PROCESS PLANNING FOR HYBRID MANUFACTURING WITH DIRECTED ENERGY DEPOSITION AND MACHINING PROCESSING

Zane Weldon Hughes

Thesis Prepared for the Degree of

MASTER OF SCIENCE

UNIVERSITY OF NORTH TEXAS

December 2022

APPROVED:

Hector Siller Carrillo, Major Professor
Maurizio Manzo, Committee Member
Reza A. Mirshams, Committee Member
Yijie Steven Jiang, Committee Member
Herman Shen, Chair of the Department of Mechanical Engineering
Shengli Fu, Interim Dean of the College of Engineering
Victor Prybutok, Dean of the Toulouse Graduate School

Hughes, Zane Weldon. *Process Planning for Hybrid Manufacturing with Directed Energy Deposition and Machining Processing*. Master of Science (Mechanical and Energy Engineering), December 2022, 118 pp., 20 tables, 36 figures, 1 appendix, 35 numbered references.

This thesis details the creation and application of a generalized process plan for the hybrid manufacturing of AISI 316L stainless steel, using direct energy deposition (DED) and ball-nose end-mill machining, that includes the inspection and measurement of objects created by that hybrid manufacturing process plan. The proposed process plan progresses through the selection of substrate thickness, single-track, multi-track, and multi-layer depositions, then on to machining processing. A manufacturers' recommended set and range of DED parameters were used to create a designed experiment that aided in the analysis of objects created in each of the DED process planning steps; those objects were then machined in the same enclosure using a set of machining parameters screened from industry recommendations for ball-nose milling of stainless steel, after which measurements were taken for surface roughness, some material characteristics, and for tool deterioration. The results, analyses, and discussions collected herein show that the proposed process plan can provide models for geometrical outputs for each step in the plan, some improvements in substrate stability, surface roughness, tool deterioration, and material porosity due to voids. Current research in hybrid manufacturing does not show generalized process planning influences. The process plan as demonstrated by the work in this thesis will help operators, designers, and researchers in the future by defining a generalized workflow that can be applied to other materials used in hybrid manufacturing.

ACKNOWLEDGMENTS

I acknowledge the infrastructure and support of Center for Agile & Adaptive and Additive Manufacturing funded through State of Texas Appropriation (#190405-105-805008-220).

I would like to thank the following people:

- Dr. Dahotre for his vision, support, understanding, and enthusiasm, without which this project, and every other project that comes out of the CAAAM, would not exist.
- Rick Pearson, his wealth of knowledge in machining and fabrication, and willingness to give of it, makes everyone that works around him that much more capable.
- Bobby Grimes for always being ready, willing, and able to help, no matter what has been asked of him.
- Dr. Rajarshi Banerjee and Dr. Mohan Sai Kiran Nartu for their invaluable assistance in assisting with sample polishing and back scattered electron diffraction microscopy, without which the microstructural analysis in this work would not have been completed.

In addition, I thank the members of my thesis committee: Dr. Maurizio Manzo, Dr. Reza A. Mirshams, and Dr. Yijie Steven Jiang for their time and efforts in helping me to make the best of the project and the thesis.

I extend the utmost gratitude to Dr. Hector Siller Carrillo, not just for his guidance in the design and execution of this project, but also for his continued friendship, measured understanding, and unwavering support of my journey through the Masters degree program that has led to this thesis.

I also thank my wife, Allison, and my family for their immeasurable support in my years at UNT. My success is just as much a product of their hard work as it is of mine.

TABLE OF CONTENTS

Page

LIST OF TABLES

Page

LIST OF FIGURES

Page

CHAPTER 1

INTRODUCTION

1.1 Abstract

Hybrid manufacturing couples additive and machining processing to create parts that would otherwise require two or more machines and can provide many beneficial opportunities in the manufacturing industry. This thesis details the creation and application of a generalized process plan for the hybrid manufacturing of AISI 316L stainless steel, using direct energy deposition (DED) and ball-nose end-mill machining, that includes the inspection and measurement of objects created by that hybrid manufacturing process plan. The proposed process plan progresses through the selection of substrate thickness, single-track, multi-track, and multi-layer depositions, then on to machining processing. A manufacturers' recommended set and range of DED parameters were used to create a designed experiment that aided in the analysis of objects created in each of the DED process planning steps; those objects were then machined in the same enclosure using a set of machining parameters screened from industry recommendations for ball-nose milling of stainless steel, after which measurements were taken for surface roughness, some material characteristics, and for tool deterioration. The results, analyses, and discussions collected herein show that the proposed process plan can provide models for geometrical outputs for each step in the plan, some improvements in substrate stability, surface roughness, tool deterioration, and material porosity due to voids. Current research in hybrid manufacturing does not show generalized process planning influences. The process plan as demonstrated by the work in this thesis will help operators, designers, and

researchers in the future by defining a generalized workflow that can be applied to other materials used in hybrid manufacturing.

1.2 Objective

The main objective for this work is to create a generalized process plan for the form of hybrid manufacturing that couples the two processes of direct-energy deposit and conventional-subtractive milling. Creating a part with this type of process requires extensive testing in each of the many and varied steps; and those steps will generally not benefit well from empirical or theoretical models created for application with differing manufacturing techniques or materials. Successfully manufacturing a part with a new material on any setup of comparable equipment would be difficult without a process plan and would risk the loss of expensive materials and productive time in creating a new plan for every material or setup.

Currently, the hybrid manufacturing industry has many useful models for individual steps in this type of process. Most of those models are empirical and are based on the characteristics of one material when applied to one machine. That very limited approach restricts the use of the knowledge base in any new type of material or on a new machine. For each new researcher or operator that wants to start from basic additive manufacturing inputs and hopes to create a useful part at the end of their work, this creates the need for an extra step in their process, which is to plan the entirety of their process. This requirement, created by the lack of a standardized process plan, affects every research team and industry operator using this type of technology.

1.3 Definitions, Nomenclature, and Abbreviations

To establish the definitions, nomenclature, and abbreviations that are used in this thesis,

Table 1.1 presents specific terms that have already been defined by the standards creating bodies: The American Society for Testing and Materials (ASTM) and the International Organization for Standardization (ISO). All entries in the Table 1.1 are quoted directly from the reference document, ISO/ASTM 52900:2015(E) (1), to preserve the meaning of the terms.

Table 1.1: ISO/ASTM standard nomenclature for additive manufacturing terminology

Directed energy deposition (DED)	Process in which focused thermal energy is used to fuse materials by melting as they are being deposited
Process parameters	Set of operating parameters and system settings used during a build cycle or a subtractive manufacturing cycle
3D scanning	Method of acquiring the shape and size of an object as a 3-dimensional representation by recording x, y, z coordinates on the object's surface and through software the collection of points is converted into digital data
Post-processing	Process steps taken after the completion of an additive manufacturing (2.1.2) build cycle (2.3.3) in order to achieve the desired properties in the final product
Fully dense	State in which the material of the fabricated part is without significant content of voids
Repeatability	Degree of alignment of two or more measurements of the same property using the same equipment and in the same environment

Table 1.2 lists some terms and abbreviations that need a definition to be used well in this thesis. These terms have not been formally defined elsewhere as in a published standard but have been used frequently in literature wherein they have meanings that are consistent with what is presented herein.

Table 1.2: Abbreviations for geometry and equipment

HD	Hatch Spacing, the distance between the center line of one track of cladding and the center point of another track of cladding. Generally expressed in mm.
OL	Overlap, the amount of one deposition track that is cover by the next deposition track in the same layer. Relates to Hatch Spacing. Generally, a percentage of TW.
FVM	Focus Variation Microscope or Microscopy as is used by the Alicona Infinite Focus.
BLI	Blue-Light Interferometry as is used by the GOM Atos 3D scanner.
AHM	Ambit Hybrid Machining center as is discussed in the equipment section

AM	Additive Manufacturing
MP	Machining Processing
BUE	Built up edge, material deposition on a tool edge during MP, contrasted with flank wear.

There are some terms that are used in this thesis that require symbolic abbreviation in some forms and equations. Table 1.3 lists these terms, with any abbreviations or symbols that may be used as a substitute for their full spellings or for their units of measure.

Table 1.3: Abbreviations and symbols for parameters and measurements

P	Laser Power, in watts.
F	Powder Flow Rate, in grams per minute
S	Scanning Speed in, millimeters per minute.
V_c	Cutting Speed, in millimeters per minute.
n	Spindle Speed, in revolutions per minute.
f_z	Feed per tooth, in millimeters.
D_e	Effective diameter of cutting tool, millimeters.
a_e	Radial depth of cut, percent or millimeters.
D	Vertical Substrate Distortion, in mm. The distance to which a substrate has moved upward after a deposition. Also called Deformation in some figures.
h	Clad Height, the distance between the substrate surface, and or the surface of the preceding layer of deposition and the surface of the current deposition. Generally expressed in mm.
h_m	Multi-layer clad height, the distance between the substrate surface and the top of the first layer or a deposition. Also, the distance between each layer. Used to program the step-up value in deposition G-codes. Generally expressed in mm.
h_c	Calibrated multi-layer clad height. Essentially the same as h_m, except calculated and adjusted iteratively after at least one multi-layer deposition has been measured for single-layer height.
w	Track Width, measured from a single-track deposition. Generally expressed in mm.
t	Substrate thickness, in mm.
E	Energy Density, synthetic parameter combining laser power and scanning speed.
d	Laser spot size. In this set of experiments this is always 1mm diameter.

CHAPTER 2

LITERATURE REVIEW

2.1 Additive Manufacturing Literature

Qi et al. (2) performed a study on adaptive tool paths for DED processing that also included data on geometric response of deposited material. The inputs they used for their experiments included laser power, powder flow rate, and travel speed, among others, which is very similar to those used in this study. The levels that were used in that study, as they relate to the inputs used in this thesis, were between 200 and 400 watts, between 2 and 4 grams per minute, and between 60 and 480 mm/minute: these recommendations were compared with those from the AHM manufacturer to establish the levels used in this study. The geometric results they obtained for wall thickness, between 0.9mm and 1.46mm, and layer height, between 0.102mm and 0.330mm, agree closely with the results shown later in this study.

In an investigation of DED parameter effects on microstructural characteristics Amine et al. in (3) showed that power and speed were both significant, and that the interaction between them was also significant. That study, like this one, used powder-based DED and stainless steel 316L powder. With factors of power, speed, and feed considered at levels of 600-900W, 300-450mm/min, and 8-12g/min respectively, the study showed that optimal microstructure could be found at 600W and 450mm/min: however, those levels are not considered in this study as they are significantly higher than what has been recommended as a good set of initial parameters. Even though powder feed rate was excluded from the study's conclusions on optimal parameter levels, they did mention the interaction between power and feed in the material

hardness response: which means that all three parameters should be controlled for overall quality of finished product.

In a thesis on AM processing for application in die and mold industry, much like this one, Camarena et al. (4) determined that the best parameters for use in AM processing of stainless steel were laser power at 400 watts, scanning speed of 400mm/min, and layer thickness of 0.3mm. While the laser power and scanning speeds are very similar to those used in this work, Camarena used the layer thickness as an input instead of measuring it as an output of the process parameters.

Simulations have been used in some studies to reduce the need for lab experimentation. Cheng and Chou showed in their study (5) that these simulation results can be regarded as close approximations, as they were able to correlate the results of their study with measurements taken from comparable objects created with the same parameters, although that was with some considerable error in specific cases. The major finding that they reported was that all the factors considered in their study had significant effect on the melt pool surface area and ratio of length to depth: power, speed, and beam diameter. The levels used in the comparison portion of this study are not relevant to this review as the technique and material where not DED or 316L stainless steel.

In a study on melt pool energy balance and the effect it has on the DED process, Yu et al. showed several findings that support a comprehensive approach to parameter adaptation (6). In microstructural development, solidification time in very important: this study showed that the most significant factor in cooling time is scanning speed. To include speed and feed to the list of significant factors in the study it was shown that mass inputs and melt pool energy must be

balanced for consistent results. And to move the results into the area of geometric concern Yu et al. showed that pool temperatures only stabilize for 304 stainless steels in DED after the sixth layer has been deposited which indicates that melt pool spreading is dependent not only on progressive geometry during the cladding operations but also on the number of layers used to create those geometries. In this study, like the others presented here, it was shown that parameter interactions should not be ignored. Which further supports a case for a comprehensive approach to process planning in direct energy deposition and hybrid manufacturing.

Another avenue for finding precedent and background for this project in the existing literature can be found in a sampling of the models that have been presented in other works. This project provides data for the creation of several models that should be able to describe the behavior of process parameters in terms of clad geometries. There are several proposed models that address geometry as a response and or accept geometry as an input that could be considered for application; however, despite the advantage that using a predefined model would provide, these models all show significant limitations.

One such model was proposed in (7) by Walker et al. They used a physics-based heat-transfer model coupled with several analytical models to propose a function that can describe transient track profiles based on process inputs similar to those that were used in this study and specific material properties. One of the interesting developments in this model was that the melt pool area was not assumed to be symmetrical or constant: in contrast to other studies this model included a process for predicting the shape of the melt pool before using it in further calculations, these can be seen in the bounds for the integral term shown in Eq. 2.1, the details of which are

excluded here for brevity. The major limitation seen in this model is that it can only be used to predict single-track and single-layer cladded objects. This could be seen as another point supporting the creation and application of a generalized process plan over that of any attempt at generalized models for a particular portion of a process.

Equation 2.1: Modeling for single-track single-layer clad profiles adapted from [8

$$h_z(x) = \frac{\eta_c(t_n)}{\rho V(t_n)} \int_{Yr}^{Yf} q_{pf} dy$$

where:

$h_z(x)$ = clad height

$\eta_c(t_n)$ = powder catchment eff.

ρ = powder density

$V(t_n)$ = scan speed

$\int_{Yr}^{Yf} q_{pf} dy$ = melt pool area

Another modelling technique based partially on physics of heat transfer and material properties was proposed by Picasso et al. in (8). This model incorporated predictions on energy absorption, temperature fields, and melt pool shape. The inputs for that model included laser power, laser radius, powder jet geometry, as well as desired clad height. That desired clad height was used along with the other inputs to determine the required process parameters of scan speed, powder feed rate, catchment efficiency, and power absorption. So, in many ways the Picasso model was a reversed approach compared to the Walker model. However, much like the Walker model, the Picasso model has only been validated for single-track single-layer claddings, which would again support the creation of a comprehensive and generalized process plan that includes portion of the hybrid process that these studies exclude.

One of the models presented in the existing literature body on this topic was presented in a study authored by Huang et al. (9), in which they applied a particle thermal physics-based approach, focused on thermal field accumulation and melt pool anisothermality to propose a model for clad height and width based on the laser power, feed rate, scan speed, as well as a variety of apparatus geometries like beam waist radius an position. This model, unlike the others discussed herein, presents a method for predicting geometries in multi-track claddings. And without detailing how, also implies that the model can be adapted to multi-layer geometries as well. The major disadvantage in this is that the model was built to predict behaviors in laser powder-bed fusion systems, wherein the thermal dynamics are notably different compared to direct energy deposition systems where the powder bed and un-melted mass surrounding the clad is not present.

Equation 2.2: Model of clad height and width in multi-track depositions, adapted from Huang et al. [9]

$$h = \frac{\sqrt{w_0 h_0 \tan(\alpha_w)}}{2}$$

$$w = 2\sqrt{\frac{w_0 h_0}{\tan(\alpha_w)}}$$

$$\alpha_w = \tan^{-1}\frac{4h_0}{w_0}$$

where: α_w = wetting angle; w_0 = initial width; h_0 = initial height

Another model that is relevant to the topic was developed by Bhardwaj et al. in (10) and is purely empirical (Eq. 2.3). In that study data was collected through experimentation using direct energy deposition with varied parameters of laser power, scan speed, and powder feed rate. Based on an analysis of variance in the results that showed all three parameters, as well the

interactions to be statistically significant to the geometric responses, the authors were able to build and validate models representing clad object height, width, depth of penetration and dilution. In Eq. 2.3 adaptations of the height and width models are shown, depth and dilution being excluded. As with the other models presented in this section of the review, this model also has limitations that preclude its application for this project: the material used in that study was a titanium alloy. That limitation, and the fact that it also does not predict multi-track or multi-layer geometries makes it interesting for review, but ultimately not applicable herein or in industry.

Equation 2.3: Model for clad height and width as a function of input parameters adapted from Bhardwaj [10]

$$Height = 26.30 - 0.02986P + 0.00582V - 0.484f + 0.000002P * V + 0.000162P * f + 0.00025V * f$$

$$Width = 85.3 - 0.0927P - 0.01029V + 0.270f + 0.000009P * V + 0.000121P * f + 0.000044V * f$$

where: P = laser power; V = scan speed; f = power feed rate

One aspect of inquiry in the work presented herein was concerned with clad height, or in other terms, layer thickness. Shim (11) has made some experiments and analyses of the effect of layer thickness and points out that the "effects of DED parameters on the dimensional accuracy […] of fabricated parts have not been well researched." Shim set out to design the process parameters for specific layer thicknesses and improved mechanical properties. However, Shim used a slicing software with user accessible slicing parameters with which they could adjust the layer thickness settings in the software, which would output as the G-Code for the deposition. Shim also did not perform the same level of process planning with the single-track to single layer parameters. The work done by Shim was performed using two different materials: M4 high-speed tool-steel as the powder, and structural carbon steel 1045 as the substrate. While the

contribution serves the industry on a conceptual level, the findings are anecdotal when applied to any other material, which serves to further emphasize the need for a generalized process plan instead of a set of generalized models for any specific output in the process.

In an article focused on creating a physics-based model for AM geometry, Wang (12) proposed to create a mathematical model for the clad track geometries deposited during a DED process based mainly on the powder flow during the process. One major assumption that Wang makes in creating their model is that all of the laser energy is entirely absorbed by the substrate and powder during the deposition. This assumption disregards the reflectivity of many materials, which can have a large effect on the amount of energy available for the deposition process. Wang makes acknowledgement of the deficiency created in the aforementioned assumption in the conclusions, as they stated that their model can predict "the surface of a single track with different parameters except for the situations where laser power cannot melt powder particles." This should be another point of emphasis that the creation of generalized models that require assumptions will be less accurate in industry applications and should be preceded by and couple with a comprehensive and generalized process plan.

Picasso et al. (8) state clearly and simple that in metal additive manufacturing the "process parameters are numerous." And that it is "possible to obtain clads of the same height at different beam velocities." This should indicate that the creation of generalized models for predicting outputs in AM may yield misleading results if the input parameter sets are not comprehensive: which would support the case of creating generalized process plans over the creation of generalized models.

While Bax et al. (13) state that their experimentation on systematic evaluation of process

parameters validates the generalized application of some empirical models for laser cladding across different machines, they state that at the least, proposed models for dilution and powder efficiency from literature sources do not seem to be applicable for their experimental setup. And in their conclusions, Bax et al. state that the "correlation between the three selected parameters and the geometrical characteristics as described [are] only applicable for single tracks." Which should serve as support for a process plan that can be applied from single-track on into multi-track experimentations, and beyond.

To make this study more comparable to others like it, one term that should be defined that can relate the laser energy to the scanning speed is energy density. Energy density is a synthetic parameter that combines the laser power, scanning speed, and the spot size of the laser as shown below, which can be found in this form in several works including articles by Wolff et al. (14), and by Kim et al. (15).

Equation 2.4: Energy density as a synthetic parameter formed from laser power, scanning speed, and laser spot size, in units of Joules per square millimeter

$$E\left(\frac{J}{mm^2}\right) = \frac{P}{S \times d}$$

where:

P = laser power in watts

S = scanning speed in mm/min

d = spot size of the laser

This synthetic parameter is only presented herein to allow for comparisons with other studies as the data collected in this set of experiments has shown that the synthetic combination of the original parameters was not statistically significant.

2.2 Machining Processing Literature

While the machining strategy employed in this study was not a factor used in the design of experiments, it may seem necessary to establish the nomenclature for that particular strategy for reference and or comparison with other studies in future works. As noted in their study on the effects of milling strategy, Vakondios (16) et al. have termed the strategy and orientation between the end mill and workpiece as oblique-push down milling, as is depicted in Figure 2.1.

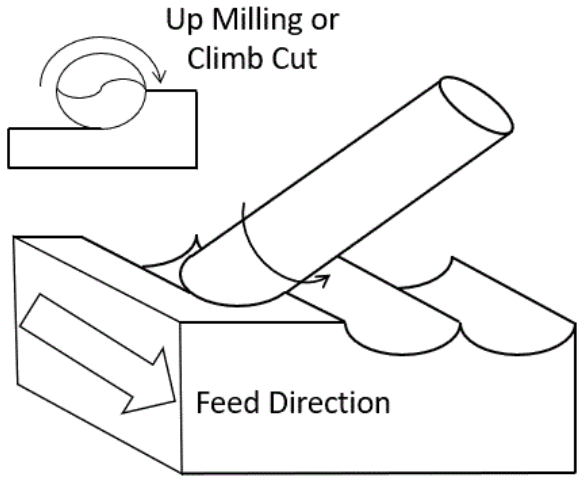

Figure 2.1: Diagram of oblique up milling or climb cut with feed direction and revolution direction relative to workpiece. Adapted from Vakondios [19]

Surface quality was not an output of interest in terms of the designed experiments discussed herein; however, in terms of establishing a good process plan, a target surface roughness was required. A good target was predicted using a model based on empirical evidence that has been cited in several works, the reference for which, as it was found in the literature review being discussed herein, is attributed to Grzesik (17). That empirical model is as shown in Equation 2.5. To make good use of the prediction for surface roughness the cutting speed and cutting-edge radius were required. The cutting-edge radius is discussed in the methodology section.

Equation 2.5: Theoretical surface roughness as adapted from [17]

$$R_a = \frac{0.0321 \times f^2}{r}$$

where

f = cutting speed in mm/rev

r = cutting edge radius of tool

The cutting speeds used in this set of experiments was selected from recommendations made by the ball nose end mill manufacturer ISCAR (18). In their reference materials cutting speeds and chip loads, i.e. chip per tooth, are recommended for semi-finish processes as were expected in this project. Those recommendations are also discussed in the methodology section as they are most relevant there.

In an article focused on the surface quality and porosity of parts created using a hybrid of AM and MP processes, Kaynak (19) states that in general, as-built 316L SS parts have surface roughness values around 7 µm, which compared to the less than 2µm roughness values of parts that are manufactured using conventional subtractive manufacturing, is less than desirable; they go on to use that as support for promoting that coupled DED and CNC processing can contribute to the advancement of additive manufacturing applications in industry. Kaynak uses the same method of predicting a surface roughness in machining as was seen in the article from Grzesik as was shown in equation five. Kaynak concludes that "finish machining […] substantially reduces porosity […] on the surface" of the part. They also conclude that microstructure grain size is reduced at and near the machined surface, which indicates that the machining process imparts a benefit to the as-built material. This benefit is also related to the strain-hardening effect that leads to an increase in the microhardness of the material. As a comparison, that agrees well the

results gained in the project detailed herein, Kaynak cites the as-built hardness of SLM produced 316L stainless steel is 260 +- 7 HV. The results from the hardness testing in this set of experiments are discussed in the results section.

In preparation for measurements of tool deterioration that this work required, the ISO standard for tool wear testing (20) was included in the literature research. The standard for tool wear testing recommends that each tool in an experiment by checked for radial and axial runout, which should not exceed 50µm and 30µm respectively. The tools used in this experiment were checked and met this requirement; the collected data for those checks is shown in the appendix. The standard recommends the use of cutting fluid when cutting steel. However, cutting fluid is not available in the AHM and as such was not used in the MP portions of this work. From the depiction of flank wear in the 7.3.1.2 section, the tool wear in this study has been identified as localized flank wear. As such any measurement describing flank wear as tool deterioration will be expressed as a positive numerical value. This is due to the reduction of flank landing material exposing a larger area underneath, thereby increasing the length of the facet being measured.

In a study of the effect of built-up edge as it relates to tool deterioration, Cassier et al. (21) have attempted studies on the dynamics of BUE as tool deterioration because "no mathematical models exist that allow users to estimate […]" tool wear as a function of built-up edge. An increase in tool wear rate related to the effects of built-up edge has however been identified by Cassier et al.

2.3 Process Planning in Hybrid Manufacturing Literature

In their review of hybrid manufacturing processes, Grzesik (22) details a process plan for uncoupled manufacturing of parts that begins with a 3D CAD model, and for the AM portion of

the process relies entirely on the slicing software to determine the geometric parameters prior to the cladding process. The MP portion of the process relies entirely on the same 3D CAD model as well. It is not well described how these two approaches meet in terms of geometric responses, especially considering that the geometric response of the AM portion is so critical to the success of the MP portion of that process. Another Process plan that Grzesik details uses an "in-house layered manufacturing or slicing software" that begins with a CAD model and relies on predictions of geometry based on melt pool dynamics. This type of process plan is not easily accessible to the industry without access to the “in-house” software. This type of process plan may also lack the flexibility to work with new or experimental materials as it was developed for one material.

In their article on AM in industry, Ituarte et al. (23) point out that while there is a vast collection of studies on additive manufacturing input parameters and the resulting characteristics of microstructure and mechanical properties, there are too few resources for process planning in additive manufacturing for the full benefit of the technology to be of use in any industry. They go on to state that the “geometric stability” of AM produced parts depend on the process plan as much as they do the machine itself, or on the process input levels.

Alvarez, in a work on the influence of process parameters in hybrid manufacturing (24), proposes a process plan that begins with selecting AM process parameters and move on to evaluating the appearance of characteristics in a single-track deposition, and then studying the characteristics in an overlapping multi-track deposition. A similar approach has been proposed in this work, however, the process approach as proposed by Alvarez neglects the effect of multi-layer processing. The study done by Alvarez used a similar AM equipment setup, with a coaxial powder fed nozzle with a central laser. However, the laser power used was very high in

comparison, 2k and 3k watts compared to the 300 to 400 watts used herein, and the powder flow rate was also very high at 12 to 31 grams per minute compared to the 2 to 3 grams per minute. As such, the results from the AM portion of this study would not be directly applicable to this thesis as the deposition geometry was not at the same scale. This should help to emphasize the importance of a generalized process plan over that of a generalized model for any portion of such a plan.

In planning a process for LPBF Ramirez et al. (25) proposed only two fabrication steps: the first to test the weldability of the material, and the second to test multi-layer fabrication. This type of process plan neglects the steps that would investigate important factors like single-track dimensionality. They then suggest analyzing the surface roughness and mechanical properties to optimize the process parameters without assessing the dimensional outputs. This type of twostep process neglects the intermediate steps that could provide useful empirical evidence that would improve the process as a whole as well as the quality of parts produced using that plan.

A good process plan should have some technique for assessing repeatability and traceability of measure; in a review of dimensional artefacts Carmignato (26) comments on this. They describe the importance of creating "dimensional artefacts" that are objects that can help define and evaluate the traceability and repeatability of dimensional outputs in manufacturing. Gauge blocks, or other types of calibrated workpieces add value to a manufacturing process by ensuring the repeatability of the process through inspection and comparison. The process plan proposed herein has built-in artefacts for each stage of the process, which is one reason it should be a positive contribution to the industry. While the work in this project was focused in part on

creating dimensional artefacts specific to the process itself, there were several dimensional artefacts that were required for the evaluation portions of this project: one that is also mentioned in Carmignato's article is a surface texture artefact. The surface roughness measurements done via FVM required several software settings to be adjusted. Matching the output of calibration measurements with the known values of the roughness calibration objects provided confidence in the measurements of the experimental pieces themselves.

In a review of adaptive control in AM processing, laser based deposition in particular, Wang et al. (27) describe a planned process that involves ex-situ geometry measurements as well as in-situ temperature monitoring. This kind of process control may afford some benefits, namely in-situ adaptive control: however, it does pose an extra cost to the adopter of this type of planning. That extra cost could support the creation of a process plan that does not require in-situ monitoring.

Additive manufacturing quality being dependent on substrate condition, Denlinger et al. (28) attempted to study the effect of dwelling between deposition layers. Denlinger et al. discovered that a substrate, used for DED depositions, will distort downward during deposition, and upward during cooling. work, was "most prominent [in] depositions with no dwell time."

As it relates to the substrate condition, Cabanettes et al. (29) In their articles that examined the topography and microstructure of as built surfaces in metal additive manufacturing, Cabanettes et al. experimented with and confirmed that heat treatment can release residual stress developed in AM processes. As the substrates suggested for use by this work would resist Distortion during deposition, residual stress would be induced, and any future

work based on the process plan proposed herein should investigate the effectiveness of heat treatment post-processing, as suggested by Cabanettes.

2.4 Substrate Condition Literature

In their work concerning the effect of substrate conditions on the additive manufacturing process, Sikan (30) states that "Complex thermal history" is one of the major issues standing as a barrier to widespread adoption of AM technologies like DED. The intensity of heat required by the process leads to extreme changes in substrate, and previously deposited layers. The effect of this is seen and addressed herein by the examination of substrate warping in various substrate thicknesses. However, one aspect of this dilemma would require processes outside the scope of the proposed process plan in this work, and that would be post- process heat-treatment to mitigate the effects of residual stress imparted during the deposition process.

After this investigation into the state of current modeling techniques and products created by similar studies it should be evident that a generalized process plan will prove useful in the field of hybrid manufacturing. Sikan goes on to express that residual stress is not only a defect of the process, as in when a technique like DED is used to repair a part, but it is also a defect that should be expected in the part to be repaired. The existence of residual stress prior to the deposition process would influence the characteristics of the part just as much as any stress imparted during the process. In the study presented by Sikan, while it does present some useful information about the effects of laser-powder based depositions as a repair technique, and some negative effects to be considered therein, the empirical results are anecdotal when applied to materials other than the Titanium alloy that was used in the study. Here again the

literature has shown that generalized models may not be available, therefore a generalized process plan should be produced that can help provide material and process specific models.

2.5 Microstructure and AM Literature

In a study on the effects of input parameters on the microstructure of DED process materials, Zhuqing Wang et al. (31) described that the grain structure in the deposited material was slightly larger and its morphology was elongated. They took care to note that although there was anisotropy in the elongation with respect to transverse and longitudinal cross-sections, there was no anisotropy measured in the yield or tensile strength of the objects created in their study. The elongation shown in their study was clearly in the direction of the deposition travel, which was in one direction for every track. This is contrary to the scanning strategy employed herein, where a meander strategy was used, meaning that the travel of the deposition was reversed for each proceeding track. However, the coarsening of the grain structure as the deposition moved further up and away from the substrate, and the elongation of the grain morphology in the same direction can be used as comparison to the microstructures as is shown in this study.

In a journal article describing experiments in DED using stainless steels Yazar et al. (32) cited that their results showed a transition in the deposited layers moving away from the substrate. Near to the surface they found that the morphology was mixed with “cellular, dendritic, columnar, and planar structures.” But that “in the interior region […] grains were columnar in nature.” Yazar et al. also noted that in their study the hardness of the materials was not significantly affected by the processing parameters. While the processing parameters specified in their study are different when compared to those used herein, the ratio of laser

power to scanning speeds are very close for some of the parameter sets, therefore the qualitative results of microstructure analysis presented in this study can be readily compared.

CHAPTER 3

METHODS

3.1 Experimental Setup

This set of experiments and analyses were designed to develop and demonstrate a good process planning regime for hybrid manufacturing that involves CNC controlled direct energy deposition and conventional subtractive CNC milling. By varying input parameters of substrate thickness, laser power, powder feed rate, and scanning speed, correlations to geometric responses in each step of the planned process can be created that will facilitate the design and execution of each subsequent step in the AM portion of the process. The depositions can then be subjected to MP processing based on best practices and recommendations; after which measurements of surface roughness can be taken and analyzed to confirm suitable machinability as would be expected in a die and mold making industrial application.

As shown in Figure 3.3, the process plan began with material selection and preparation. The material selected for this set of experiments was Stainless Steel 316L as it is a very common material to be used in the die and mold making industry. The powder selected for this set of experiments was SS316L powder in a size range of 45-110µ as per recommendations from the AHM manufacturer. That powder was sieved to less than 90µ so that the powder sizing aspect ratio would be within 2:1 as that is a recommendation for the AHM with respect to the effect of powder size on laser beam blockage.

The next step in the process plan was to determine the minimum substrate thickness required to mitigate the effects of induced Distortion in the substrate. To achieve this determination varying thicknesses of substrate were used to deposit a set amount of the selected

powder material as cladding, the same amount for each of the substrate thicknesses. The different thicknesses of substrate were then scanned using BLI and measured in the GOM software to determine the amount of thermal Distortion created during deposition. That data was then analyzed to determine the optimal substrate thickness.

With the minimum substrate thickness determined, the process continued into selecting the parameters for the AM portions of the experiment. Choosing parameters near to those suggested by the literature and the manufacturers recommendation (33) provided a basis for the designed experiment. Those parameters are discussed in the section on DED parameters. The first step in the main designed experiment of this project was to make single-track depositions for each of the parameter set combinations. Those depositions were then measured using FVM and analyzed using Excel to determine the width of track created for each parameter set. Those track widths were then used to determine the hatch spacing for the multi-track depositions for each of the same parameter sets. This is the first calibration step as shown in Figure 3.1.

The multi–track depositions were measured using FVM and the data was analyzed using Matlab to determine the average track height for each parameter set. Those average track heights were then used to determine the step-up values for the multi-layer depositions of each of the parameter set combinations; this is calibration step 2 as shown in Figure 3.1.

For calibration step 3, those multi-layer depositions where measured and the data analyzed using Matlab to compare the multi-layer heights with the step-up values, from calibration step 2, that were used for that deposition, the data was then used to create re-calibrated step-up values for each of the parameter sets, as is shown at bottom of Figure 3.1.

Calibration Step 1: Deposit single track objects. Measure for width. Use measured width to set hatch-spacing for multi-track depositions.	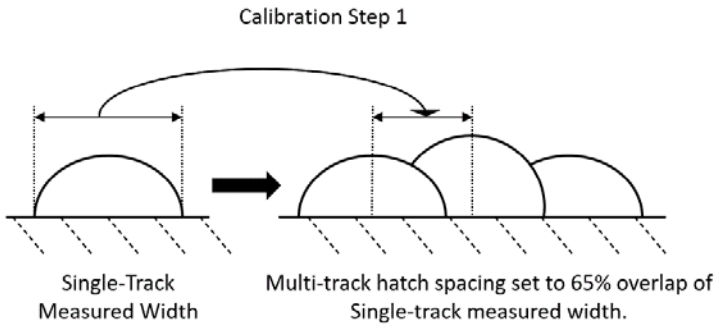
Calibration Step 2: Measure multi-track average height and use that value to establish a step-up value for multi-layer depositions.	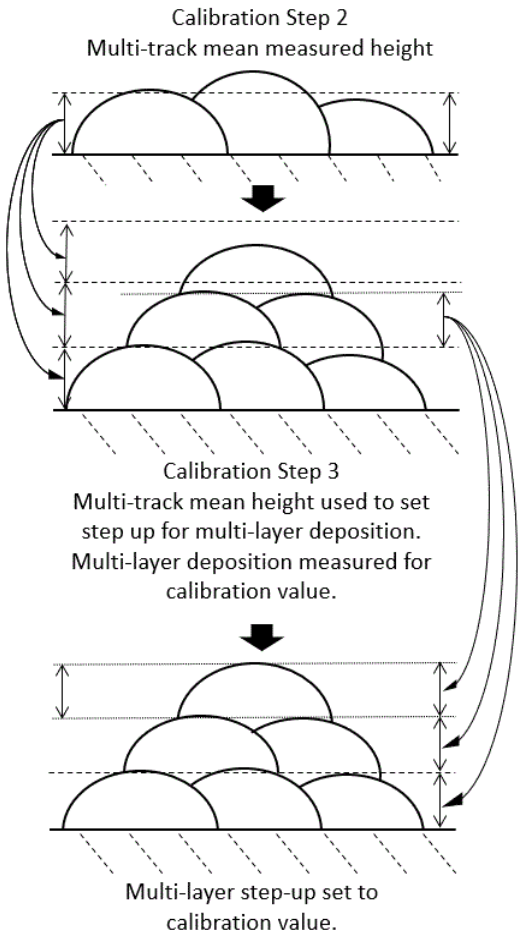
Calibration Step 3: Measure multi-layer depositions, divide the overall measure by the number of layers and use this value to re-calibrate the step-up values created in calibration step 2.	

Figure 3.1: Schematic and description of all geometric calibration steps

The next step in the process was to select the parameters for the machining processing steps. Suggestions from literature and industry recommendations were used to create a designed screening of the subtractive parameters that would yield the best surface roughness. In that screening several depositions were made using one set of input parameters which were then

subjected to the machining processing. The machined faces of those samples were then measured using FVM and the data was then analyzed to validate the selection of subtractive process parameters that yielded the best surface roughness.

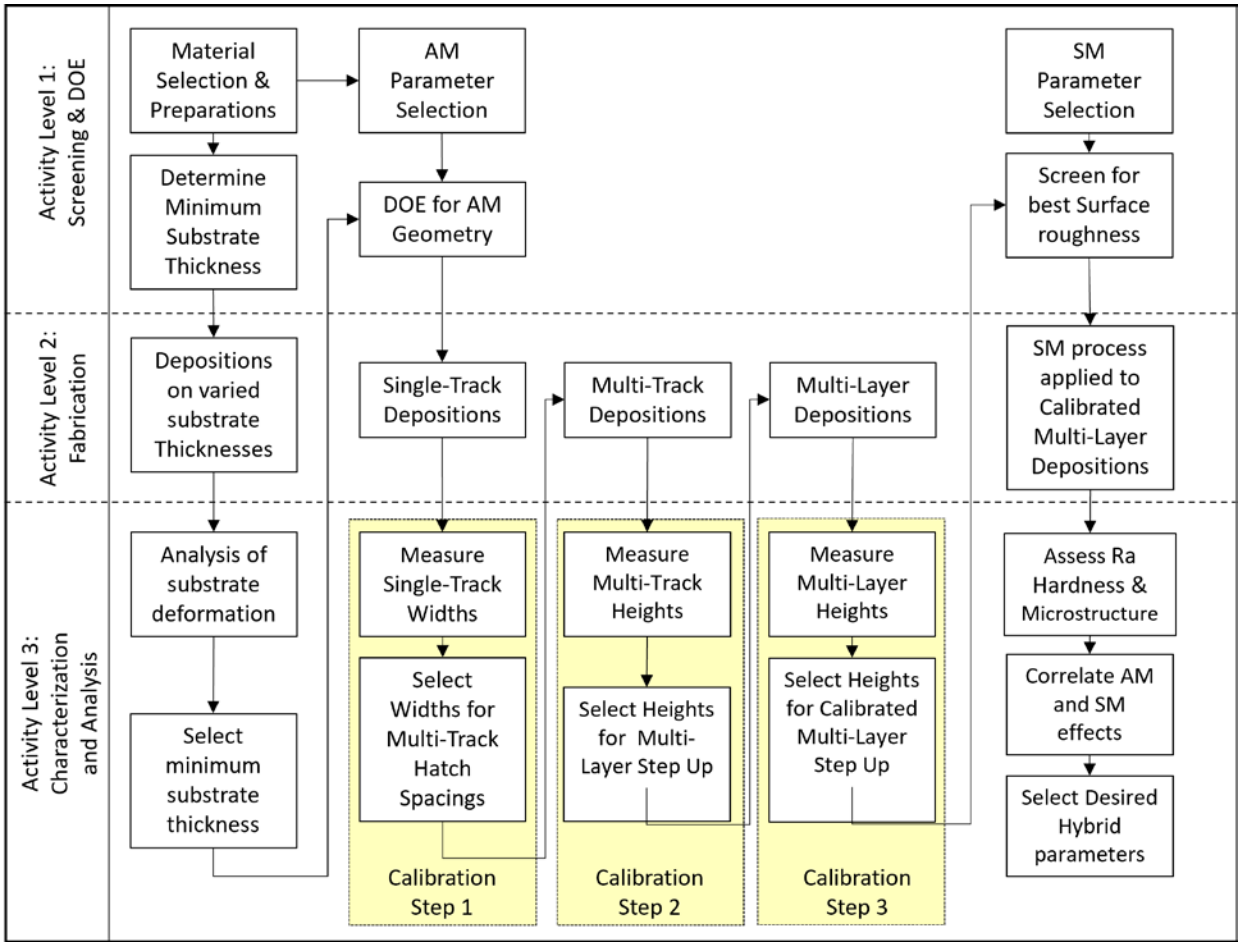

Figure 3.2: Process plan for coupled hybrid manufacturing with separation of activity levels and outputs

Those subtractive process parameters where then used in the next step of the process, wherein both the calibrated and uncalibrated step-up values were used to make depositions of each of the AM parameter sets that were also subjected to machining processing. The surface finish, hardness and microstructure of each deposition were then measured using the appropriate equipment. The results were then analyzed to assert or exclude any correlation between the inputs, calibrations and outputs. All the steps above are represented graphically in

Figure 3.2. Some steps were taken intermediate to those as described to validate the process as it was being developed; but those steps are not part of the proposed process plan. Those steps may however be described in this document in appropriate detail where neccessary.

3.2 Equipment

3.2.1 Hybrid Manufacturing Equipment

The work and experimentation in this thesis project is performed mainly on a CNC controlled direct energy deposition (DED) machine, the Ambit Hybrid Machining center. The DED portion of the machine is an addition to the existing components: the machine is a hybridization of a Haas Mini-Mill that maintains its subtractive manufacturing capabilities with the added additive manufacturing capabilities provided by the DED systems. As such it is a hybrid manufacturing system.

This machine could be seen as a natural evolution of the DED process: to achieve high quality surface finish and tight tolerances, most parts created using DED are designed with post process subtractive operations in mind. Even though it is a complimentary pairing of technologies that allow both techniques to be utilized within the same workspace, both processes are limited by the same physical mechanisms; and as such both techniques, even at their optimal capacities, are limited to the basic tolerances that could be expected from the Haas Mini-Mill. This is important to keep in mind when evaluating expectations for outcomes in the project and others where work is to be done on the Ambit Hybrid.

This machine has a few distinguishing characteristics that are worth mentioning, as they separate it from many of the DED machines that have been examined in academic projects like this one. It has a co-axial powder feeding head, which avoids the disadvantages in directionality

and low powder efficiency that might be expected from single or multi-nozzle off-axis powder feeding systems by effectively collimating the powder flow. It also has an integrated controller that operates the laser and powder feeding system via relay calls that can be initiated in the G-Code that also controls the tool pathing. This means that control of the machine can be fully realized in just the G-Code without adjustments from separate controllers, knobs, or switches.

It should be noted that in this set of experiments the DED head used in the AHM has a 1mm spot diameter. The machine can use different DED heads that have larger diameters, but the scope of this work limited that to just the 1mm spot size head.

Figure 3.3: AHM inside work enclosure with original Spindle and adapted DED Head

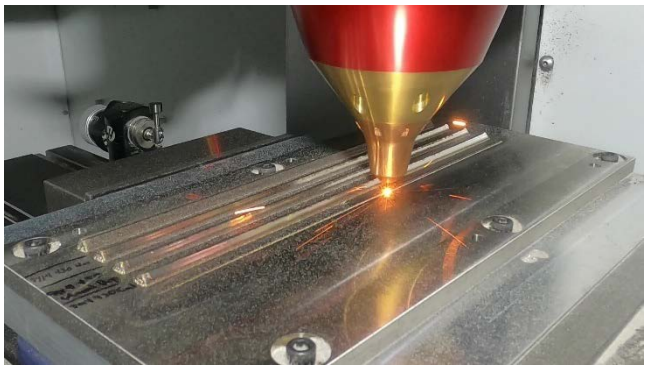

Figure 3.4: DED Head Depositing Material

Figure 3.5: Ball-nose end milling of material deposited by DED Head

3.2.2 Focus Variation Microscopy (FVM)

Measurements of form and surface roughness in single track, multi-track, and multi-layer sets of experiments were taken on a focus variation microscope built by FVM on the Alicona Infinite Focus SL. Alicona proprietary software was used to process the focus variation scans into usable data that could be exported to other software for analysis.

The FVM was calibrated by first measuring the surface roughness of samples with known roughness values using a surface profilometer. After which those samples were measured using the FVM as validation. The two measurements were compared to establish the validity of the FVM equipment and software setup. The two sets of measurements agreed to within a small percentage on all test samples.

In general, the figures in this document that include images from the FVM software include axis measurement values on the micrometer scale anywhere there is a data set shown. However, those images are for visual reference only. The purpose of including those data point images is to show the shape of the data. The data itself was in all cases exported from the FVM software and analyzed in Matlab.

3.2.3 Blue Light Interferometry (BLI)

Form measurements of substrate flatness were taken from blue-light fringe projection scans of the substrates on a GOM Atos Core. Those scans were then analyzed using proprietary GOM software to compare the substrate surface flatness before deposition to the flatness after deposition. The BLI was calibrated using a proprietary calibration device and procedure. The calibration process was indicated to be successful in the GOM software.

3.2.4 CNC 3-Axis Vertical Machining Center and EDM

The substrates used in each set of experiments were prepared using a Haas VF2 CNC Mill. G-Codes for substate preparation were created using SolidWorks CAM. Samples from each experiment were cut to manageable sizes for use on the FVM using a Mitsubishi ML1200V EDM. G-Codes for sample preparation were created on the EDM manually.

3.2.5 Hardness Tester

The hardness testing done in this project was performed on a Service Diamond, Model 12SSA Rockwell Hardness Tester Lab Testing by Louis Small.

3.3 Materials

Die and mold making being such an integral part of so many industries, the application of hybrid manufacturing to these efforts is of great interest. Many die and mold makers use stainless steel to create their products due to the hardness and corrosion resistance of the material. With this in mind, 316L stainless steel has been selected for use in these experiments.

3.3.1 Powder Selection and Preparation

316L Stainless Steel powder was purchased for use in these experiments. Powder sized from 45-110µm was selected as per the AHM manufacturers recommendation. The powder was then sieved to less than 90µm to achieve the optimum sizing aspect ratio of 2:1 which is also recommended by the AHM manufacturer.

Table 3.1: Chemical Composition of Stainless Steel 45-110µm Powder (34)

Mo	2.00-3.00%
N	0.10%
C	0.03%
Cr	16.00-18.00%
Mn	2.00%
O	0.10%
S	0.03%
Ni	10.0-14.0%
Si	1.00%
P	0.05%
Fe	Balance

3.3.2 Substrate Selection and Preparation

Interactions between disparate substrate and deposition material being undesirable in terms of scientific inquiry, the material selected for substates in these experiments is the same

as the material selected for the powder – 316L Stainless Steel. The substrates were prepared for the experiments by being squared on all sides first, then by being face milled on the sides that would be used for the subsequent depositions. All these operations were performed on a Haas VF2. The G-codes for these operations were prepared using SolidWorks CAM software and models created in SolidWorks.

3.3.3 Subtractive Tooling Selection

As the process planning effort in these experiments is mainly focused on an application in the die and mold making industry, ball nose end mills were selected for the subtractive tooling in these experiments. Ball nose end mills are the most used tools in creating non-planar shapes that require high quality surface finishes in the die and mold making industry. Specifically, with respect to the size of the deposition to be machined and the hardness of the material, quarter inch 4-flute ball-nose end mills composed of solid carbide with a physical vapor deposition coating of AlTiCrSiN, produced by ISCAR were selected for these experiments. A fresh ball nose end mill was used for every experimental iteration in the MP portion of the process to remove any cumulative tool wear from consideration.

3.4 Methodology

The proposed process plan that this thesis intends to show began with the substrate. To mitigate the effects of thermal Distortion on the deposition process, the minimum thickness of substrate required for a set of material and input parameters was first found. To find this minimum thickness three sets of substates with different thicknesses were first scanned using blue-light fringe projection scanning, then subjected to a set of depositions, then scanned again.

The before and after scans were then compared to determine at what thickness thermal warping had been eliminated. Once a minimum substrate thickness was determined, the cladding geometries were determined. The process of determining the cladding geometries began with single track depositions using the full set of input parameters. Those single-track depositions were then measured using focus variation microscopy to find a correlation between the relevant input parameters and the track widths. That track width was then used to create cladding paths for multi-track depositions using an appropriate overlap for hatch spacing. For this set of experiments the hatch spacing was held constant at 65% of single-track width for all experiments. Those multi-track deposition were then measured using focus variation microscopy for an average clad height produced by a given set of input parameters. Then the average clad heights were used to program a multi-layer deposition, that was subsequently measured using focus variation microscopy to determine the multi-layer clad height and relevant error from multi-layer clad height expectations based on the multi-track average clad height. After eliminating any sets of input parameters and multi-layer tool paths that had high levels of error in multi-track clad heights, the remaining sets of parameters and clad geometries were used to write tool paths for long depositions that could then be subjected to machining processing. After the machining processing, samples from each deposition were removed from the substrate to be examined through hardness testing on the machined surfaces and to have surface roughness evaluations performed using focus variation microscopy and proprietary software.

3.4.1 Process Parameters

3.4.1.1 Direct Energy Deposition (DED) Parameters

The DED parameters used in this thesis are laser power, powder flow rate, and scanning

speed. The levels of these parameters were selected to be close to those found in the manufacturers recommendations (33) and to those found in the relevant literature. A simple but full factorial designed experiment to evaluate the geometric responses of these DED inputs was created using the inputs levels as shown in Table 3.2.

Table 3.2: DED input parameters: $\mathbf{P}$, $\mathbf{F}$, $\mathbf{and}$ $\mathbf{S}$ with levels for designed experiment

AM Input	Levels
Laser Power, in watts	300 – 400
Powder Flow Rate, in grams per minute (mass flow rate)	2, 3, 4
Scanning Speed, in millimeters per minute	350 – 450

These values were used to establish a full-factorial designed experiment in which all of the combinations of the inputs and levels were used, similar in structure to a 2^3 full factorial experiment in which each of the three inputs would have two levels, with the exception that one input, the powder flow rate, initially had one extra level. That structure required twelve experiments when all the input levels were included. Later in the process some input levels were excluded, and one input was added, for various reasons which changed the number of experiments required. Those exclusions and the one addition are discussed herein where relevant.

So that this study can be readily compared with others, the inputs of laser power and scanning speed can be considered in terms of linear energy density, which is a term that can be found in many other studies on this topic. Linear energy density, as a synthetic parameter, is the combination of the laser power, scanning speed inputs, and laser spot sectional area, which is generally expressed as the amount of power per area scanned: in this case it is expressed as joules per square millimeter, which makes the 1mm spot size of the DED head selected for these

experiments convenient for calculation. The input levels converted to linear energy density are shown in Table 3.3. Those values were calculated using the form of equation four as described in the DED parameter section of the literature review. As it relates to the literature sources, these values are within the same range as used by Kim et al. in their study on microstructure and direct energy deposition of 316L stainless steel; that range being 35 to 177 J/mm^2 (15). The preference for using the individual parameters over the synthetic energy density parameter in this study is discussed briefly in the results sections.

Table 3.3: Energy density for DED parameters

P – Laser Power in $watts$	S – Scanning Speed in mm/min	E - Energy Density in J/mm^2
300	350	51.4
300	450	40
400	350	68.6
400	450	53.3

3.4.1.2 Machining Processing Parameters

Some of the MP parameters used in this set of experiments like feed per tooth, spindle speed, and depth of cut were selected using industry recommendations based on the type of machining to be done, and the capabilities of the machine being used. Typical MP in the die and mold industry is focused on finish machining as the products require a very good surface roughness in most cases. The characteristics of the material chosen for this set of experiments would have required a spindle speed and power much higher than what the AHM is capable of; therefore, recommendations for semi-finishing were used to determine most of the machining processing parameters herein.

Determination of MP parameters requires analysis of tool geometry as the first step,

specifically the tool diameter and depth of cut. The chosen tool for this set of experiments is a ball-nose endmill, and the tool was only engaged with the workpiece using a portion of the cutting edge, an assessment of the effective tool diameter is required. Literature and industry recommendations have several methods for approximating the effective diameter. In this case, the effective diameter can easily be measured for each of the different AM parameter sets by modeling the workpieces and the tool in Solidworks using the manufacturers recommended depth of cut for the semi-finish approach of five percent [iscar die and mold guide] of the overall tool diameter, which for the one quarter inch tool would be 0.0125in or 0.312mm. An example of this is shown in Figure 3.6.

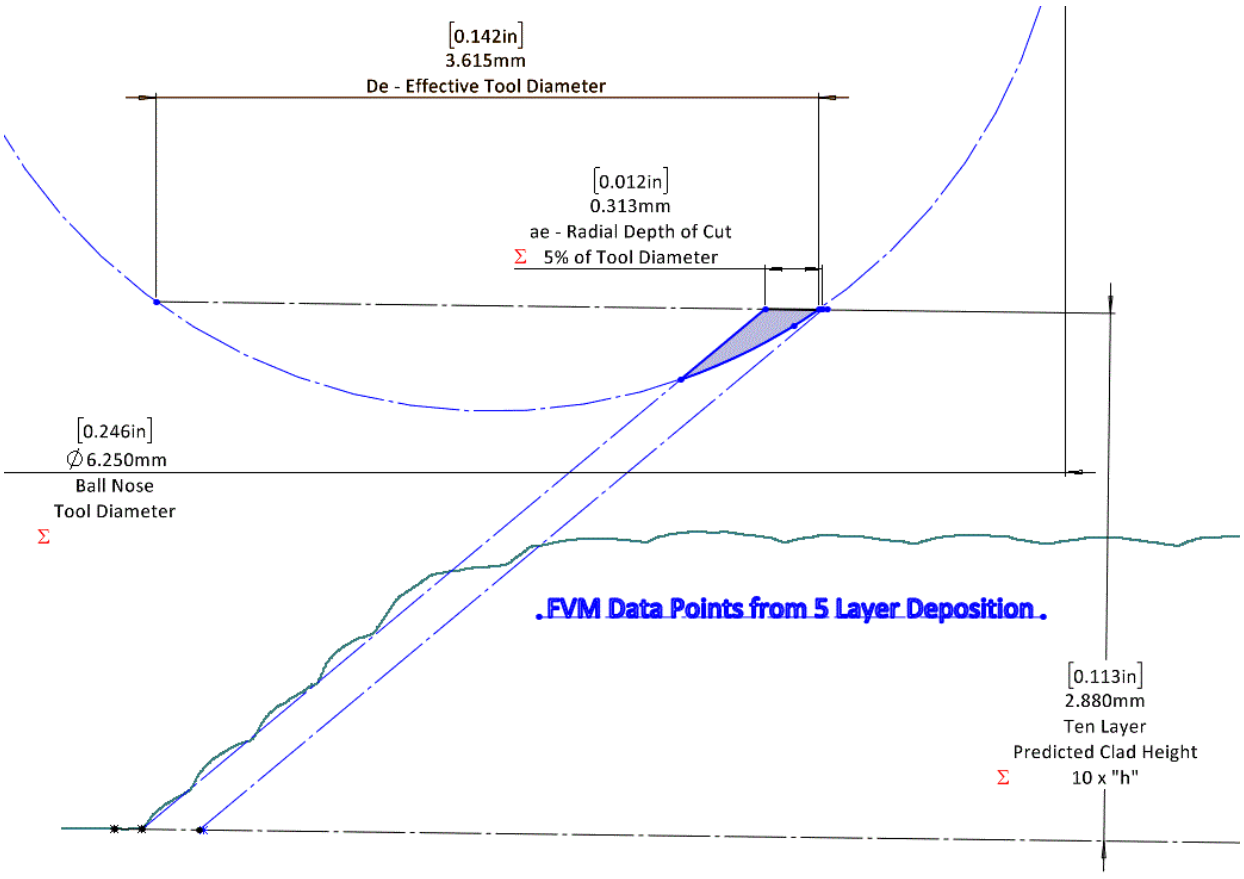

Figure 3.6: Effective diameter approximation by 3D modeling using CSV data from FVM imported to Solidworks

The tool path offset for each parameter set as approximated using the 3D modeling approach was adjusted for each AM parameter set such that the radial depth of cut and the effective diameter would be constant across the AM parameter sets.

For each of the parameter sets, using the approximated effective tool diameter from the 3D modeling approach and the recommended cutting speeds from the tool manufacturer, the spindle speed was calculated using Eq. 3.1:

Equation 3.1: Industry standard spindle speed equation as a function of cutting speed and effective diameter

$$n = \frac{V_c \times 1000}{\pi \times D_e}$$

Feed per tooth can also be calculated with an industry standard equation. That equation involves the chip thinning factor, which in the case of the objects in this set of experiments is very close to one, which makes it negligible, and as such the feed per tooth values recommended are just those as recommended by the manufacturer.

The manufacturers recommendation for cutting speed, to start calculations, for this application was 150 m/min; the calculated spindle speed using that cutting speed far exceeded the spindle capabilities of the AHM. To adjust for this limitation the highest acceptable spindle speed was used to reverse engineer the calculations to obtain a set of parameters that could be screened for the best-case surface finish. The highest allowable spindle speed of the AHM being 5900 rpm, indicates a cutting speed of 100 m/min. To establish a screening experiment for these parameters a middle and low level of the cutting speed were chosen at 50 and 25 m/min, which would create a set of spindle speed values of 5714, 2863, and 1428 rpm. These spindle speeds were paired with recommended feed per tooth values for finishing and semi-finishing with the chosen tool geometry, which are 0.0007 and 0.0013 inches. Along with these values, the type of

cutting was also screened: conventional and climb cutting were used as the third input of the screening experiment. The screening inputs and levels as described above are shown in Table 3.4. The results of the screening is discussed in the results section.

Table 3.4: MP Parameter Screening Inputs and Levels

Input	Levels
Spindle Speed – n (rpm)	1428, 2863, 5715
Feed per Tooth – f_z (mm)	0.018 – 0.033
Method	Conventional – Climb

The target of surface roughness used to compare the results of the MP parameter screening, and to compare the results of the final full hybrid cycle experiments, was calculated using an equation published in several sources in literature, as was shown in equation five, where R_a is surface roughness in µm, and f is the cutting speed in mm per revolution, and r is the cutting-edge radius of the tool.

The cutting speed for use in equation six, as calculated from the V_c of 100 m/min selected in the machining processing screening, in mm per revolution, was 0.0003 mm per revolution, and the quarter-inch ball-nose tool-edge radius as measured using FVM was between 10 and 20 µm, we expected the surface roughness values to be close to 0.65µm. This is discussed in more detail in the results section on surface roughness.

Figures 3.7 and 3.8 are examples of the attempts at tool edge radius measurement using FVM and FVM software.

3.4.1.3 Substrate Distortion Parameters

One step, arguably the first step, in a good process plan for hybrid manufacturing should be to ensure that the substrate will remain geometrically stable during the deposition process.

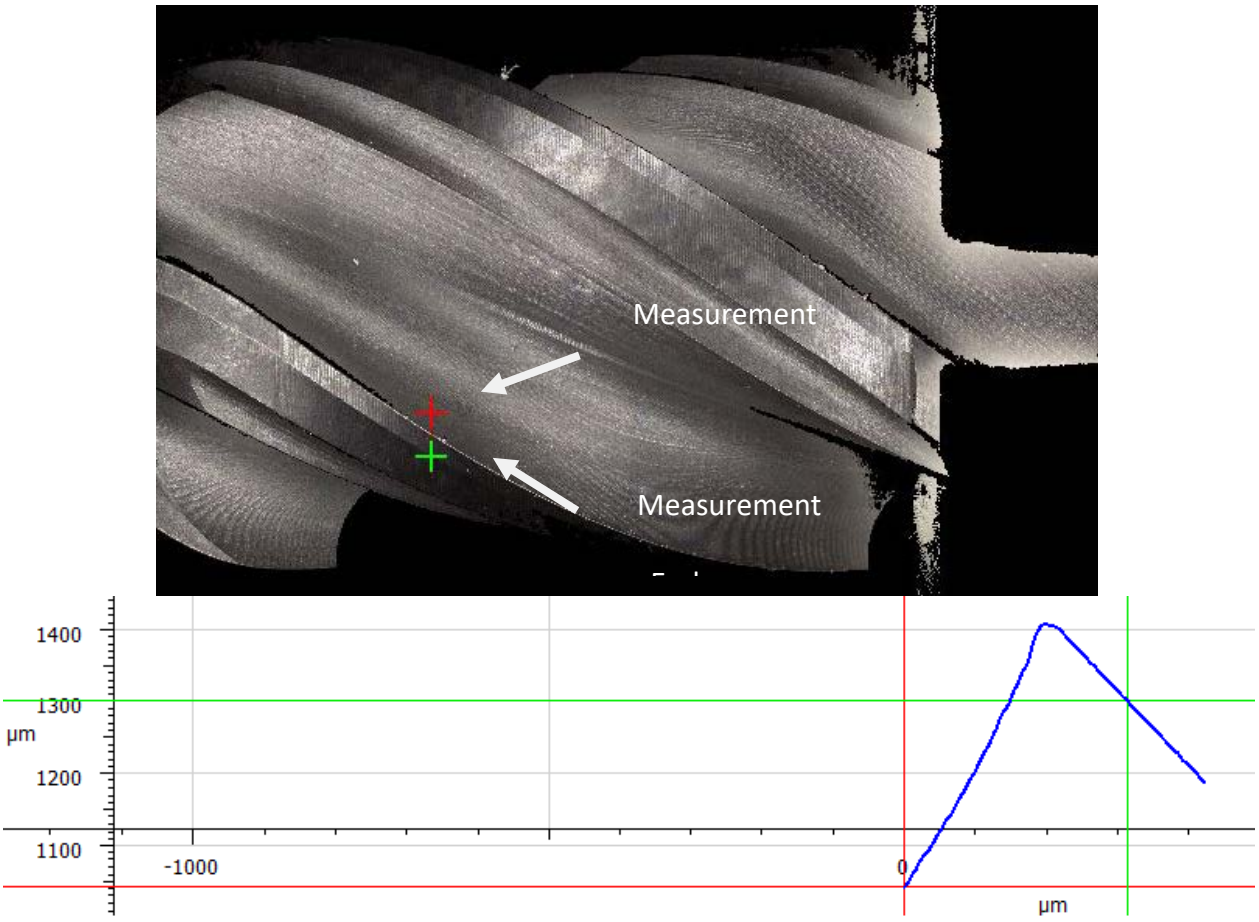

Figure 3.7: FVM scan of ball-nose end-mill tool-edge radius with data point measurements shown in blue

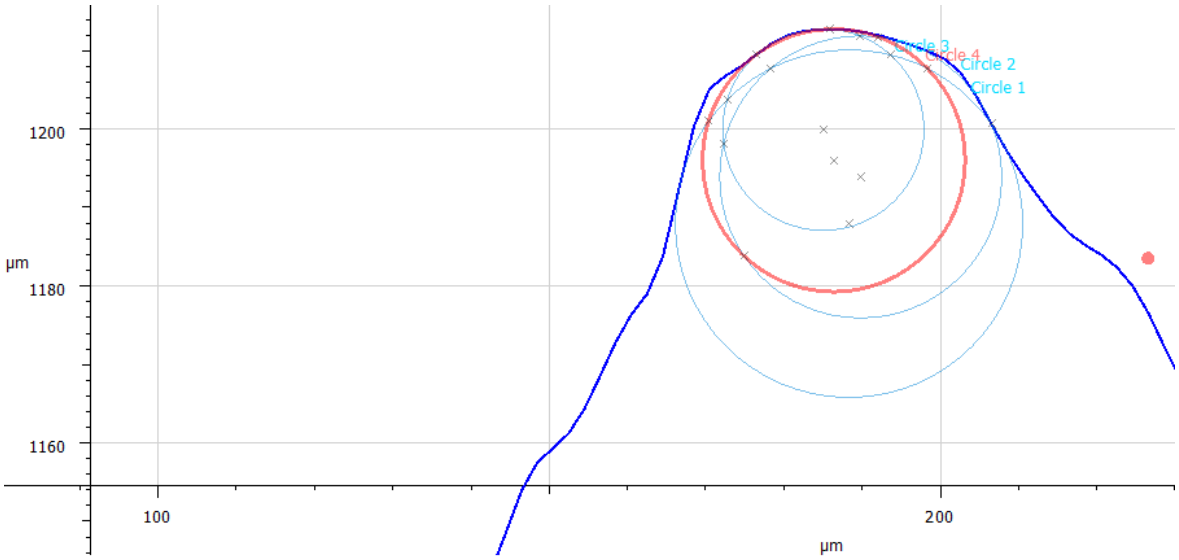

Figure 3.8: Measurement of cutting-edge radius attempt in FVM software. Radius value output from drawn circles not shown. Profile shown is from data collected in scan shown in Fig. 3.7.

As in many heating processes, DED processing can cause substrates to distort during the deposition process. This is undesirable as the spot size and focal length of a DED processing laser is generally fixed, and if the substrate surface and focal point of the laser are not well aligned, or become misaligned during the process, the quality of the deposition negatively affected.

Any specific material to be used in a DED process will require various levels of laser energy for good results. As such any planned process should include an initial assessment of the minimum substrate thickness required for that material to avoid excessive Distortion of the substrate during deposition.

In this set of experiments three different thicknesses of substrate, with the same surface area, were subjected to the same deposition process: those thicknesses were 9.52mm, 17.145mm, 25.4mm, and the surface area was 11582 mm^2 (18 in^2). The depositions for each thickness of plate were the same and used 149.6-watt hours each based on the laser input level, the scanning speed, and the length of cladding tracks combined.

3.4.2 Software

Matlab, FVM software, GOM Inspect, SolidWorks, SolidWorks CAM. Short descriptions of how each software was used. FVM software software was used in the FVM process to view and measure the form and surface roughness of most of the samples created in this project. It was also used to output form measurements as comma separated value data sets for further analysis in Matlab and graphic representation in SolidWorks. BLI software was used in the BLI process to compare the 3D form scans of the substrates before and after the deposition process as described in the substrate warping section above. SolidWorks and SolidWorks CAM were used to create the CAD models and G-codes that were used to prepare the substrates for all the

depositions in this project. SolidWorks was also used to graphically present comma separated value data taken from the FVM software in modeling the depositions and tool geometry as described in the subtractive process parameter section above. Matlab was used to analyze most of the data taken from the FVM software, the results of which are shown in the sections detailing the analyses of data below.

CHAPTER 4

RESULTS

4.1 Vertical Substrate Distortion

The substrates, having been scanned using BLI before deposition, were scanned using BLI again afterwards. The scans were then processed using the BLI software. Figures 4.1 and 4.2 show the thinnest and the thickest of the substrates (the blue surfaces in the figures), along with the overlain scans of the post-deposition distorted substrate (the color mapped surfaces), as they were compared in the BLI software.

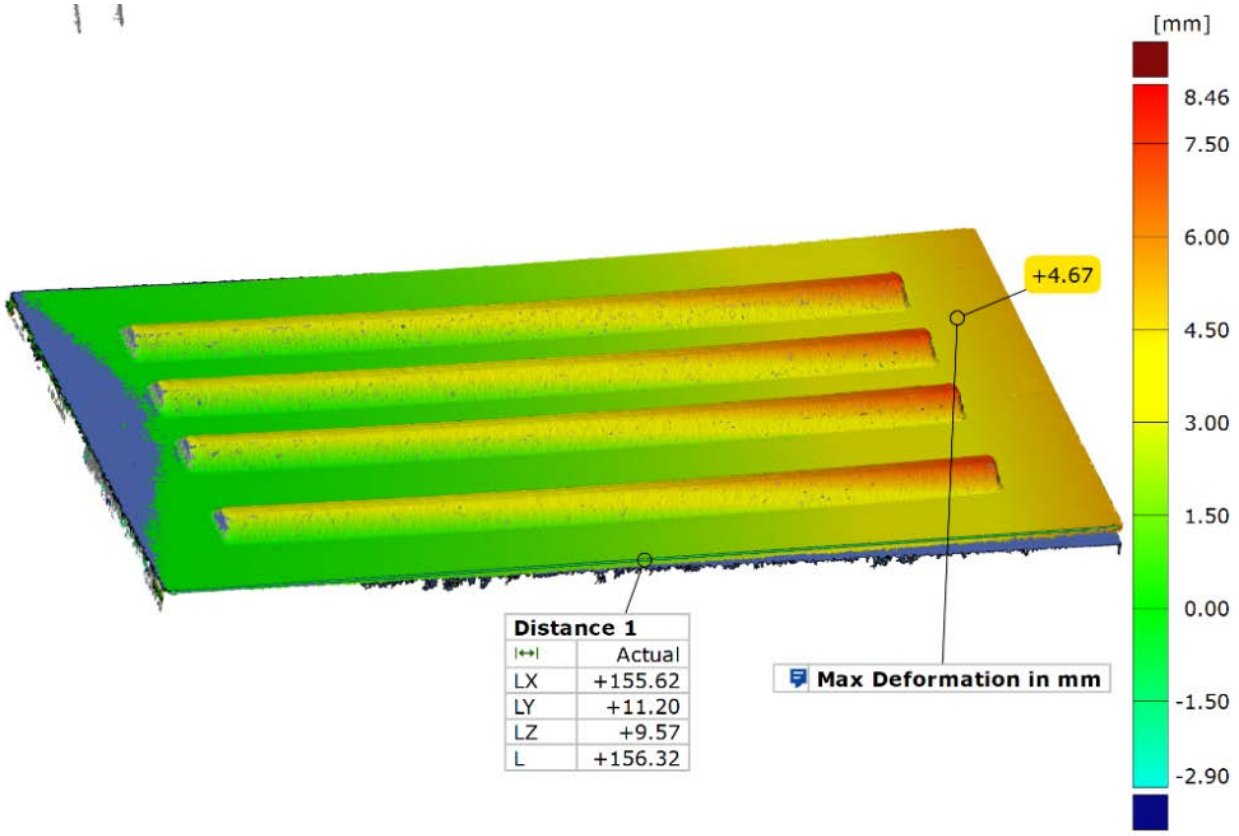

Figure 4.1: 9.5mm thick, 150mm long, 75mm-wide vertical substrate distortion after deposition, with the original form of the substrate underneath, in blue. The BLI software outputs this term as "Deformation," the two should be considered interchangeable in this image

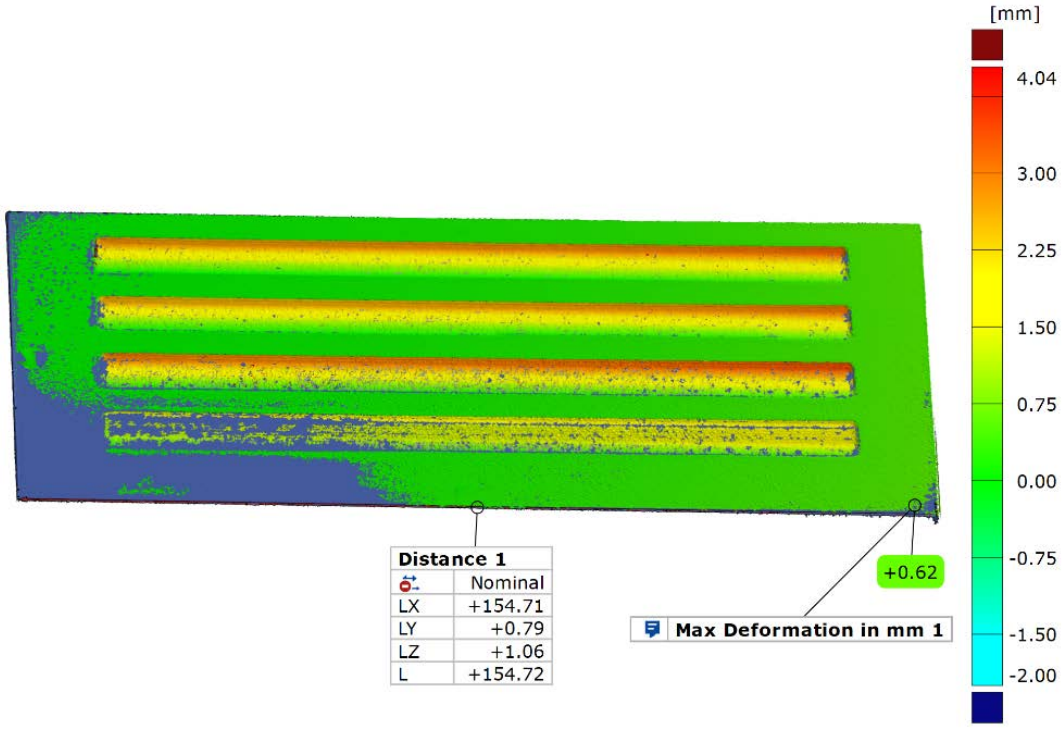

Figure 4.2: 25.4mm thick, 150mm long, 75mm-wide vertical substrate distortion after deposition, with the original form of the substrate underneath, in blue.

The data collected from the BLI scans of the substrates before and after deposition show clearly that thicker substrates experience significantly less Distortion during the deposition process. As is shown in Figure 4.3, the relationship is not linear, which may indicate that the behavior is asymptotic and will never be eliminated entirely by simply increasing the substrate thickness. However, future studies on the combined rigidity of thick substrates and thick fixture plates may achieve a Distortion free deposition process. As in Figure 4.3, the distortion in the 9.5mm plate was highest, at an average of 4.28mm across the two iterations of the experiment at that thickness. At the other extreme of the data set can be seen the relatively small Distortion of 0.62mm that was measured on the 25.4mm thick substrate. From the data collected we can show a correlation between the substrate thickness and the thermal Distortion when energy input is held constant.

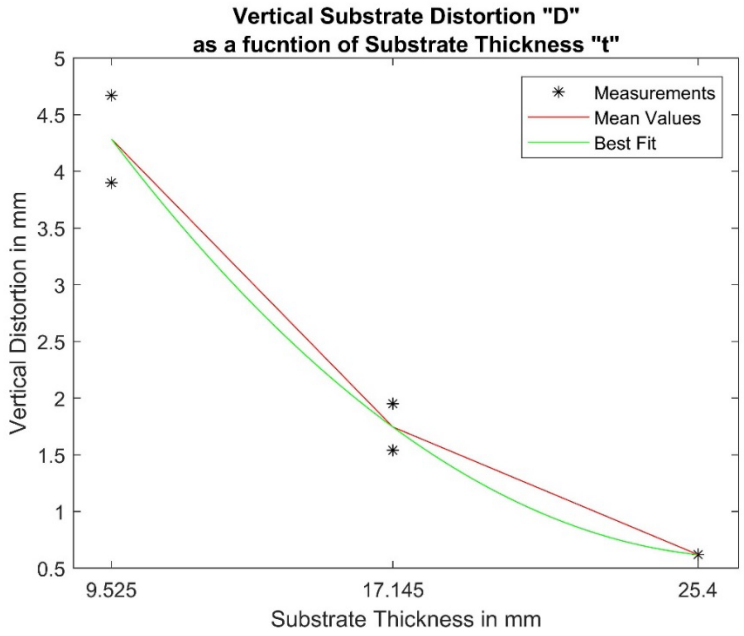

Figure 4.3: Plot of maximum substrate distortion as a function of substrate thickness in mm

4.2 Single Track Deposition

Figure 4.4 shows a FVM scan of a single-track deposition that was measured for track width and height using the FVM software.

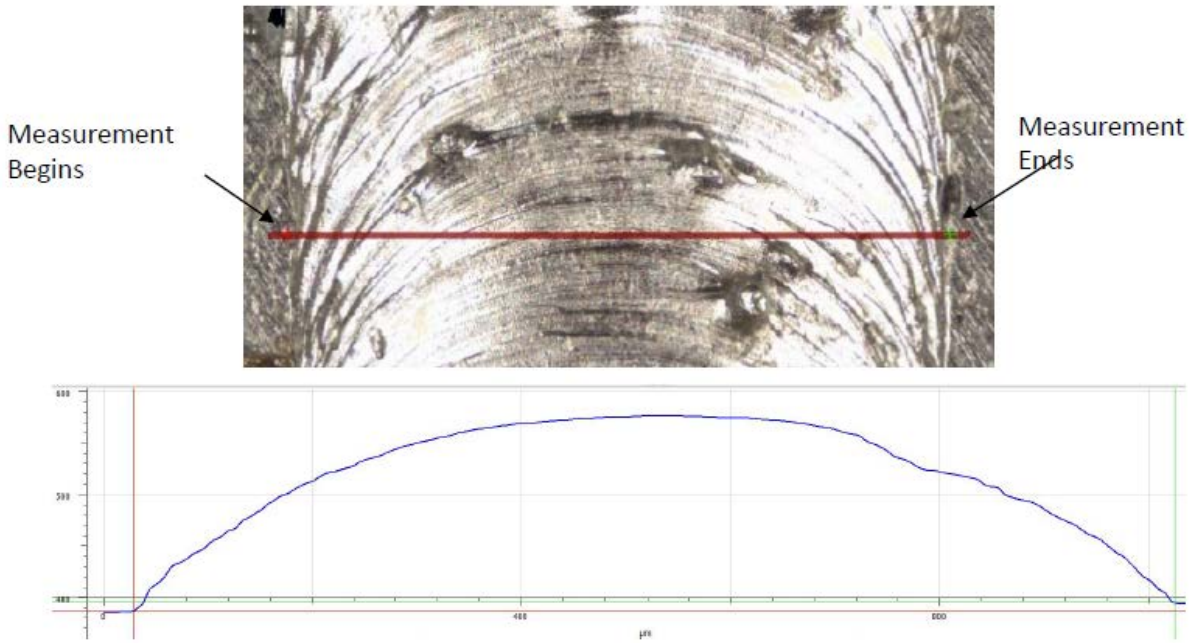

Figure 4.4: FVM scan of single-track deposition with data points displayed in µm scale

The data collected from scans such as those shown in Figure 4.4 were collected and imported to Matlab; the analyses in Table 4.1 show the results of that Matlab analysis of variance.

Table 4.1: ANOVA for Single-Track Width with F, P, S inputs and interactions

Source	Sum Sq.	d.f.	Mean Sq.	F	p
Powder Flow	0.010436	2	0.005218	8.477363	0.017858
Laser Power	0.292581	1	0.292581	475.3207	6.08E-07
Scan Speed	0.016366	1	0.016366	26.58839	0.002102
Powder Flow * Laser Power	0.000693	2	0.000346	0.562672	0.597085
Powder Flow *Scan Speed	0.000105	2	5.23E-05	0.084964	0.9193
Laser Power * Scan Speed	2.11E-05	1	2.11E-05	0.034344	0.859084
Error	0.003693	6	0.000616		
Total	0.351287	15			

In examining the ANOVA table above it should be noted that the ‘p’ values for the interactions are all well above the standard value of 0.05 to be considered statistically significant. As such they were ignored, and the ANOVA was performed again.

Table 4.2: ANOVA for Single-Track Width without F, P, and S Interactions

Source	Sum Sq.	d.f.	Mean Sq.	F	p
Powder Flow	0.010436	2	0.0052182	12.72249	0.001376
Laser Power	0.31861	1	0.31860964	776.8027	1.48E-11
Scan Speed	0.017729	1	0.01772932	43.22589	4.00E-05
Error	0.004512	11	0.00041016		
Total	0.351287	15			

In the analysis of variance shown in Table 4.2, it should be noted that the ‘p’ values are very good and indicate that the variance in the output can be accounted for by the inputs. From this analysis a model can be created to correlate the inputs of laser power, powder flow rate, and scanning speed with the single-track clad width, as is shown below; that model is discussed in the

results section. A main effects plot for the single-track width shows that the main effect for the width is laser power (Fig. 4.5).

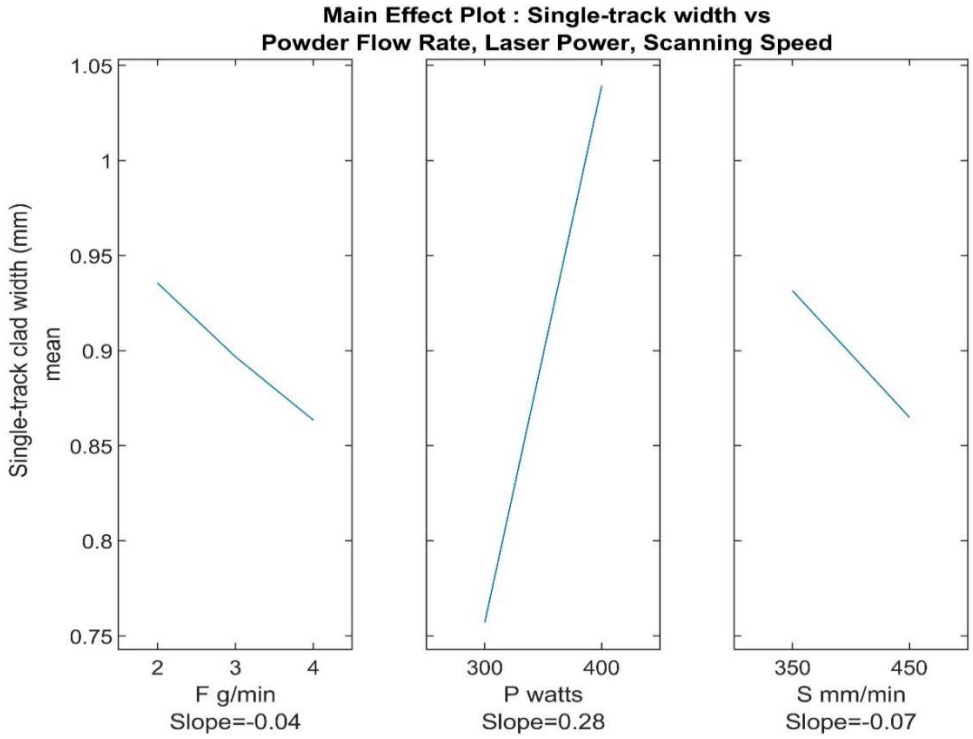

Figure 4.5: Main effect plot of single-track width for powder flow rate, laser power, and scanning speed

An analysis of variance can be created in a similar manner for the single-track height as well, and is shown in Table 4.3. As it was found in the single-track width analysis that the interactions may not be statistically significant, the analysis has been recalculated without the interactions of the inputs and shown in Table 4.4.

Table 4.3: ANOVA for Single-Track Height with F, P, S inputs and interactions

Source	Sum Sq.	d.f.	Mean Sq.	F	p
Powder Flow	0.013	1	0.0130002	41.48204	0.023269
Laser Power	1.15251	2	0.5762551	1838.758	0.000544
Scan Speed	0.006211	1	0.0062110	19.81858	0.046934
Powder Flow * Laser Power	0.002343	2	0.0011716	3.738447	0.21104
Powder Flow *Scan Speed	0.002071	1	0.0020706	6.607855	0.123841
Laser Power * Scan Speed	0.001416	2	0.0007082	2.259774	0.30677

Source	Sum Sq.	d.f.	Mean Sq.	F	p
Error	0.000627	2	0.0003133		
Total	1.178179	11			

Table 4.4 – ANOVA for Single-Track Height without F, P, and S Interactions

Source	Sum Sq.	d.f.	Mean Sq.	F	p
Powder Flow	0.013	1	0.01300021	14.0929	0.00713
Laser Power	1.15251	2	0.57625518	624.6905	1.29E-08
Scan Speed	0.006211	1	0.00621102	6.733063	0.035694
Error	0.006457	7	0.00092247		
Total	1.178179	11			

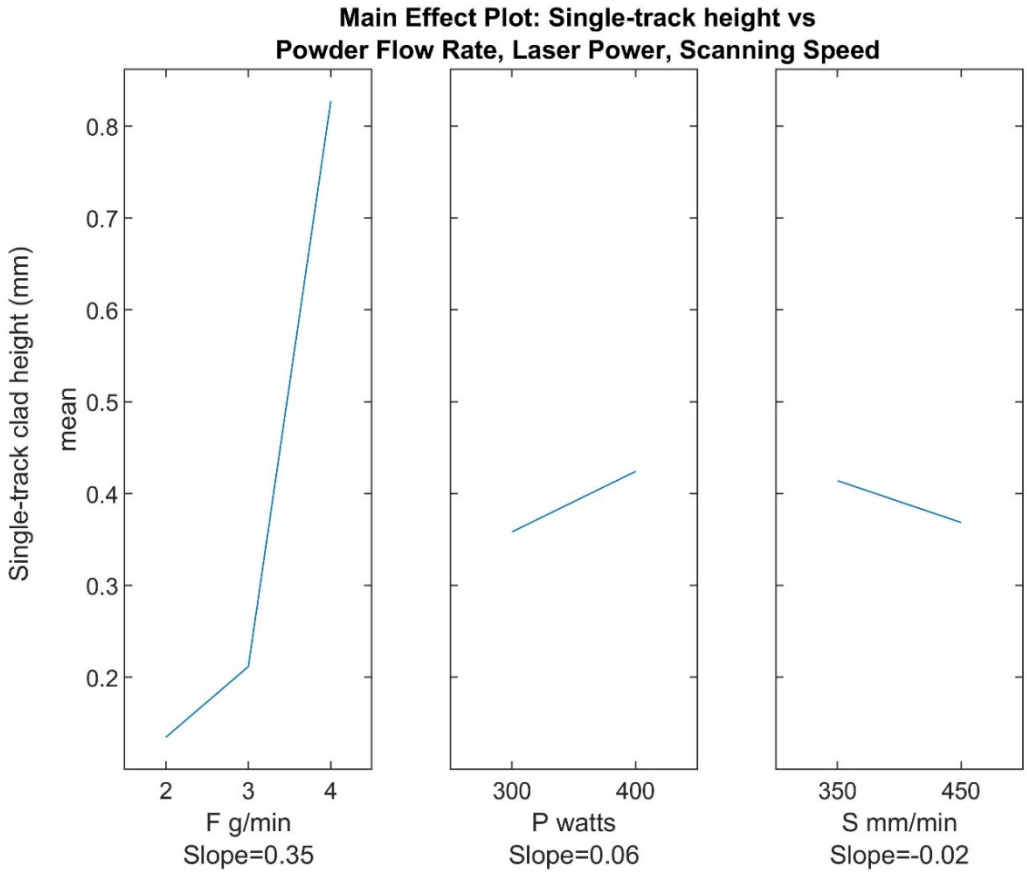

Figure 4.6: Main effect plot of single-track width for powder flow rate, laser power, and scanning speed

A main effect plot for the single-track height shows similar behavior when compared to the single-track width, except in the case of powder flow rate which shows a positive influence

in the height (Fig. 4.6). Further analysis of these results and the correlation taken from them are discussed below in the results section.

It is worth noting that for the single-track width, the width output was very sensitive to the powder flow rate, especially at the four grams per minute level. This may be related to the effect that promoted the exclusion of that particular input level later on in the experiments, and that are detailed later in this document.

4.3 Multi-Track Deposition

The multi-track depositions were scanned using the Alicona. Data from the Alicona scans were then exported in comma separated value format and imported to Matlab for further analysis. The Alicona scan shown in Figure 4.7 shows the actual contour of a multi-track deposition.

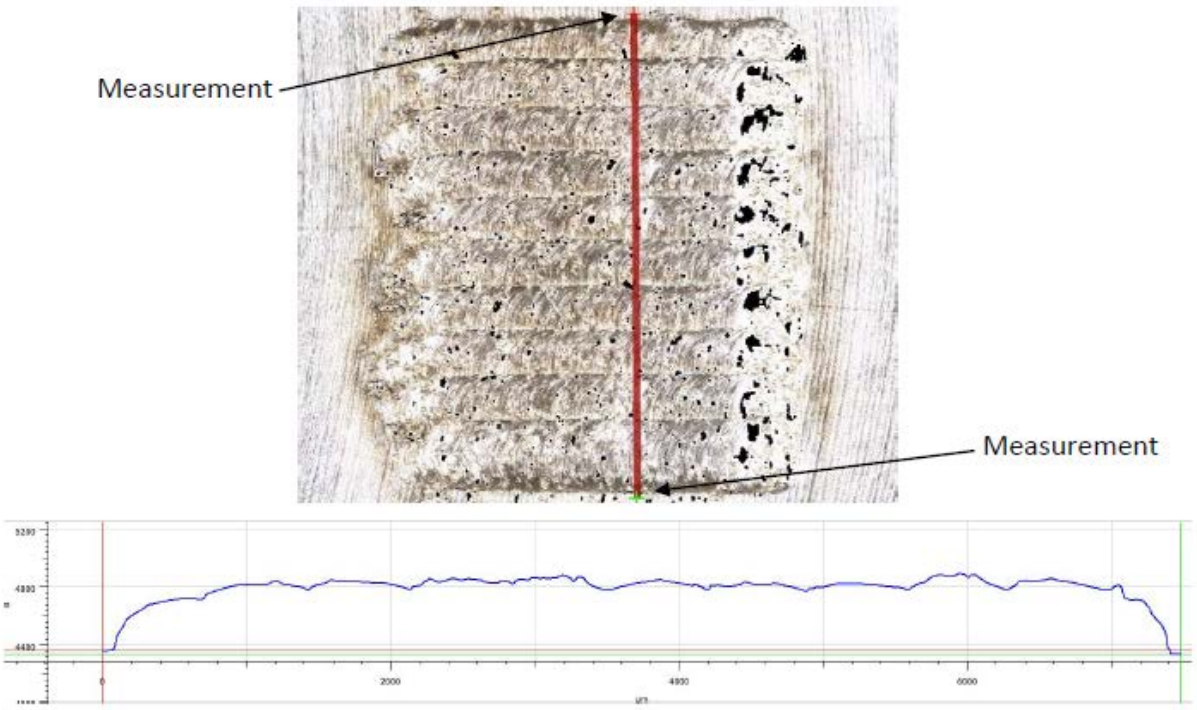

Figure 4.7: FVM scan of multi-track height deposition with data points displayed in µm scale

Each of the three iterations of multi-track depositions were scanned and the data from them imported to Matlab so that the results of each iterations multi-track clad height average could then be averaged. It is worth mentioning that in most of these iterations there was inconsistent data from the first iteration when compared to the second and third iterations, that both agreed well with each other. This observation should inform any designer or operator that intends to plan a process on a DED machine that there is some error in process outputs that are associated with the machine itself, and that identifying those would be integral for the success of any process plan. Figure 4.8 shows the output of a Matlab analysis on one iteration.

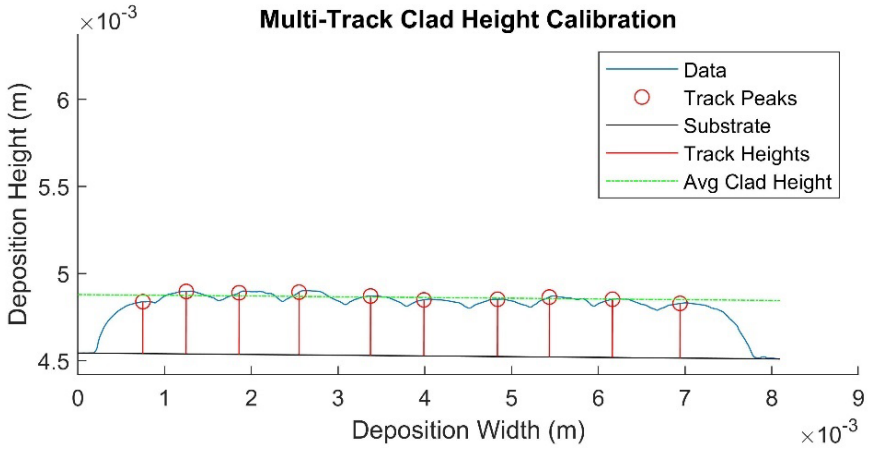

Figure 4.8: Plot of Multi-Track Height data points taken from FVM with individual track peaks and average clad height indicated

The data from the FVM profile measurements of the multi-track depositions was analyzed in another Matlab LiveScript, as was the data from the single-track experiments. In this analysis, the interactions were excluded as they had been found to be less than statistically significant for either the single-track height or width. As was the case in the previous sets of analysis of variance, it is shown in Table 4.5 that the powder flow rate, laser power, and scanning speed were all significant factors in the multi-track height output. As the interactions between the inputs were shown to be less than statistically significant in the previous analyses they are ignored herein.

Table 4.5: ANOVA of Multi-Track Height with F, P, and S inputs

Source	Sum Sq.	d.f.	Mean Sq.	F	p
Powder Flow	0.042927	1	0.04292743	105.6914	0.000505
Laser Power	0.011997	1	0.01199701	29.53775	0.005562
Scan Speed	0.01137	1	0.01137032	27.99479	0.006124
Error	0.001625	4	0.00040616		
Total	0.067919	7			

The correlation that can be taken from this analysis is discussed in the results and discussion section below. As was shown for the single-track width and height, a main effect plot of the multi-track height should be examined for comparison with the effect levels in the previous step of the process plan. As shown in Figure 4.9, the powder flow rate seems to dominate the output. In keeping with the trend shown in the single-track main effect plots, increasing laser power does increase clad height, and increased scanning speed does also reduce the output of clad height.

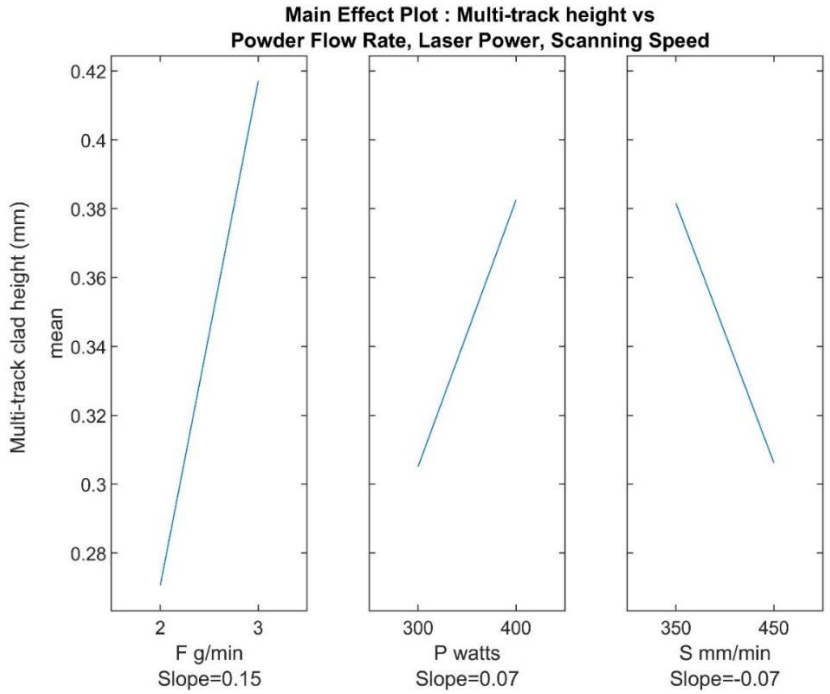

Figure 4.9: Main effect plot of multi-track height for powder flow rate, laser power, and scanning speed

4.4 Multi-Layer Deposition

The multi-layer objects were scanned and analyzed in the same methods as the previous objects were. Figure 4.10 shows the result of the FVM scan and the data that it yields.

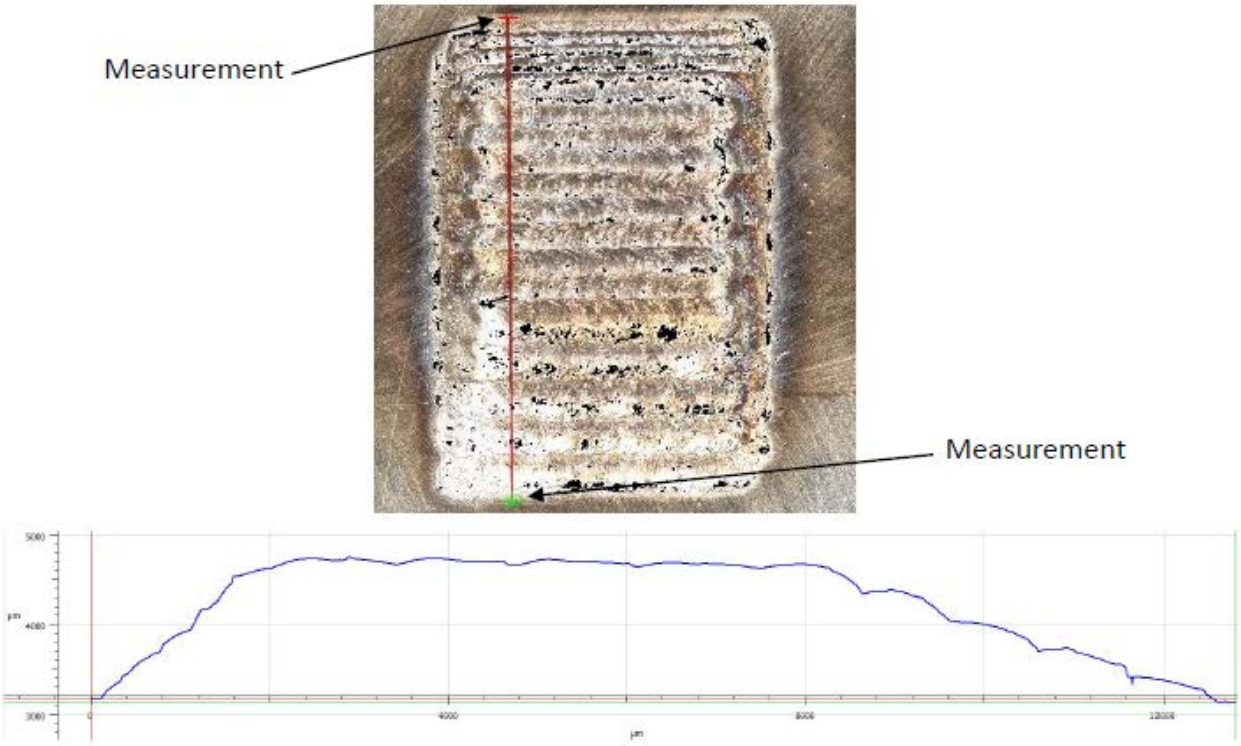

Figure 4.10: FVM scan of multi-Layer deposition with data points displayed in µm scale

The data from this scan was output from the FVM software as a comma separated value data set and imported to Matlab for analysis. Where this data differs from the data in the single layer iterations is that the clad heights at five layers are measured, then that value is divided by five to yield the single-track height average between the five layers. This process is recommended by Ambit as the least complex way to establish the proper step-up value with which to program a tool path for deposition for a particular set of inputs.

That data yielded an analysis of variance from which a correlation between the AM inputs of L, P, and S and the output of multi-layer clad height can be made. Table 4.6 shows the analysis of variance.

Table 4.6: ANOVA of Multi-Layer Average Measured Height with F, P, and S inputs

Source	Sum Sq.	d.f.	Mean Sq.	F	p
Powder Flow	0.083273	1	0.083273	54.17848	0.001815
Laser Power	0.003681	1	0.003681	2.394794	0.196651
Scan Speed	0.013448	1	0.013448	8.749462	0.041639
Error	0.006148	4	0.001537		
Total	0.10655	7			

This ANOVA result shows a clear departure from the results of the previous steps in the process plan. In this step, the “p” value for laser power indicates that it is not statistically significant in the multi-layer measured heights. The ANOVA was run again without the laser power to determine more accurate levels for the statistical significance of the other inputs, as is shown in Table 4.7.

Table 4.7: ANOVA of Multi-Layer average measured height with F and S inputs

Source	Sum Sq.	d.f.	Mean Sq.	F	p
Powder Flow	0.083273	1	0.0832728	42.3614	0.001279
Scan Speed	0.013448	1	0.013448	6.841082	0.047352
Error	0.009829	5	0.0019657		
Total	0.10655	7			

In the ANOVA above the powder flow and scan speed are both shown to be statistically significant even in the absence of the laser power as an input. In analyzing the data at this point in the process, it was clear that certain combinations of input parameters had higher levels of error in when comparing the expected clad heights to the measured clad heights. In an industry

setting, if a particular set of inputs was required for some quality expectation, those errors could be resolved through successive iteration of the previous steps in the process plan. A main effect plot of the three inputs for this multi-layer clad height output indicates, as did the ANOVA results, that the powder flow rate is dominant for this output, and that the laser power had little effect. See Figure 4.11. As compared with the other main effect plots for the previous steps in the process, increased scanning speed also reduces the clad height output. This main effect plot may look identical to that of the multi-track main effect, the only difference is that the maximum value on the y-axis is slightly higher.

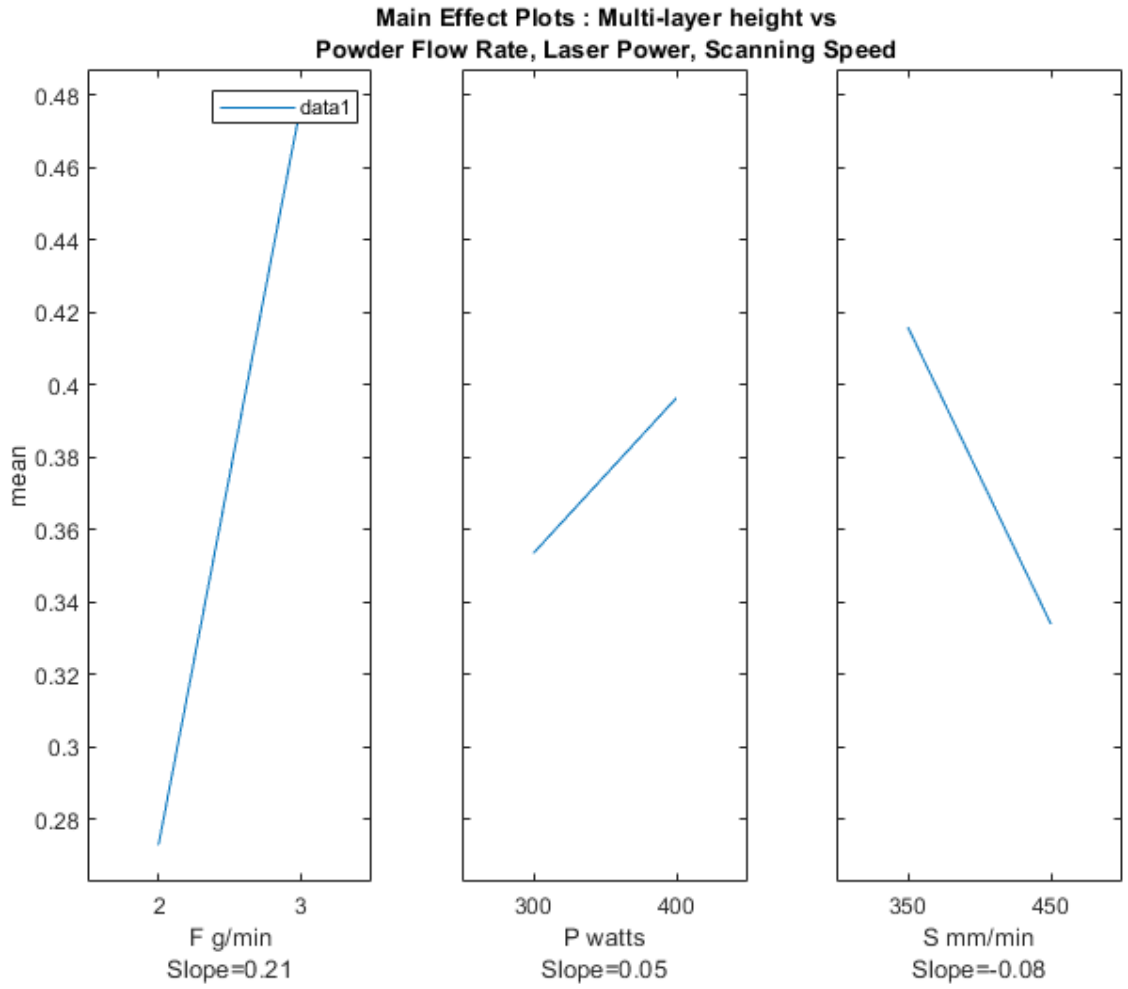

Figure 4.11: Main effect plot of multi-layer clad height for powder flow rate, laser power, and scanning speed

For the exploration of the later portions of the process plan imposed upon the work in this thesis, the four input sets with the highest error were eliminated from the experimentation, the data for that step-in elimination is shown in Table 4.8. One point that should be noticed in the table is that all the parameter sets using 300 watts have been excluded for excessive error in clad height, as such they do not appear in any subsequent analysis sections.

Table 4.8: Exclusion of 300-Watt parameter sets based on percent error of multi-layer measured height compared to expected height

Powder Flow Rate	Laser Power	Scan Speed	Percent Error	Status
2	300	350	12.97	Excluded
2	300	450	13.85	Excluded
2	400	350	9.93	Kept
2	400	450	5.23	Kept
3	300	350	23.22	Excluded
3	300	450	23.21	Excluded
3	400	350	10.37	Kept
3	400	450	4.76	Kept

4.5 Machining Processing

4.5.1 Hardness Testing

The depositions created during the multi-layer experiments, and those created using the full AM and MP Hybrid processing, were tested for harness using a standard indentation tester. Prior to creating and testing the full hybrid specimen the multi-layer uncalibrated specimen was tested for hardness to ensure that the material conditions were close to those as expected in reviewing the recommendations for subtractive parameter selection.

While there does not appear to be any trend in the data that could suggest a correlation between the inputs and the measured hardness of each sample, the hardness values collected

from the multi-layer experiments were higher than would be expected from as purchased stainless steel 316L. And the hardness values measured from the full hybrid experiments were slightly higher those measured from the multi-layer experiments. This could indicate that some part of the MP process has granted the depositions and the machined surfaces a higher level of hardness, which would be beneficial in a die and mold making process. More testing would be required to confirm this finding formally.

Table 4.9: Hardness measures from multi-layer depositions

Powder Flow Rate (g/min)	Laser Power (watts)	Scan Speed (mm/min)	Calibration State	Hardness HRC
2	400	350	Uncalibrated	30
3	400	450	Uncalibrated	29.5
3	400	350	Uncalibrated	29
3	400	450	Uncalibrated	30.5

Table 4.10: Hardness measures from full hybrid specimen

Powder Flow Rate (g/min)	Laser Power (watts)	Scan Speed (mm/min)	Calibration State	Hardness HRC
2	400	350	Uncalibrated	30
2	400	350	Calibrated	33.5
2	400	450	Calibrated	31
3	400	350	Uncalibrated	31.5
3	400	350	Calibrated	33.5
3	400	450	Uncalibrated	31
3	400	450	Calibrated	34.5

4.5.2 Tool Deterioration

The tools used in the subtractive testing portion of this thesis were scanned and their flank landing width were measured before and after use. The difference in a tools flank landing

length can be used to ascribe a degree of tool wear; an example of this measurement, post machining processing, is shown in Figure 4.12.

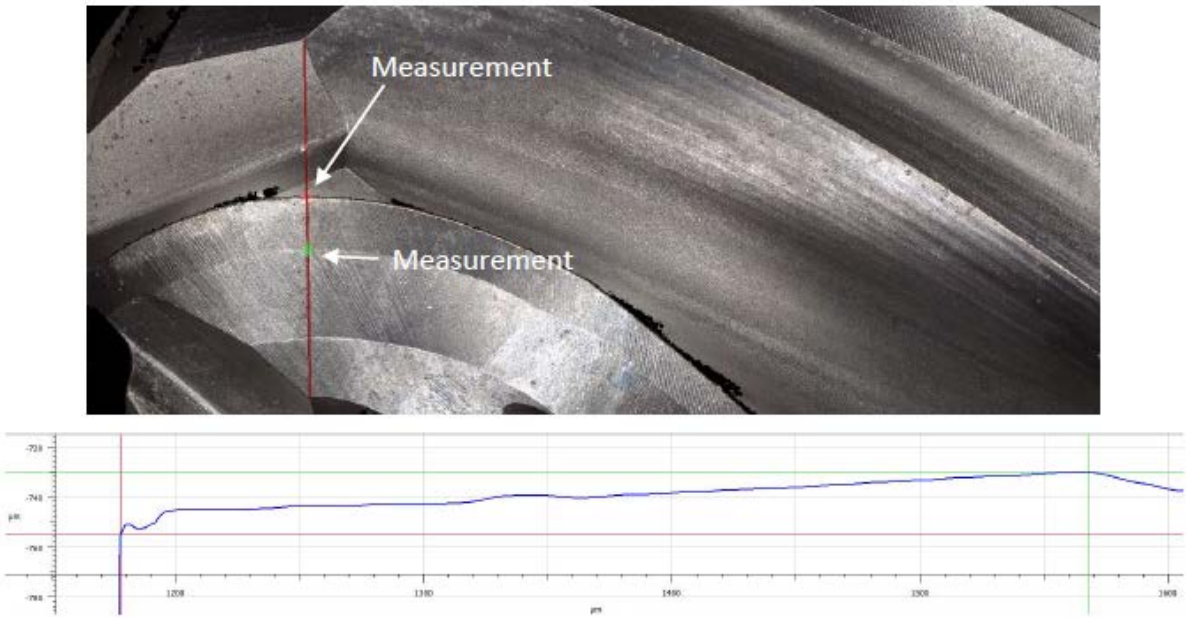

Figure 4.12: FVM scan of Ball Nose Flank Landing Wear with data points displayed in µm scale

As shown in the figure, the distance between the leading and trailing edge of the flank was measured for each of the tools. If that distance increased after use, that would indicate that some material had been lost and now there is a shorter, wider flank. A decrease in that distance might indicate that there was some built-up material that could be seen as a raised or widened flank. The data from these measurements was analyzed for trends or correlations, but as is shown in Table 4.11, there may not be any trends that can be inferred from this particular set of experiments.

Table 4.11: ANOVA of Tool Wear with F, P, S and interaction inputs

Source	Sum Sq.	d.f.	Mean Sq.	F	p
Powder Flow	67.03243	1	67.03243	0.175465	0.679553
Scan Speed	529.4643	1	529.4643	1.385936	0.252264
Calibration	976.786	1	976.786	2.556854	0.124755

Source	Sum Sq.	d.f.	Mean Sq.	F	p
Powder Flow * Scan Speed	44.3546	1	44.3546	0.116103	0.736685
Powder Flow * Calibration	128.4726	1	128.4726	0.336292	0.568148
Scan Speed * Calibration	47.23126	1	47.23126	0.123633	0.72863
Error	8022.557	21	382.0265		
Total	11607.93	27			

As is shown in Table 4.11, the 'p' values for all the inputs, and for the interactions between them, are all very high. This would normally indicate the lack of statistically significant correlation between any of the inputs and the outputs themselves. In Figure 4.13 the tool wear measurements have been plotted for each of the uncalibrated and calibrated parameter sets to show that while there is no clear correlation between the AM parameters as inputs and the tool wear.

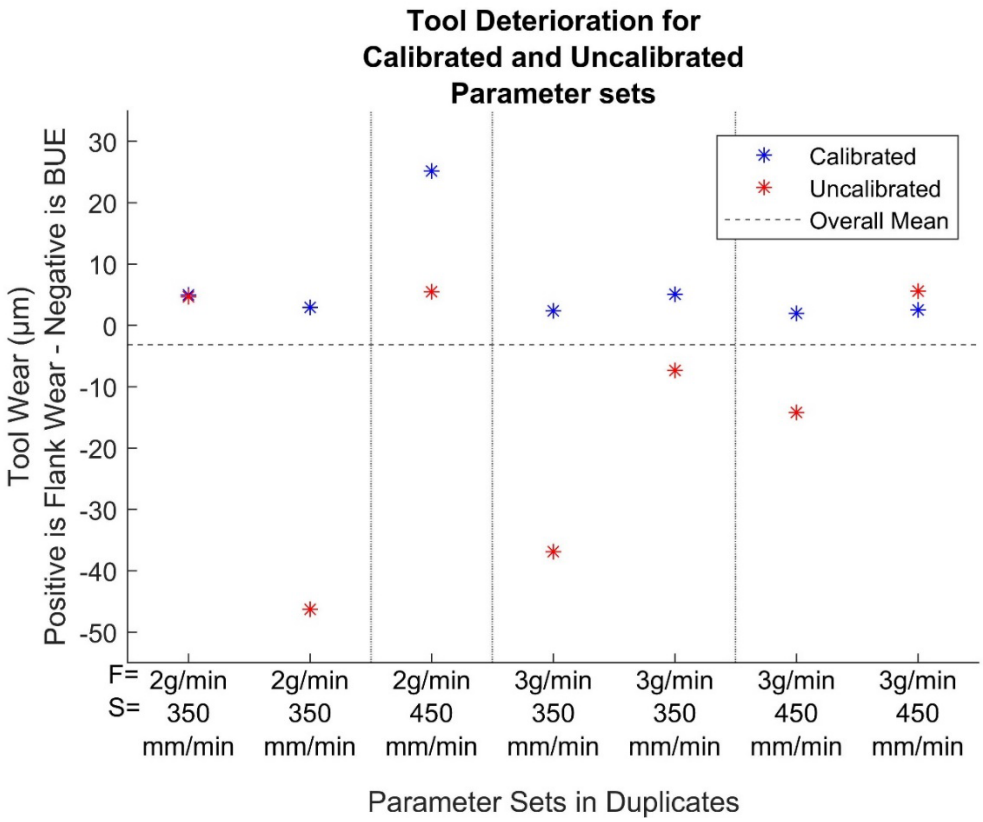

Figure 4.13: Plot of Tool Wear for each parameter set and calibration state

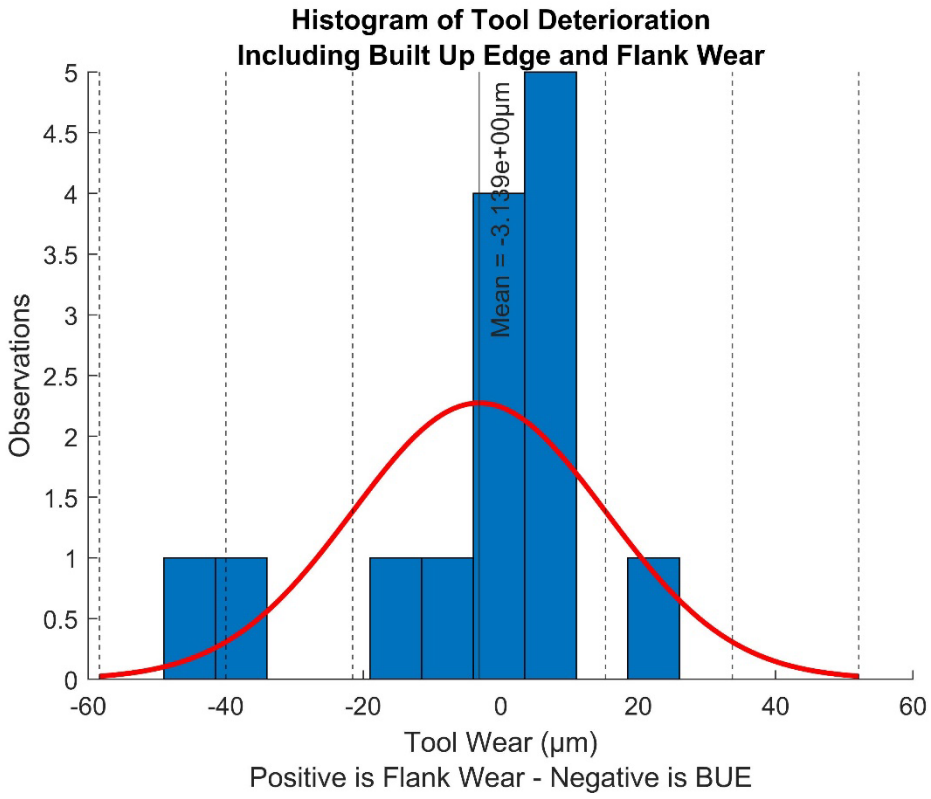

Figure 4.14: Tool Wear Histogram

As is shown in Figures 4.13 and 4.14,the data from the tool wear measurements shows that while the tool wear data shows no particular trend that can be correlated to the inputs and level used in the experiments discussed herein, the data is however normally distributed around a mean value of -3.14µm of flank wear with a standard deviation of 0.184µm.

To illustrate the appearance of BUE and tool wear as it was measured in these experiments, Figures 4.15 and 4.16 can be compared: Figure 4.15 is an FVM scan of an unused ball-nosed endmill, and Figure 4.16 is an FVM scan of a ball-nosed endmill with some BUE. BUE is when material from the workpiece become attached to the surface of the tool. This is generally due to either poor material characteristics or to improper tool engagement. It becomes unpredictable for in terms of surface quality because the built-up material changes the shape of the cutting edge, which was shown to be integral to the theoretical predictions on surface quality

in equation five. The tool life expectancy changes when BUE is present because the extra material and poor cutting conditions increase the effects of retained and generated heat during the process, which can cause rapid and unpredictable behavior if the BUE becomes dislodged during the process.

Figure 4.15: FVM scan of an unused ball-nose end mill with flank landing measurement in µm scale

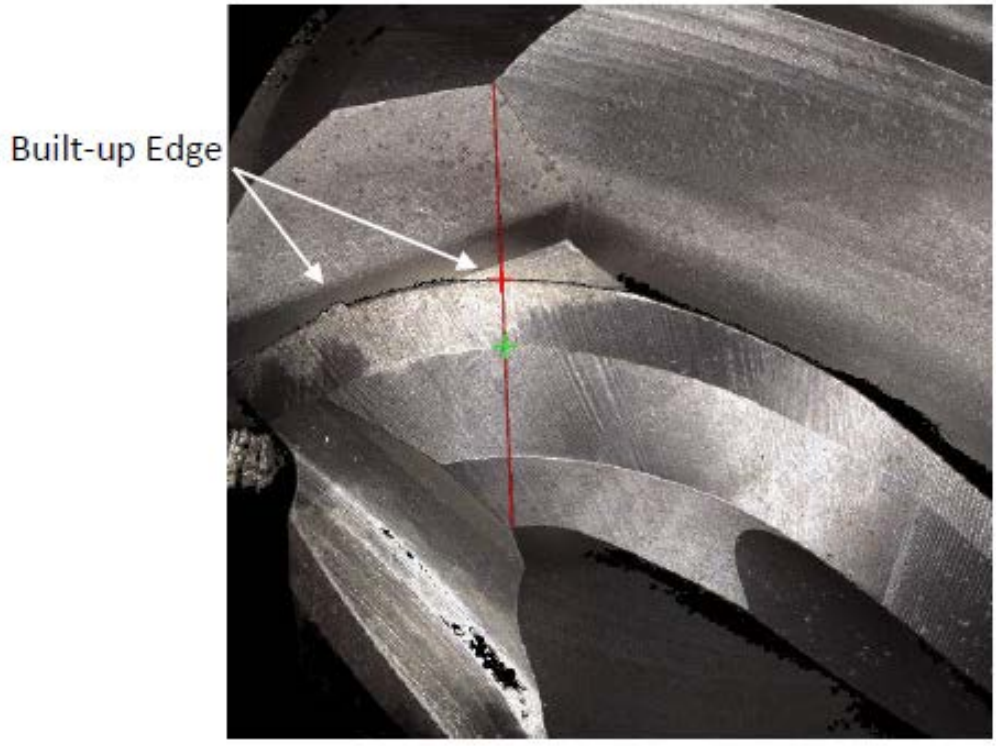

Figure 4.16: FVM scan of used ball-nose endmill with BUE

One interesting point that can be shown from the tool wear data is that the set of observations from the calibrated experiments has a much lower standard deviation, as is shown in Table 4.12. So, while each set, and the combined set, are all normally distributed, the calibrated set displays a much lower range of variation which could indicate that there is some benefit to tool wear to be gained from properly calibrated depositions.

Table 4.12: Tool Wear: Comparison of Calibrated and Uncalibrated Distributions

Source	Mean (μm)	St. Deviation (μm)
Full Set	-3.139	18.413
Uncalibrated	-12.698	21.252
Calibrated	6.419	8.3546

The experiments in this section were duplicated once, except for the 2 gram per minute 450 mm per minute set which was not duplicated as it showed nearly zero error in moving from the multi-track expected height to the multi-layer experiment measurements. All of the data collected from measurements in this part of the study are plotted on Figure 4.13. Further duplication of these experiments could be performed in the future to establish more detailed an descriptive statistics for the data set.

4.5.3 Surface Roughness

Each of the objects having been subjected to the full Hybrid process were scanned and measured for surface roughness using FVM and the FVM software. An example of the scan and the measurement data is shown in Figure 4.17. The measurements used in the following analyses were taken from close to where the tool path would have started; this was an effort to mitigate the errors created by other factors that may have been present.

The data from these scans were collected and imported to Matlab for plotting and an

analysis of variance. As is shown in Figure 4.18, there is no apparent trend in the data as it relates to calibrated parameter sets versus uncalibrated. However, it is clear that the surface roughness measurements were very close to the predicted values based on the material, the subtractive inputs and the tool geometry.

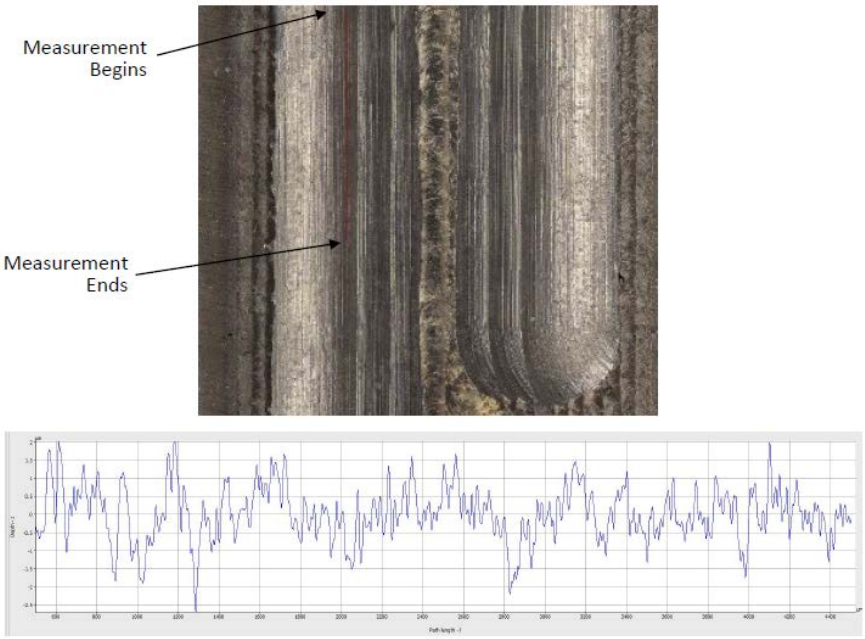

Figure 4.17: FVM scan of post-machined deposition surface roughness

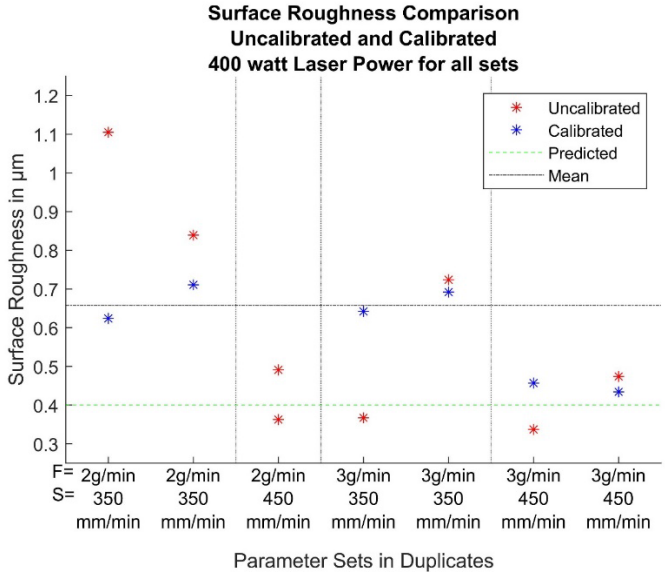

Figure 4.18: Plot of surface roughness measurements taken from FVM scans of post-machined deposition

As is shown in Table 4.13, the ‘p’ values for each of the inputs being very high which indicates that there is little to no statistical significance between these inputs and the output of surface roughness measured on the objects in these experiments. This observation would agree with the analysis of the plot in that there is no clear trend between the AM inputs and the surface roughness measurements. In the surface roughness plot it should be noticed that there is a significant outlier in the data, this could affect the calculation of the mean and move it closer to the predicted value if it were to be excluded.

Table 4.13: ANOVA of post-machined deposition surface roughness measurements with F and S inputs

Source	Sum Sq.	d.f.	Mean Sq.	F	p
Powder Flow	0.040323	1	0.040323	1.315758	0.334543
Scan Speed	0.151044	1	0.151044	4.928699	0.113036
Calibration	0.005336	1	0.005336	0.174122	0.704538
Error	0.091938	3	0.030646		
Total	0.335463	6			

The experiments in this section of the study were duplicated once except for the 2 gram per minute 450 mm per minute set which did not require changes in G-code step-up during calibration. All the data points collected in the experiment are shown on Figure 4.18. Further studies on this topic could expand the available data set such that more detailed and descriptive statistics for the surface roughness behavior could be described.

CHAPTER 5

CONCLUSIONS AND DISCUSSION

5.1 Correlations and Discussion

5.1.1 Substrate Distortion Model

The correlation that can be formed from the data collected in measuring the Distortion of the substrates after deposition is shown in Eq. 5.1, where "D" is the induced Distortion in mm, and "t" is substrate thickness in mm, is:

Equation 5.1: Vertical distortion of substrate by thickness model

$$D = 0.012t^2 - 0.664t + 9.487$$

This model does not lend itself well to deciding on a substrate thickness that would yield no substrate distortion at all, as that would be an extrapolation. More experiments on this topic would be required to make that determination.

This model is also entirely empirical and would not be suitable for application with other materials in its current form; more experimentation based on other materials would be required to establish a generalized model for substrate distortion in this respect: and any model generated in such expanded experimentation would certainly require the inclusion of other characteristics.

Another important point to consider for thicker substrates in this field is that residual stress should be expected, not just in the substrate but also in the deposited material itself whenever the substrate is not allowed to distort during the deposition process. Future studies in this area should include experimentation on residual stress relief through careful heat treatment after the deposition process. Preheating the substrates was considered as a pre-emptive solution to the warping effect. However, the AHM enclosure has several subsystems that may be sensitive

to prolonged exposure to that level of ambient temperature, as such that solution should be avoided in the AHM for the future.

5.1.2 Single Track Width Model

The analysis of the single-track width data yields a model that can correlate the AM inputs to the output of deposition height as is shown in Eq. 5.2.

Equation 5.2: Single-track width as a function of F, P, and S

$$w = 0.391 \times F - 0.033 \times P + 0.033 \times S$$

The r^2 value for this correlation is very high, at 0.9945. Modeling single-track height may not be as directly useful for proceeding in a process plan as the single-track width will prove more useful; however, it can be useful in a recursive study on the effects of hatch overlap on the deviation of track height from a particular mean in track height of a multi-track deposition.

A comparison of the main effect plots (Figs. 4.6 and 4.7) of single track width and height should reveal some interesting analyses: that powder flow rate may have a contrary effect on the two outputs – width and height, although it is a small effect, and that the laser power has a large effect increasing the measured output with increased levels in both cases, and that increasing the scanning speed reduces the measured height and width to a similar degree as is seen in the powder flow rate. So, while it is shown that all three inputs are statistically significant it is clear that laser power dominates the regime. And as was the case for the model of substrate distortion, this model is also entirely empirical and as such would not be suitable for application with other materials.

5.1.3 Multi-Track Height Model

Using the coefficients of correlation from the ANOVA as presented in the results section,

a model correlating the input parameters to the multi-track height output was created and is shown in Eq. 5.3.

Equation 5.3: Multi-track height as a function of F, P, and S

$$h\ (mm) = 0.344 \times F - 0.073 \times P + 0.073 \times S$$

Much like the single-track correlation, this correlation also carries a high level of confidence in predicting the output of multi-track height as a function of the inputs laser power, powder flow rate, and scanning speed, with an r^2 value of 0.9761. Like the other models discussed herein, this model is entirely empirical and would not be suitable for application with other materials.

5.1.4 Multi-Layer Height

As was shown in the ANOVA of the multi-layer experiment data, two of the inputs considered in the rest of the experiments are statistically significant with respect to the multi-layer clad height; from that ANOVA we can show the correlation between those two inputs and the multi-layer height in Eq. 5.4.

Equation 5.4: Multi-layer height as a function of F and S

$$h\ (mm) = 0.375 \times F + 0.102 \times S$$

While this correlation does carry a reasonably high level of confidence, with a an r^2 value of 0.9078, other inputs should certainly be considered when attempting to model this output. This model is also entirely empirical and based on the data collected herein. As such it would not be suitable for application with other materials. Further experimentation would be required to include other materials and material characteristics.

5.1.5 Tool Deterioration

In comparing the data from the set of tools used for the depositions with uncalibrated

step-up values to those used on the depositions with calibrated step-up values it can be shown that tool deterioration is favorable from the sets with calibrated step-up values, as is shown in Figure 5.1. The overall tool deterioration (Fig. 4.15) was in the negative region, indicating that built-up edge was the dominant form of deterioration. BUE is less desirable as it becomes less and less predictable as it increases. It can also deteriorate the work piece surface in the form of redeposition of material. As it changes the tool edge radius unpredictably it is also less likely to produce a good or predictable surface roughness. On the other hand, tool wear, which is shown in Figure 5.1 as the dominant form of deterioration observed from tools used to process depositions with calibrated step-up values, is generally very predictable as the industry has been familiar with it for a very long time. This finding might indicate that another benefit of good process planning in hybrid manufacturing would be a more predicable tool wear.

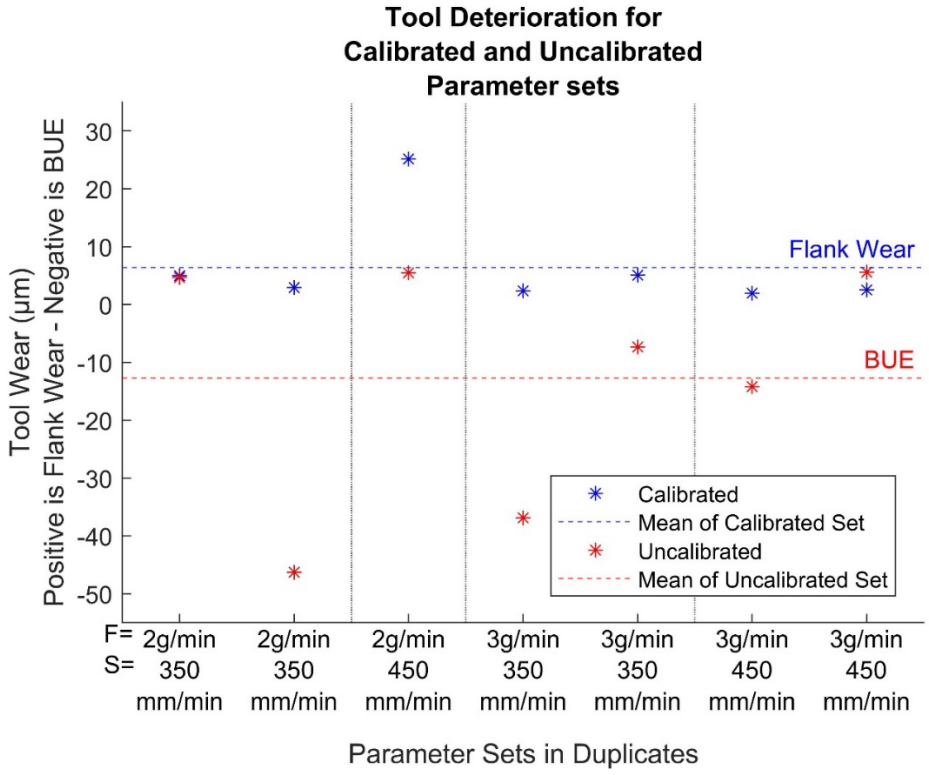

Figure 5.1: Comparison of tool deterioration from depositions with uncalibrated and calibrated step-up values

5.1.6 Surface Roughness

The analysis of surface roughness values can show that in the measurements taken from the depositions with calibrated step-up values, the surface roughness mean was slightly lower than in the depositions with uncalibrated step-up values, as is shown in Figure 5.2.

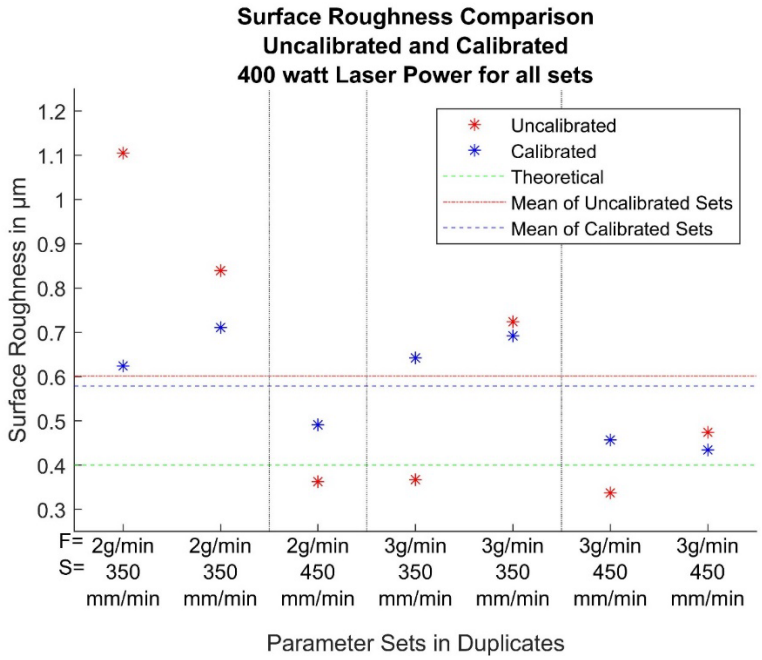

Figure 5.2: Comparison of mean surface roughness between depositions with calibrated and uncalibrated step-up values

5.2 Quality of Deposition

To assess the microstructural quality of the depositions created through the process plan proposed herein, transversal cross sections of the deposited and machined objects were prepared for and scanned using back scattered electron diffraction. As is shown below in Figures 5.3 to 5.6, the microstructure of the deposited materials exhibits an increased grain size when compared to that of the substrate. The grain morphology in the depositions is also different from that of the substrate, in that it is not equiaxed and cellular but is rather columnar like and directional towards the surface of the depositions.

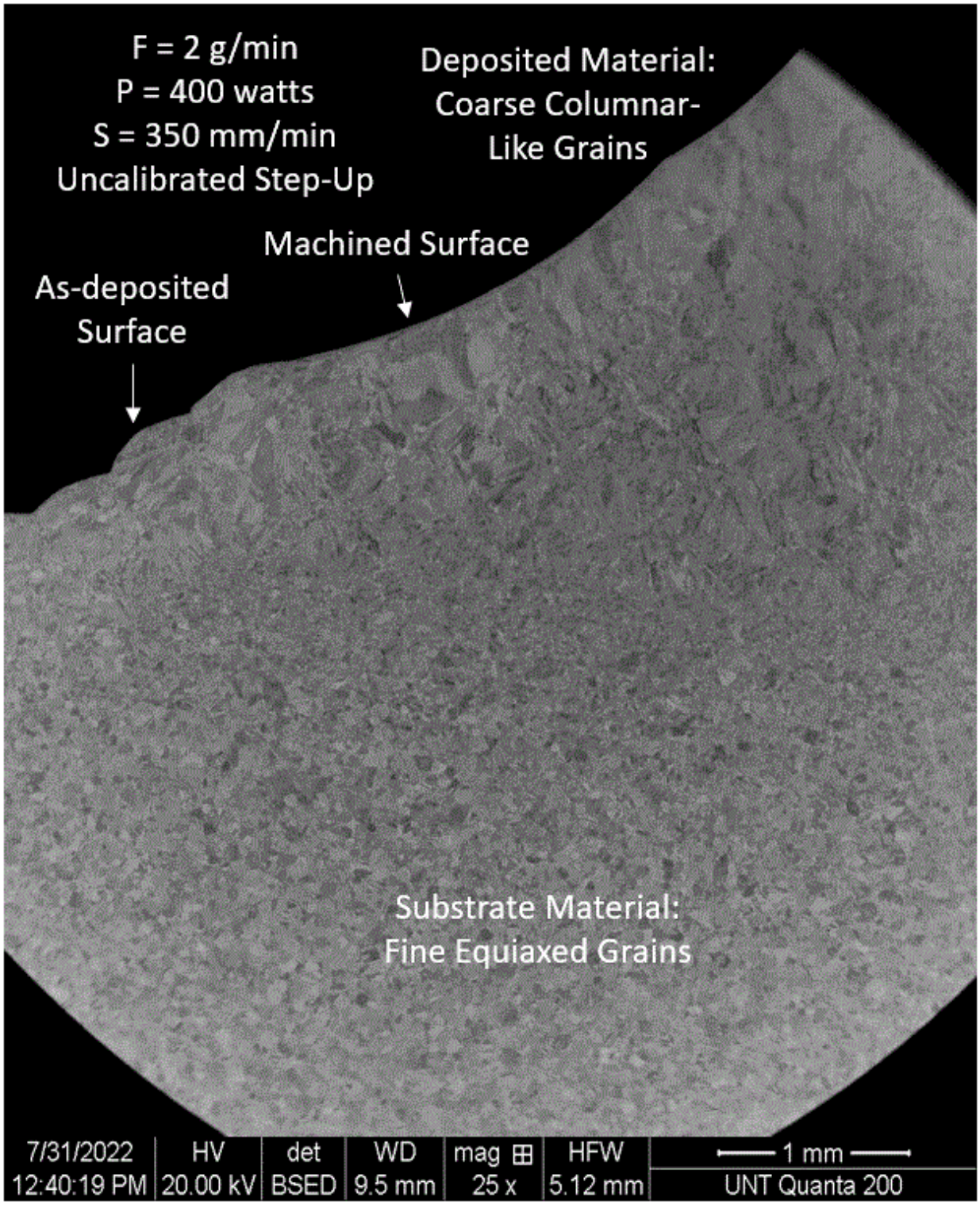

Figure 5.3: BSED image of 2 g/min 350 mm/min Uncalibrated Step-up deposition

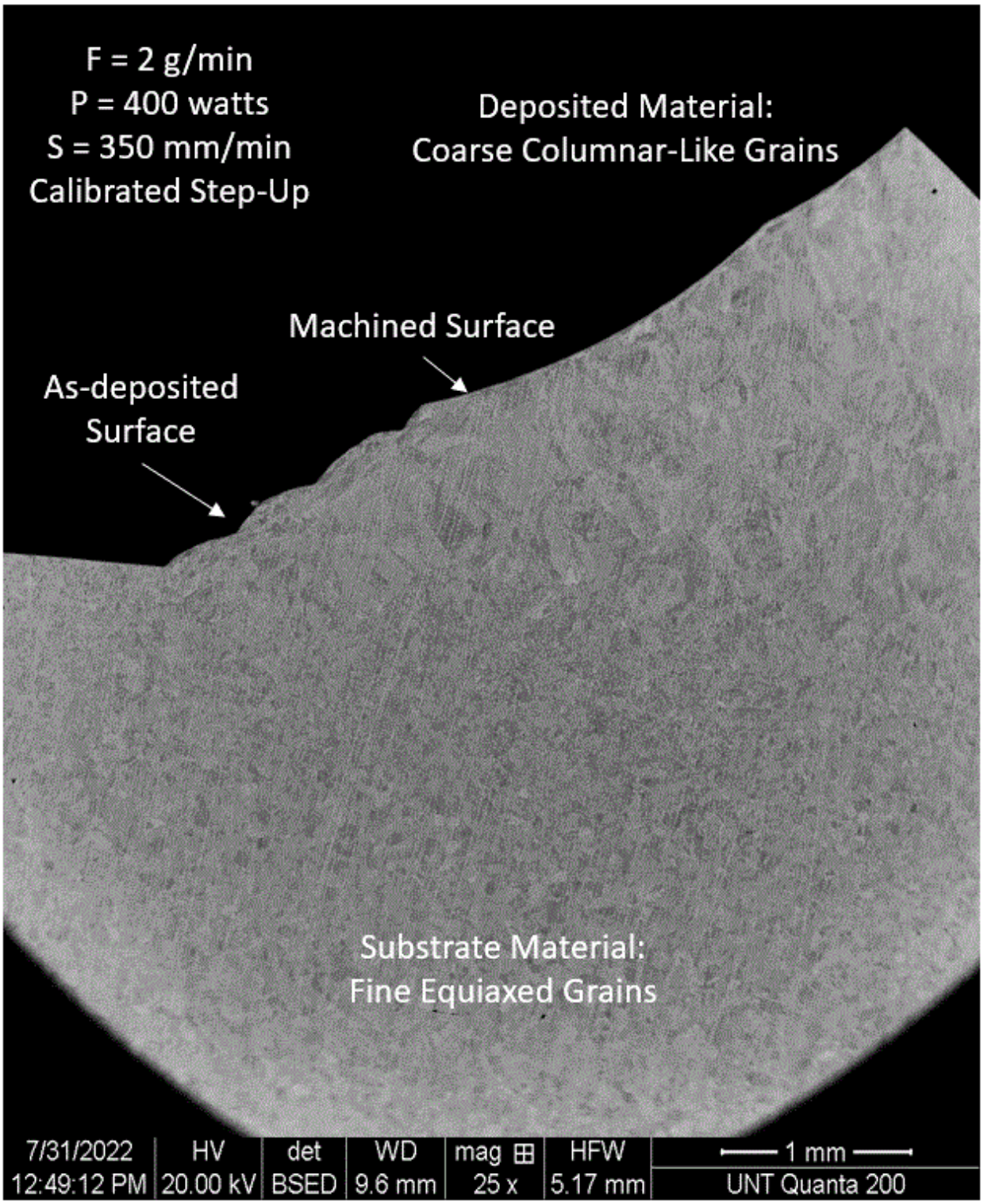

Figure 5.4: BSED image of 2 g/min 350 mm/min Calibrated Step-up deposition

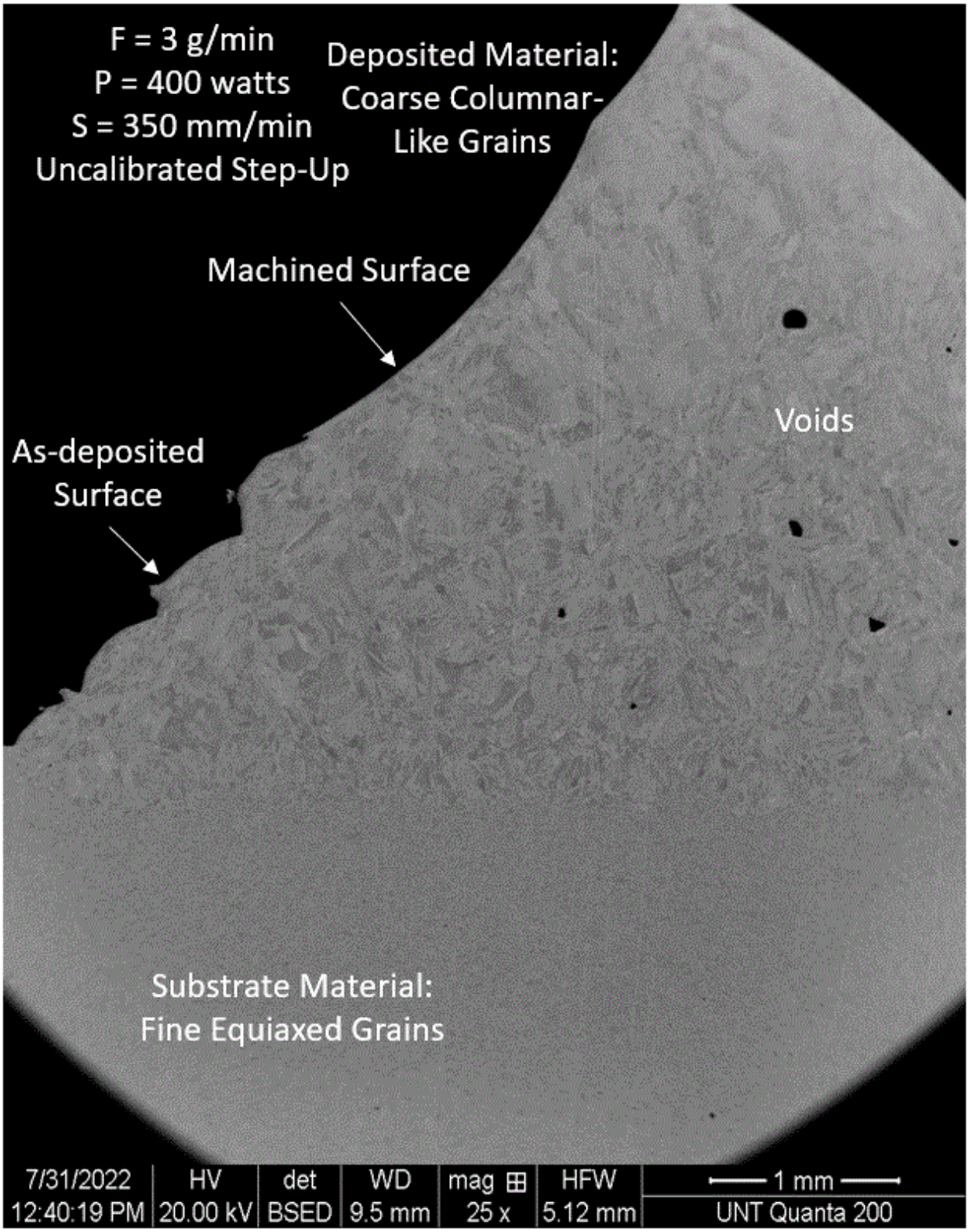

Figure 5.5: BSED image of 3 g/min 350 mm/min Uncalibrated Step-up deposition, with voids

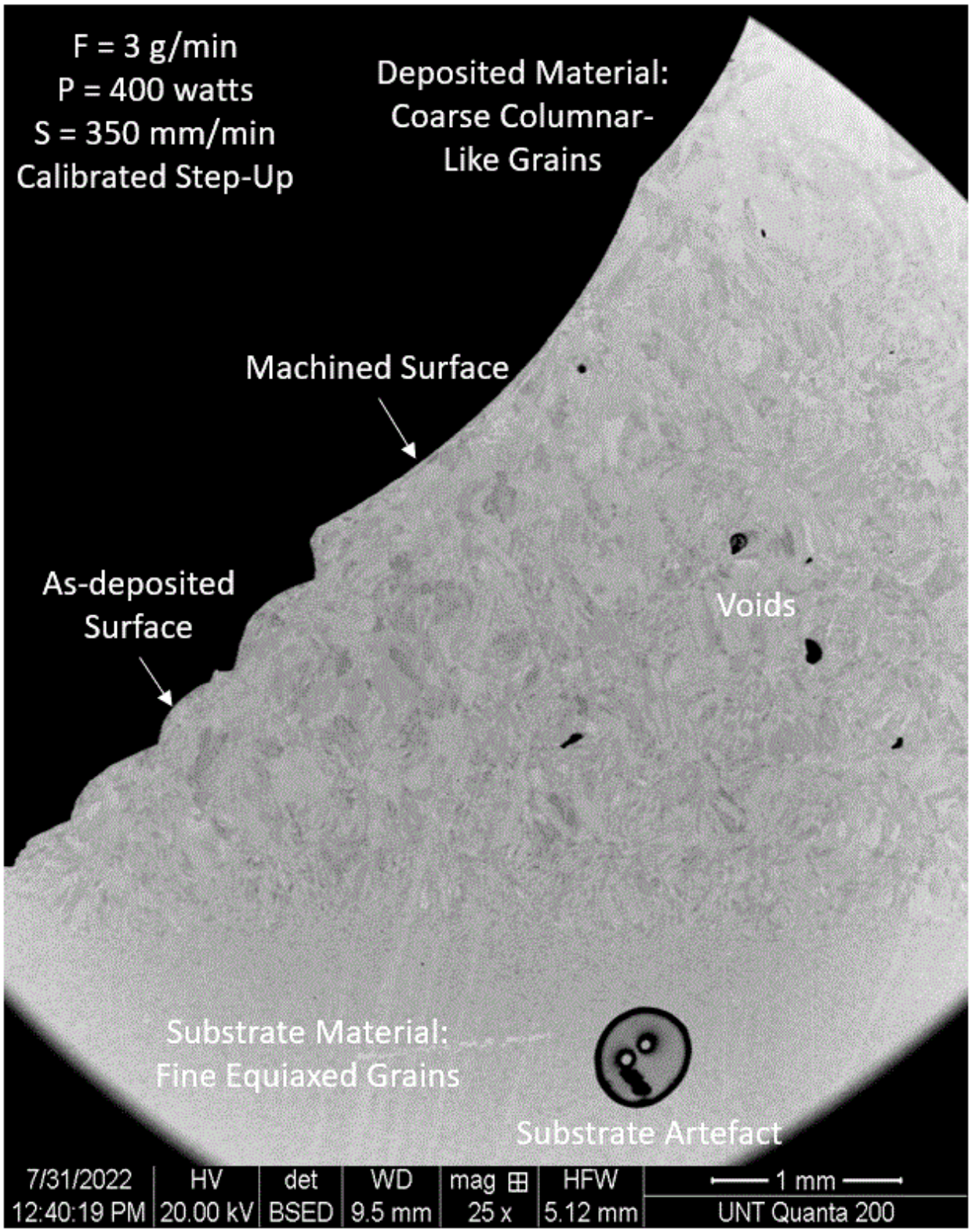

Figure 5.6: BSED image of 3 g/min 350 mm/min Calibrated Step-up deposition, with voids

As it relates to the literature, these findings agree well in that the grain sizes increase in the depositions, and that the grain shapes become columnar. The directionality of the columnar grain morphology is also in agreement with what is stated in the literature in that the columnar shapes have developed in the direction of the surface which is the most direct path for heat as it leaves the deposited material.

As it relates to the influence of machining processing on the deposited materials, the images in the figures above show that, at the surfaces were the depositions were machined, there are no apparent changes in the microstructure. This finding is contrary to that as described in (19) which reported that microstructures near the machined surfaces had been affected. There are several factors including machine stability and tooling quality that could influence this in both the case of Kaynak and the work herein.

As can be seen in Figures 5.5 and 5.5, for the three gram per minute parameter sets, both for the calibrated and the uncalibrated versions, there are several voids apparent in the deposition. The inputs and levels used for this portion of the experiment sets indicate that the higher powder flow rate is responsible for the voids. Further investigation should be made to confirm this finding.

5.3 Enhanced Process Planning Proposal

The process plan in Figure 5.7 shows the initially proposed process plan (Fig. 3.2), but also includes some necessary feedback loops. The first feedback loop allows for an iterative investigation of the effects of overlap on the multi-track single-layer variation in height, which would be intermediate to the first and second calibration steps. The next feedback loop allows for iterations of the multi-layer clad height calibration process to accommodate excess errors

when comparing measured multi-layer height with the expected height produced in previous steps, which would be intermediate to the second and third calibration steps. Each of the feedback loops should create an iterative process for minimizing error in the output for that particular step in the process.

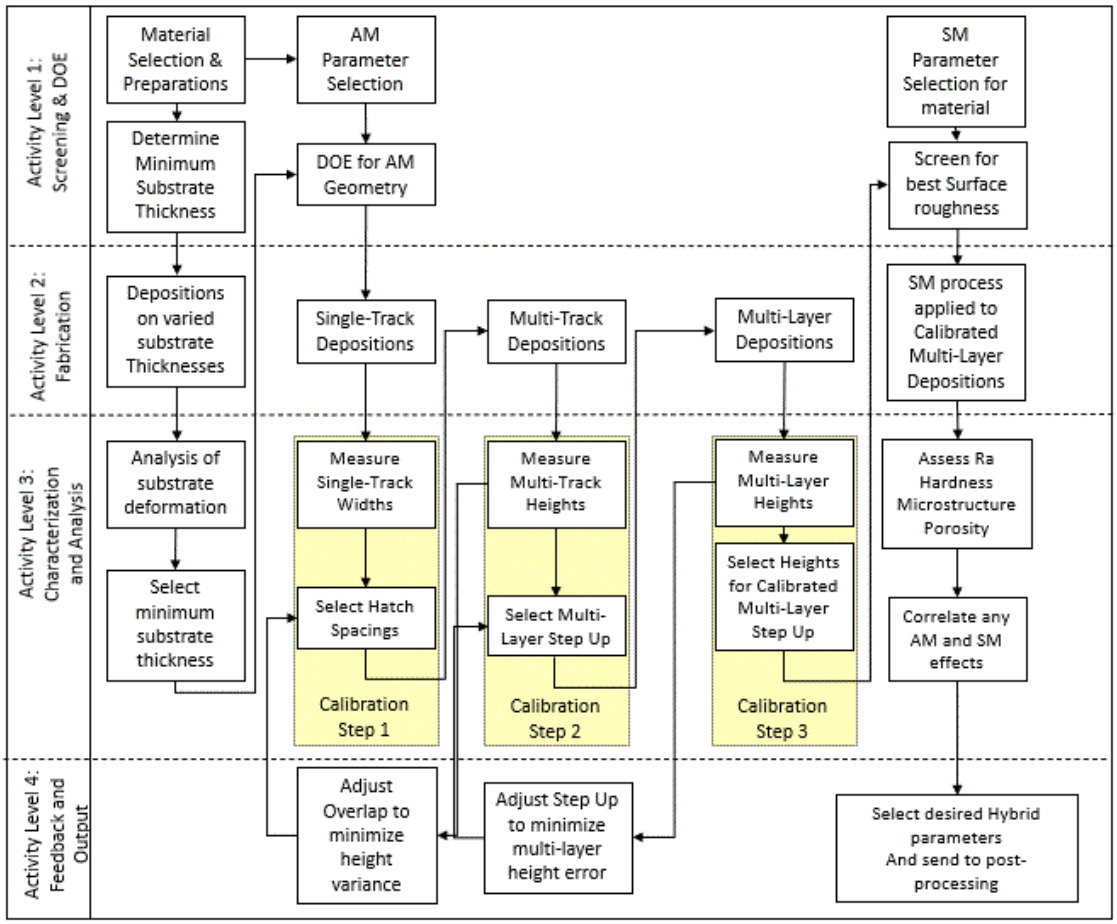

Figure 5.7: Enhanced process-plan proposal for hybrid manufacturing

As has been discussed, the benefits of controllable tool deterioration and surface roughness values closer to the theoretical values gained from application of industry standards, and more in line with the expectations in the die and mold industry, can be increased if the results of the iterative portions of the process plan are optimized.

To illustrate the additions to the enhanced process plan Figures 5.8 and 5.9 show that the

overlap value used in the single-layer depositions can be varied to minimize the error from clad height as it was predicted in the single-track depositions. And that the height calculated after measuring a multi-layer deposition can be used to further refine the calibration iteratively.

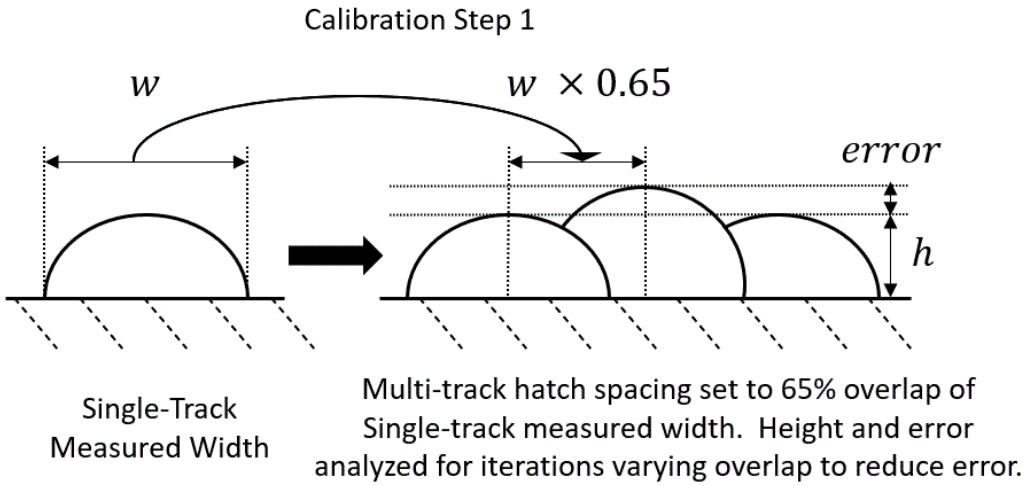

Figure 5.8: Schematic of single-track width measurement for determination of multi-track hatch spacing enhanced to reduce error

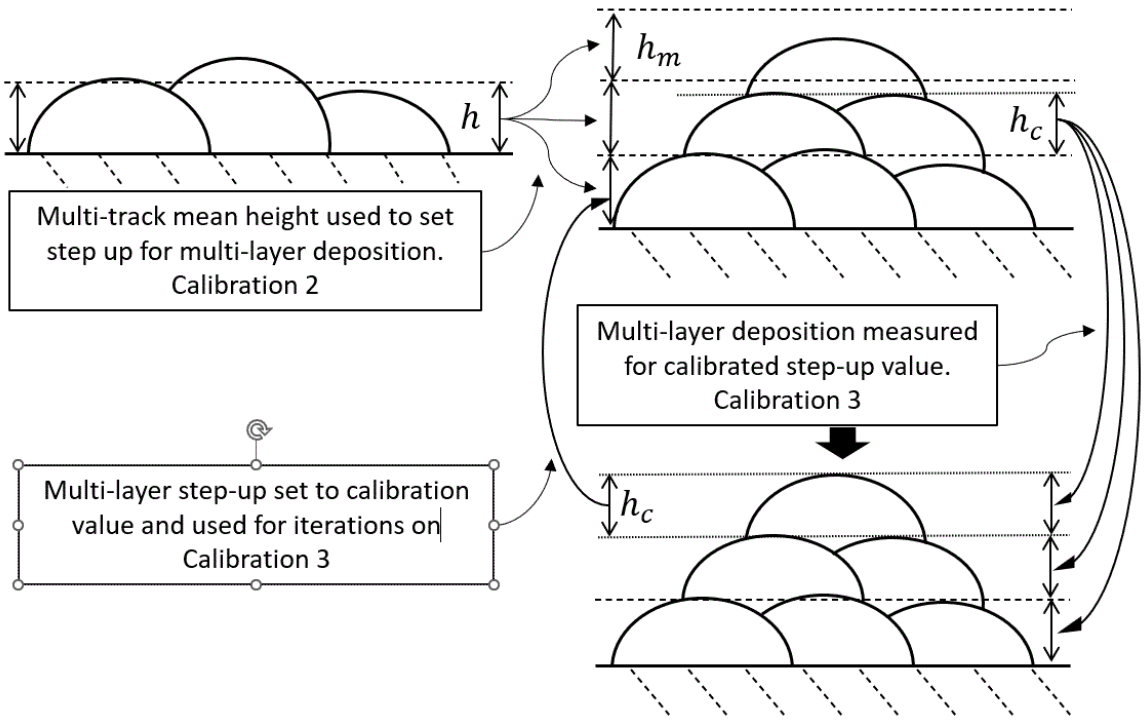

Figure 5.9: Schematic of multi-track height used to set step-up values for multi-layer deposition enhanced for iteration

5.4 Contributions

The first and major contribution this work makes to the knowledge base of hybrid manufacturing is a generalized process plan that goes beyond the scope of other works on process planning. The process plan proposed by Alvarez (24) stops at single-layer depositions, this process plan goes well beyond that with multi-layer depositions and subsequent machining processes. Shim (11) focuses on single-layer height while this study begins ahead of that with single-track depositions, and again, goes well beyond. The process proposed Zhu (35) is comprehensive almost to the same level as that of the process proposed herein, however, their work is focused on an entirely different material set and deposition mechanism - fused deposition modeling with plastics to be specific; so while it may carry similarities it does not contribute to the knowledge base of hybrid manufacturing with metals in the same way.

The process plan will also contribute to the efforts of any design or research process that already has optimized AM input parameters by providing the framework with which they can proceed without the need for further empirical modeling.

Another contribution this work offers to the industry is the process step and modeling of substrate Distortion due to deposition processing. The control of substrate flatness will benefit every aspect any other process plan. When considering that laser-based deposition requires a precise alignment of laser and powder flow focal points, any substrate Distortion will impact the quality of a deposition by moving the work surface out of the otherwise optimal position, which makes this contribution important not just for anyone hoping to follow the process plan proposed herein, but also important for other research endeavors that will follow other process plans, or none at all.

The empirical modeling of single-track geometries is not novel, but when it is combined with the iterations proposed in the enhanced process plan it contributes to the industry by providing a method for achieving an optimized flatness in single-layer depositions that will benefit every step thereafter. This is also the case for the empirical modeling of the multi-layer depositions and the geometric calibration values. That process, when preceded by the iterative single-layer calibration, in following the context of the overall process plan, should provide a geometrically predictable work piece for subsequent machining processing, which presents the opportunity for realizing two more contributions. The empirical modeling also provides a basis for metrology artefacts, like those mentioned by Carmingnato [4] that are invaluable to manufacturers engaged in larger batch productions that require inspection during as well as after production runs.

Another contribution that this work offers is a further improvement of tool deterioration, towards the more predicable flank wear as opposed to built-up edge, as provided for by the calibration processes that have been described in this work, which allow manufacturers to better plan their tooling inventory and deployments when engaged in hybrid manufacturing. This will allow more of the industry to benefit from this technology where it had previously been unattractive for the lack of predictability among many other reasons.

Much like the improvement of the tool deterioration, the improvements of surface finish, as shown to be present in the calibrated cases compared to the uncalibrated, reduces the need for successive roughing and finishing cycles in the machining processing stages of hybrid manufacturing thereby contributing to the ability of hybrid manufacturers to meet customer expectations in the die and mold industry.

One specific contribution that can be gleaned from this work is a recommendation of a set of AM processing parameters which should the best behaviors herein. The parameter sets that used 300 watts as laser power were excluded because of the errors in step-up value, from calibration step one, when compared to the multi-layer measurements that used those step-up values; this effectively eliminated 300 watts from the pool of desirable parameter levels. The microstructural analyses showed that the three gram per minute powder flow rate produced depositions with large voids; as such, that level of input for powder flow rate should also be discarded. Considering that the tool deterioration, and surface roughness measurements for the 450 mm per minute objects that also used the 400-watt laser power and 2 gram per minute powder flow rate, the 450 mm per minute level for scanning speed can be considered best in these cases. So, the results of this study support the proposal that the best set of parameters for use on the AHM would be 400 watts laser power and 2 grams per minute of powder flow and 450 mm per minute scanning speed.

5.5 Future Work

Future works in the development of hybrid manufacturing would do well to follow a process plan similar to what has been proposed in this work. The process plan in Figure 5.7 includes feedback loops to investigate the effects of overlap on the multi-track single-layer variation in height, as well as iterations for the multi-layer clad height calibration process to accommodate excess errors. Optimizing the reduction of error in geometric responses could produce a large body of future works.

In line with the concept of feedback, the addition of a closed-loop, in-situ measurement setup would be a project worth investing in for the future. The integration of such technologies

would require cooperation between several multi-disciplinary studies ranging from metrology to computer science, with material sciences positioned well in between.

Other portions of the plan that should be developed in the future should include post process heat treatment aimed at the mitigation of residual stress as will be induced by the rigidity of the substrates during the deposition process. As relates to the microstructural outputs, some portion of the process plan developments in future work could also investigate the cooling rates of the depositions, as they correlate strongly to the development of microstructure, and on how to affect those cooling rates through additional equipment like substrate cooling systems.

As it relates to microstructure to the process plan, future works on the effect of intra-layer dwell times could improve the deposition quality of objects made using this process plan. This set of experiments did not use or consider intra-layer dwell times as the scanning strategy was a continuous meander path. That continuous meander path, considering that each layer had a different number of tracks, could have produced differing cooling times between the layers. Similar to this would be the effect of overall cool-down time between deposition processes and machining processes. The structure of the experiments herein required that the machining system spindle in the AHM needed to be warmed up during every experiment. This created a twenty minute cool-down time between the end of every deposition phase and the beginning of every machining process phase. Future works that include spindle conditioning as part of the process plan could not only decrease processing times but could also show an effect on the microstructure and hardness of objects. Data from those experiments would be required to theorize about whether those effects would be pos

Integrating a non-contact metrology system would be a useful future project for anyone

considering reducing the process times involved in the plan proposed herein. In-line, or on-line laser-based metrology systems could be deployed in machines like the AHM and would be of great benefit if properly used.

Another avenue for useful future works related to this thesis would be the application of high isostatic pressure treatment to reduce the appearance of porosity in the depositions created during the AM portion of this process plan.

APPENDIX

EXAMPLES OF CODES

A.1 Single-track G-Code example

(----- Header Begins -----)
G91G28Z0 (Raises Z axis up to avoid any collision during first X & Y motion)
T07 (ENTER tool of assigned short tool holder to call the tool offset that is stored for the DED head & associated with the tool number called. Also having a toolholder in the spindle protects it from powder ingress)
M06 (Tool change to previously indicated tool)
G43 H07 (ENTER tool after "H" to apply the tool offset for the length of the DED heads)
G90G55G00X0.0Y0.0 (Sets the work offset to G55 which should have already been taught)
G00 Z75. (Approaches the workpiece and stops XXmm above - ensures tool length offset is correct)
M98 P9111 (PLEASE UPDATE - recipe for the program)
G04P0.3 (Short dwell to ensure the relays are set for the recipe)
M00 (The head should be XXmm above the Z0 position - CONFIRM by pressing cycle start)
(CONFIRM by pressing cycle start)
G00 Z15. (Approaches the workpiece and stops XXmm above - ensures tool length offset includes stands-off)
M00 (The head should be XXmm above the Z0 position - CONFIRM by pressing cycle start)
(CONFIRM by pressing cycle start)
M110 (Media On)
G04P30. (Dwell to let powder and gas stabilize)
G00Z15.
G00Z0.
(----- Header Ends -----)

(----- P9111 is 3g/min at 300W. P9112 is 3g/min at 400W -----)
(----- The first object recipe was called in the Header -----)

(----- Object 1 : 1 Tracks : Repetition 3 -----)
G00 G90 X0. (Sets X to Zero Position)
G00 G91 Y4. (Increment Y position)
M97 P101 L3 (Call N101 3 times)

(----- Object 2 : 1 Tracks : Repetition 3 -----)
G00 G90 X0. (Sets X to Zero Position)
G00 G91 Y4. (Increment Y position)
M97 P102 L3 (Call N102 3 times)

(----- P9111 is 3g/min at 300W. P9112 is 3g/min at 400W -----)

M98 P9112 (Call Recipe)
G00 G90 X0. (Sets X to Zero Position for Dwell)
G04 P15. (dwell to establish powder flow)

(----- Object 3 : 1 Tracks : Repetition 3 -----)
G00 G91 Y4. (Increment Y position)
M97 P101 L3 (Call N101 3 times)

(----- Object 4 : 1 Tracks : Repetition 3 -----)
G00 G90 X0. (Sets X to Zero Position)
G00 G91 Y4. (Increment Y position)
M97 P102 L3 (Call N102 3 times)

(----- P9113 is 2g/min at 300W. P9114 is 2g/min at 400W -----)
M98 P9113 (Call Recipe)
G00 G90 X0. (Sets X to Zero Position for Dwell)
G04 P15. (dwell to establish powder flow)

(----- Object 1 : 1 Tracks : Repetition 3 -----)
G00 G91 Y4. (Increment Y position)
M97 P101 L3 (Call N101 3 times)

(----- Object 2 : 1 Tracks : Repetition 3 -----)
G00 G90 X0. (Sets X to Zero Position)
G00 G91 Y4. (Increment Y position)
M97 P102 L3 (Call N102 3 times)

(----- P9111 is 3g/min at 300W. P9112 is 3g/min at 400W -----)
M98 P9114 (Call Recipe)
G00 G90 X0. (Sets X to Zero Position for Dwell)
G04 P15. (dwell to establish powder flow)

(----- Object 3 : 1 Tracks : Repetition 3 -----)
G00 G91 Y4. (Increment Y position)
M97 P101 L3 (Call N101 3 times)

(----- Object 4 : 1 Tracks : Repetition 3 -----)
G00 G90 X0. (Sets X to Zero Position)
G00 G91 Y4. (Increment Y position)
M97 P102 L3 (Call N102 3 times)

(----- Footer Begins -----)
G91Z25. (Incremental - Drive the Z axis up to avoid any collision during X & Y motion)

```
G90             ( Absolute mode)
M121            ( Laser Off - double check )
G04 P3.         ( Dwell to clear the air after laser is off)
M111            ( Media Off )
G91Z25          ( Incremental - Drive the Z axis up to avoid any collision during X & Y motion
G90             ( Absolute mode)
G91Z75.         ( Incremental - Drive the Z axis up to avoid any collision during X & Y motion )
G91G28Y0        ( Incremental - Drive the Y axis forward for convenience of the operator )
G90             ( Absolute mode - position command )
M100            ( Parks and Purges the DED head)
M30             ( Program end )
%

(----- Subroutines Only Below -----)

(----- 15mm in X direction at 350mm/min -----)
N101
G00 G91 X5.
M120 (Laser on)
G01 X15. F350.000
M121 (Laser off)
M99

(----- 15mm in X direction at 450mm/min -----)
N102
G00 G91 X5.
M120 (Laser on)
G01 X15. F450.000
M121 (Laser off)
M99

(----- End of Code -----)
```

A.2 Multi-track G-Code example

```
(----- Header Begins -----)
G91G28Z0        ( Raises Z axis up to avoid any collision during first X & Y motion )
T07             ( ENTER tool  of assigned short tool holder to call the tool offset that is stored for the DED head & associated with the tool number called. Also having a toolholder in the spindle protects it from powder ingress )
M06             ( Tool change to previously indicated tool)
```

```
G43 H07         ( ENTER tool  after "H" to apply the tool offset for the length of the DED heads)
G90G55G00X0.0Y0.0 ( Sets the work offset to G55 which should have already been taught )
G00 Z75.        ( Approaches the workpiece and stops XXmm above - ensures tool length offset is correct)
M98 P9104       ( PLEASE UPDATE - recipe for the program )
G04P0.3         ( Rapid dwell to ensure the relays are set for the recipe )
M00             ( The head should be XXmm above the Z0 position - CONFIRM by pressing cycle start )
( CONFIRM by pressing cycle start )
G00 Z15.        ( Approaches the workpiece and stops XXmm above - ensures tool length offset includes stands-off)
M00             ( The head should be XXmm above the Z0 position - CONFIRM by pressing cycle start )
( CONFIRM by pressing cycle start )
M110            ( Media On )
G04P20.         ( Dwell to let powder and gas stabilize )
G00Z15.
G00Z0.
(----- Header Ends -----)

(----- Variables Description -----)
(#1 sets the four digit Ambit recipe)
(#2 sets the scan speed)
(#3 step-over for tracks)
(#4 step-up for layers)
(#5 track length)
(#6 Number of tracks per layer)
(----- Variables End -----)

(----- Experiment 1 -----)
#1 = 9111
#2 = 350.000
#3 = 0.542
#4 = 0.5
#5 = 8.
#6 = 10.
G00 G90 X4.0 Y4.0
G00 G90 Z0.0
M98 P[#1]
G04 P20.  (Set Recipe and Dwell to let powder and gas stabilize)
(----- Repetition 1 -----)
M97 P101 L[#6]
```

```
G00 G91 X4.0
(----- Repetition 2 -----)
M97 P101 L[#6]
G00 G91 X4.0
(----- Repetition 3 -----)
M97 P101 L[#6]
G00 G91 X4.0

(----- Experiment 2 -----)
#1 = 9111
#2 = 450.000
#3 = 0.494
#4 = 0.5
#5 = 8.
#6 = 10.
G00 G90 X4.0 Y16.0
G00 G90 Z0.0
M98 P[#1]
G04 P20.  (Set Recipe and Dwell to let powder and gas stabilize)
(----- Repetition 1 -----)
M97 P101 L[#6]
G00 G91 X4.0
(----- Repetition 2 -----)
M97 P101 L[#6]
G00 G91 X4.0
(----- Repetition 3 -----)
M97 P101 L[#6]
G00 G91 X4.0

(----- Experiment 3 -----)
#1 = 9112
#2 = 350.000
#3 = 0.723
#4 = 0.5
#5 = 8.
#6 = 10.
G00 G90 X4.0 Y16.0
G00 G90 Z0.0
M98 P[#1]
G04 P20.  (Set Recipe and Dwell to let powder and gas stabilize)
(----- Repetition 1 -----)
M97 P101 L[#6]
G00 G91 X4.0
(----- Repetition 2 -----)
```

```
M97 P101 L[#6]
G00 G91 X4.0
(----- Repetition 3 -----)
M97 P101 L[#6]
G00 G91 X4.0

(----- Experiment 4 -----)
#1 = 9112
#2 = 450.000
#3 = 0.723
#4 = 0.5
#5 = 8.
#6 = 10.
G00 G90 X4.0 Y16.0
G00 G90 Z0.0
M98 P[#1]
G04 P20.  (Set Recipe and Dwell to let powder and gas stabilize)
(----- Repetition 1 -----)
M97 P101 L[#6]
G00 G91 X4.0
(----- Repetition 2 -----)
M97 P101 L[#6]
G00 G91 X4.0
(----- Repetition 3 -----)
M97 P101 L[#6]
G00 G91 X4.0

(----- Experiment 5 -----)
#1 = 9113
#2 = 350.000
#3 = 0.496
#4 = 0.5
#5 = 8.
#6 = 10.
G00 G90 X4.0 Y16.0
G00 G90 Z0.0
M98 P[#1]
G04 P20.  (Set Recipe and Dwell to let powder and gas stabilize)
(----- Repetition 1 -----)
M97 P101 L[#6]
G00 G91 X4.0
(----- Repetition 2 -----)
M97 P101 L[#6]
G00 G91 X4.0
```

```
(----- Repetition 3 -----)
M97 P101 L[#6]
G00 G91 X4.0

(----- Experiment 5 -----)
#1 = 9113
#2 = 350.000
#3 = 0.496
#4 = 0.5
#5 = 8.
#6 = 10.
G00 G90 X4.0 Y16.0
G00 G90 Z0.0
M98 P[#1]
G04 P20.  (Set Recipe and Dwell to let powder and gas stabilize)
(----- Repetition 1 -----)
M97 P101 L[#6]
G00 G91 X4.0
(----- Repetition 2 -----)
M97 P101 L[#6]
G00 G91 X4.0
(----- Repetition 3 -----)
M97 P101 L[#6]
G00 G91 X4.0

(----- Experiment 6 -----)
#1 = 9113
#2 = 450.000
#3 = 0.456
#4 = 0.5
#5 = 8.
#6 = 10.
G00 G90 X4.0 Y16.0
G00 G90 Z0.0
M98 P[#1]
G04 P20.  (Set Recipe and Dwell to let powder and gas stabilize)
(----- Repetition 1 -----)
M97 P101 L[#6]
G00 G91 X4.0
(----- Repetition 2 -----)
M97 P101 L[#6]
G00 G91 X4.0
(----- Repetition 3 -----)
M97 P101 L[#6]
```

```
G00 G91 X4.0

(----- Experiment 7 -----)
#1 = 9114
#2 = 350.000
#3 = 0.697
#4 = 0.5
#5 = 8.
#6 = 10.
G00 G90 X4.0 Y16.0
G00 G90 Z0.0
M98 P[#1]
G04 P20.  (Set Recipe and Dwell to let powder and gas stabilize)
(----- Repetition 1 -----)
M97 P101 L[#6]
G00 G91 X4.0
(----- Repetition 2 -----)
M97 P101 L[#6]
G00 G91 X4.0
(----- Repetition 3 -----)
M97 P101 L[#6]
G00 G91 X4.0

(----- Experiment 8 -----)
#1 = 9114
#2 = 450.000
#3 = 0.652
#4 = 0.5
#5 = 8.
#6 = 10.
G00 G90 X4.0 Y16.0
G00 G90 Z0.0
M98 P[#1]
G04 P20.  (Set Recipe and Dwell to let powder and gas stabilize)
(----- Repetition 1 -----)
M97 P101 L[#6]
G00 G91 X4.0
(----- Repetition 2 -----)
M97 P101 L[#6]
G00 G91 X4.0
(----- Repetition 3 -----)
M97 P101 L[#6]
G00 G91 X4.0
```

(----- End of DED Toolpath : Insert Mayka Wrapper Footer Below -----)

(----- Mayka Footer Begins -----)
G91Z25. (Incremental - Drive the Z axis up to avoid any collision during X & Y motion)
G90 (Absolute mode)
M121 (Laser Off - double check)
G04 P3. (Dwell to clear the air after laser is off)
M111 (Media Off)
G91Z25 (Incremental - Drive the Z axis up to avoid any collision during X & Y motion)
G90 (Absolute mode)
G91Z75. (Incremental - Drive the Z axis up to avoid any collision during X & Y motion)
G91G28Y0 (Incremental - Drive the Y axis forward for convenience of the operator)
G90 (Absolute mode - position command)
(----- Mayka Footer Ends -----)

(----- The End Begins -----)
M30
(----- The End Ends -----)

(----- Subroutines Only Below Here -----)
(----- This subroutine DEDs 5 layers, sinlge track -----)
N101
M120 (Laser on)
G01 G91 Y8.000 F[#2]
M121 (Laser off)
G00 G91 X[#3] Y-8.000
M99

(----- Subroutines End -----)

A.3 Multi-layer G-Code example

(----- Header Begins -----)
G91G28Z0 (Raises Z axis up to avoid any collision during first X & Y motion)
T07 (ENTER tool of assigned short tool holder to call the tool offset that is stored for the DED head & associated with the tool number called. Also having a toolholder in the spindle protects it from powder ingress)
M06 (Tool change to previously indicated tool)
G43 H07 (ENTER tool after "H" to apply the tool offset for the length of the DED heads)

```
G90G55G00X0.0Y0.0 ( Sets the work offset to G55 which should have already been taught )
G00 Z75.  ( Approaches the workpiece and stops XXmm above - ensures tool length offset is correct)
M98 P9104  ( PLEASE UPDATE - recipe for the program )
G04P0.3  ( Rapid dwell to ensure the relays are set for the recipe )
M00  ( The head should be XXmm above the Z0 position - CONFIRM by pressing cycle start )
( CONFIRM by pressing cycle start )
G00 Z15.  ( Approaches the workpiece and stops XXmm above - ensures tool length offset includes stands-off)
M00  ( The head should be XXmm above the Z0 position - CONFIRM by pressing cycle start )
( CONFIRM by pressing cycle start )
M110  ( Media On )
G04P10.  ( Short Dwell to let powder and gas stabilize, Longer Dwells later )
G00Z25.
(----- Header Ends -----)

(----- Variables Description -----)
(#1 sets the four digit Ambit recipe)
(#2 sets the scan speed)
(#3 step-over for tracks)
(#4 step-up for layers)
(#5 track length)
(#6 Number of DoubleTracks per layer)
(#7 Number of layers)
(#10 object start X)
(#12 half step over)
(#20 yposition)

(These Variable should work for all experiments)
(#14 - #19 xpositions 1 - 6)
#14 = 8.0
#15 = 27.0
#16 = 45.0
#17 = 8.0
#18 = 27.0
#19 = 45.0
(----- Variables End -----)

(----- Experiment 1 -----)
#1 = 9111
#2 = 350.000
```

```
#3 = 0.542
#4 = 0.262
#5 = 8.
#6 = 9.
#10 = #14
#12 = 0.271
#20 = 4.0

M98 P[#1]
G04 P20.  (Set Recipe and Dwell to let powder and gas stabilize)
(----- Repetition 1 -----)
M97 P101
#10 = #15
(----- Repetition 2 -----)
M97 P101
#10 = #16
(----- Repetition 3 -----)
M97 P101


(----- Experiment 2 -----)
#1 = 9111
#2 = 450.000
#3 = 0.494
#4 = 0.204
#5 = 8.
#6 = 9.
#10 = #17
#12 = 0.247
#20 = 16.0

M98 P[#1]
G04 P20.  (Set Recipe and Dwell to let powder and gas stabilize)
(----- Repetition 1 -----)
M97 P101
#10 = #18
(----- Repetition 2 -----)
M97 P101
#10 = #19
(----- Repetition 3 -----)
M97 P101


(----- Experiment 3 -----)
```

```
#1 = 9112
#2 = 350.000
#3 = 0.723
#4 = 0.327
#5 = 8.
#6 = 9.
#10 = #14
#12 = 0.362
#20 = 28.0

M98 P[#1]
G04 P20.  (Set Recipe and Dwell to let powder and gas stabilize)
(----- Repetition 1 -----)
M97 P101
#10 = #15
(----- Repetition 2 -----)
M97 P101
#10 = #16
(----- Repetition 3 -----)
M97 P101


(----- Experiment 4 -----)
#1 = 9112
#2 = 450.000
#3 = 0.673
#4 = 0.228
#5 = 8.
#6 = 9.
#10 = #17
#12 = 0.336
#20 = 40.0

M98 P[#1]
G04 P20.  (Set Recipe and Dwell to let powder and gas stabilize)
(----- Repetition 1 -----)
M97 P101
#10 = #18
(----- Repetition 2 -----)
M97 P101
#10 = #19
(----- Repetition 3 -----)
M97 P101
```

```
(----- Experiment 5 -----)
#1 = 9113
#2 = 350.000
#3 = 0.496
#4 = 0.429
#5 = 8.
#6 = 9.
#12 = 0.248
#20 = 52.0
#10 = #14

M98 P[#1]
G04 P20.  (Set Recipe and Dwell to let powder and gas stabilize)
(----- Repetition 1 -----)
M97 P101
#10 = #15
(----- Repetition 2 -----)
M97 P101
#10 = #16
(----- Repetition 3 -----)
M97 P101

(----- Experiment 6 -----)
#1 = 9113
#2 = 450.000
#3 = 0.456
#4 = 0.324
#5 = 8.
#6 = 9.
#12 = 0.228
#20 = 64.0
#10 = #17

M98 P[#1]
G04 P20.  (Set Recipe and Dwell to let powder and gas stabilize)
(----- Repetition 1 -----)
M97 P101
#10 = #18
(----- Repetition 2 -----)
M97 P101
#10 = #19
(----- Repetition 3 -----)
M97 P101
```

```
G00 G91 Z25. (move up before start of next object)

(----- Experiment 7 -----)
#1 = 9114
#2 = 350.000
#3 = 0.697
#4 = 0.507
#5 = 8.
#6 = 9.
#12 = 0.348
#20 = 76.0
#10 = #14

M98 P[#1]
G04 P20.  (Set Recipe and Dwell to let powder and gas stabilize)
(----- Repetition 1 -----)
M97 P101
#10 = #15
(----- Repetition 2 -----)
M97 P101
#10 = #16
(----- Repetition 3 -----)
M97 P101

(----- Experiment 8 -----)
#1 = 9114
#2 = 450.000
#3 = 0.651
#4 = 0.407
#5 = 8.
#6 = 9.
#12 = 0.326
#20 = 88.0
#10 = #17

M98 P[#1]
G04 P20.  (Set Recipe and Dwell to let powder and gas stabilize)
(----- Repetition 1 -----)
M97 P101
#10 = #18
(----- Repetition 2 -----)
M97 P101
#10 = #19
(----- Repetition 3 -----)
```

```
M97 P101

(----- Experiment 9 -----)
#1 = 9117
#2 = 350.000
#3 = 0.48
#4 = 0.636
#5 = 8.
#6 = 9.
#12 = 0.24
#20 = 100.0
#10 = #14

M98 P[#1]
G04 P20.  (Set Recipe and Dwell to let powder and gas stabilize)
(----- Repetition 1 -----)
M97 P101
#10 = #15
(----- Repetition 2 -----)
M97 P101
#10 = #16
(----- Repetition 3 -----)
M97 P101

(----- Experiment 10 -----)
#1 = 9117
#2 = 450.000
#3 = 0.444
#4 = 0.465
#5 = 8.
#6 = 9.
#12 = 0.222
#20 = 112.0
#10 = #17

M98 P[#1]
G04 P20.  (Set Recipe and Dwell to let powder and gas stabilize)
(----- Repetition 1 -----)
M97 P101
#10 = #18
(----- Repetition 2 -----)
M97 P101
#10 = #19
(----- Repetition 3 -----)
```

```
M97 P101

(----- Experiment 11 -----)
#1 = 9118
#2 = 350.000
#3 = 0.683
#4 = 0.654
#5 = 8.
#6 = 9.
#12 = 0.342
#20 = 124.0
#10 = #14

M98 P[#1]
G04 P20.  (Set Recipe and Dwell to let powder and gas stabilize)
(----- Repetition 1 -----)
M97 P101
#10 = #15
(----- Repetition 2 -----)
M97 P101
#10 = #16
(----- Repetition 3 -----)
M97 P101
G00 G91 Z25. (move up before start of next object)

(----- Experiment 12 -----)
#1 = 9118
#2 = 450.000
#3 = 0.683
#4 = 0.499
#5 = 8.
#6 = 9.
#12 = 0.318
#20 = 136.0
#10 = #17

M98 P[#1]
G04 P20.  (Set Recipe and Dwell to let powder and gas stabilize)
(----- Repetition 1 -----)
M97 P101
#10 = #18
(----- Repetition 2 -----)
M97 P101
#10 = #19
```

```
(----- Repetition 3 -----)
M97 P101

(----- End of DED Toolpath : Insert Mayka Wrapper Footer Below -----)

(----- Mayka Footer Begins -----)
G91Z25.     ( Incremental - Drive the Z axis up to avoid any collision during X & Y motion )
G90         ( Absolute mode)
M121        ( Laser Off - double check )
G04 P3.     ( Dwell to clear the air after laser is off)
M111        ( Media Off )
G91Z25      ( Incremental - Drive the Z axis up to avoid any collision during X & Y motion )
G90         ( Absolute mode)
G91Z75.     ( Incremental - Drive the Z axis up to avoid any collision during X & Y motion )
G91G28Y0    ( Incremental - Drive the Y axis forward for convenience of the operator )
G90         ( Absolute mode - position command )
(----- Mayka Footer Ends -----)

(----- The End Begins -----)
M30
(----- The End Ends -----)

(----- Subroutines Only Below Here -----)
(----- This subroutine DEDs 5 layers, sinlge track -----)

N101
G00 G90 Z25.0
G00 G90 X[#10] Y[#20]
G00 G90 Z0.0
M97 P102 L5
#6=9.
G00 G90 Z25.0
M99

N102
M97 P103 L[#6]
#10=#10+#12
#6=#6-1.
G00 G91 Z[#4]
G00 G90 X[#10]
M99
```

```
N103
M120 (Laser on)
G01 G91 Y[#5] F[#2]
M121 (Laser off)
G01 G91 X[#3]
M120 (Laser on)
G01 G91 Y-[#5]
M121 (Laser off)
G01 G91 X[#3]
M99

(----- Subroutines End -----)
```

A.4 Full hybrid G-Code example

```
(----- Initialize Variables with Descriptions -----)
#1 = 9112       (sets the four digit Ambit recipe)
#2 = 350.000    (sets the scan speed)
#3 = 0.723      (step-over for tracks)
#4 = 0.332      (step-up for layers)
#5 = 25.        (track length)
#6 = 14.        (Total Number of Tracks in Bottom layer)
#7 = 10.        (Total Number of layers)
#10 = 6.0       (X Position Additive Start)
#11 = 6.0     (Y position Additive Start)
#12 = 0.362     (Half step over for layers up X increment)
#13 = 25.4      (Safe Height)
#15 = 1.        (Flip Flop Variable)

#18 = 6.0       (Subtractive X Start Location)
#19 = 2.0       (Subtractive Y Start Location)
#20 = 3852.     ('n' RPM Spindle speed as calculated for this model)
#21 = 418.      ('Vf' feed rate mm/min as calculated for this model)
#22 = 0.938     (Left Hand Cutter Compensation for this model)
#23 = 16.0      (Length of Subtractive tool path)
#25 = 200.0     (Use as slow speed feed rate of mm/min for positioning moves)
#30 = 1.        (Subtractive Pass Counter)

M00 (Press Cycle Start to Confirm Variables have been loaded)
```

(----- Header Begins -----)
G91G28Z0 (Raises Z axis up to avoid any collision during first X & Y motion)
T07 (ENTER tool of assigned short tool holder to call the tool offset that is stored for the DED head & associated with the tool number called. Also having a toolholder in the spindle protects it from powder ingress)
M06 (Tool change to previously indicated tool)
G43 H07 (ENTER tool after "H" to apply the tool offset for the length of the DED heads)
G90G55G00X0.0Y0.0 (Sets the work offset to G55 which should have already been taught)
G00 Z75. (Approaches the workpiece and stops XXmm above - ensures tool length offset is correct)
M98 P9104 (PLEASE UPDATE - recipe for the program)
G04P0.3 (Rapid dwell to ensure the relays are set for the recipe)
M00 (The head should be XXmm above the Z0 position - CONFIRM by pressing cycle start)
(CONFIRM by pressing cycle start)
G00 Z15. (Approaches the workpiece and stops XXmm above - ensures tool length offset includes stands-off)
M00 (The head should be XXmm above the Z0 position - CONFIRM by pressing cycle start)
(CONFIRM by pressing cycle start)
M110 (Media On)
G04P10. (Short Dwell to let powder and gas stabilize, Longer Dwells later)
G00Z25.
(----- Header Ends -----)

(----- Experiment -----)

M98 P[#1] (set recipe)
G04 P20. (Dwell to let powder and gas stabilize)

M97 P101 (Call the set of MultiLayer ZigZag Path subroutines)

(----- End of DED Toolpath : Insert Mayka Wrapper Footer Below -----)

(----- Mayka Footer Begins -----)
G91Z25. (Incremental - Drive the Z axis up to avoid any collision during X & Y motion)
G90 (Absolute mode)
M121 (Laser Off - double check)
G04 P3. (Dwell to clear the air after laser is off)
M111 (Media Off)

```
G91Z25          ( Incremental - Drive the Z axis up to avoid any collision during X & Y
motion )
G90             ( Absolute mode)
G91Z75.         ( Incremental - Drive the Z axis up to avoid any collision during X & Y
motion )
G91G28Y0        ( Incremental - Drive the Y axis forward for convenience of the operator )
G90             ( Absolute mode - position command )
M100            ( Parks the DED Head)
(Insert Park Command Here)
(----- Mayka Footer Ends -----)

(----- Subtractive Processing Below -----)
M00 (Confirm start of subtractive processing by pressing 'Cycle Start')
G91 G28 Z0
G54
T01 M06                     (Tool Change to Ball Nose)
G43 H01                     (Call the Height Offset for the Ball Nose: make sure to
check this before running)
G41 D[#22]                  (Sets left hand cutter compensation as measured in SW
Model)
G00 G90 X[#18] Y[#19]       (Move to XY Subtractive Start location)
G00 G90 Z[#13]              (then to safe Z height)

M04 S[#20]                  (Starts Spindle at Calculated Spindle Speed)

G01 G90 Z[[#7-2]*#4] F[#25]         (Moves to 2nd to last layer Z height at slow speed
feed rate)
G01 G91 X[#12*[#7-2]] F[#25]        (Increments to X location of 2nd to last layer start)
M97 P201 L5                         (Calls N201 Subtractive Subroutine)

(----- The End Begins -----)
M30
(----- The End Ends -----)

(----- Subroutines Only Below Here -----)

(----- This set of Subroutines Clads Multi-Layer in ZigZag path -----)
N101
G55                         (double check for work offset G55)
G00 G90 Z[#13]              (moves up for safety)
G00 G90 X[#10] Y[#11]       (moves to XY start positions)
G00 G90 Z0.0                (moves down to G55 Z0.0)
M97 P102 L[#7]              (Calls N102 #7 = number of layers)
G00 G90 Z[#13]              (moves up for safety)
```

```
M99

N102
M97 P103 L[#6]              (calls flip flop track N103 #6 Number of tracks in layer times)
#10=#10+#12                 (updates X Position to increment over a half track width)
#6=#6-1.                    (updates Number of tracks in layer for next layer)
G00 G91 Z[#4]               (moves to new Z height, up #4 Step Up value)
IF [#15 EQ 2] GOTO 1021
G00 G90 X[#10] Y[#11]       (moves to updated X Position and Original Y position)
M99

N1021
G00 G90 X[#10] Y[#11 + #5] (moves to updated X Position and Flopped Y position)
M99

N103
IF [#15 EQ 2] GOTO 1031 (Checks for flop, if true skips to N1031)
M120                (Laser on)
G01 G91 Y[#5] F[#2] (Clads in Y positive dir, at #5 track length)
M121                (Laser off)
G01 G91 X[#3]       (Incremental Drive +X dir, to #3 Step Over)
#15 = [#15 + 1]     (makes flip flop = flop)
M99                 (ends subroutine, if flip flop was equal to flip)

N1031
M120                (Laser on)
G01 G91 Y-[#5]      (Clads in Y negative dir, at #5 track length)
M121                (Laser off)
G01 G91 X[#3]       (Incremental Drive +X dir, to #3 Step Over)
#15 = [#15 - 1]     (makes flip flop = flip)
M99                 (ends subroutine, if flip flop was equal to flop)

(---- The subroutines below here are for subtractive processing -----)

N201
G01 G91 Y[#23] F[#21]       (Cuts workpiece)
G01 G91 X-[#12 * 2]         (Increments over two step over values)
#30 = #30 + 1.              (Adds to Subtractive Pass Counter)
IF [#30 EQ 6] GOTO 2011     (Looks for number of subtractive passes and sends to N2011)
G00 G91 Y-[#23]             (Increments back to Y start, at Rapid)
G01 G91 Z-[#4 * 2] F[#25]   (Increments down two layer heights)
M99
```

N2011
G01 G91 Z25. F[#25] (If 5 passes are done, this sends the tool up)
M99

(----- Subroutines End -----)

A.5 Matlab multi-track height analysis example

General Housekeeping

```
clear,clc
format long
```

Reading the data into a table from the csv and preparing the characters for good plot titles.

```
RSS = ['9114_350'];
TrialNum = ['\11';'\12';'\21';'\22';'\31';'\32'];
for i = 1:6
    fnames(i,:) = append(RSS,TrialNum(i,:));
end
titles = char(fnames);
AmbitRecipe = titles(:,1:4);
ScanSpeed = titles(:,6:8);
TrialPos = string(insertAfter(cellstr(titles(:,10:11)),1,","));
for k = 1:size(fnames,1);
    p = readtable(fnames(k,:),"ReadVariableNames",false);
```

Separate and rename the table variables for ease of use.

```
    x = p{:,"Var1"}; y = p{:,"Var2"};
    if k == 1
        ExampleData = figure();
        plot(x,y); axis image; ylim([min(y)*.98 max(y)*1.2]);
        title(sprintf('Example of Profile Measurement Data from \n Focus
Variation Microscope'))
        xlabel('Deposition Width (m)');ylabel('Deposition Height (m)');
    end
```

Create the graphics figure for plotting and turn "hold" on so subsequent plots are in the same figure. Also, add some padding to the plot with limits.

```
    DetailedPlots = figure();
```

```
    hold on;
    plot(x,y,'b');DetailedPlots.Position = [681 559 560 250];
    xlabel('Deposition Width (m)');ylabel('Deposition Height (m)');
    title(sprintf('Ambit Recipe: %s \n Scan Speed %s \n Trial Position
%s',AmbitRecipe(k,:),ScanSpeed(k,:),TrialPos(k,:)));
    yHigh = max(y)*1.3; yLow = min(y)*0.98; ylim([yLow,yHigh]);
```

Using the built-in Matlab function "islocalmax" to find the local extremes, which should represent the clad heights of the individual tracks. Then plotting those maxima. To fine tune this process I will first create some variables to control the inputs for the "islocalmax" function, then I can adjust these inputs for each data set respectively using a conditional statement for each iteration of the loop. If the data set does not behave well I can further fine tune the process by creating smaller section in the data to use in the function.

```
    CP = round(linspace(1,numel(y),12));
    offsets = [10 -20 20 0 0 0 0 0 0 0 0 0];
    CheckPoints = CP + offsets;
%     plot(x(CheckPoints),y(CheckPoints),'g*')
    for i = 1:10
        xCladSection = x([CheckPoints(i):CheckPoints(i+1)]);
        yCladSection = y([CheckPoints(i):CheckPoints(i+1)]);
        TrackHeight = islocalmax(yCladSection,'MaxNumExtrema',1);
        if i == 1
            TrackHeight = numel(yCladSection);
        end
        xp(i) = xCladSection(TrackHeight);
        yp(i) = yCladSection(TrackHeight);

    end
    plot(xp,yp,'ro')
```

Section below will sort some of the data points into sections that represent the substrate surface so that it can be plotted for visualization and track height calculation.

```
    g = 10;
    xstart = x([2:2+g]);xend = x([end-g:end]);
    ystart = y([2:2+g]);yend = y([end-g:end]);
    w(:,1,k) = vertcat(xstart,xend);
    w(:,2,k) = vertcat(ystart,yend);
```

Now I will create a function from the data points that represent the substrate surface, using "polyfit", so that I can plot the assumed surface below the depositions.

```
    substate_equation = polyfit(w(:,1,k),w(:,2,k),1);
    substrate_surface = polyval(substate_equation,x);
    plot(x,substrate_surface,'k');
```

Now I can find the distance between each of the track maxima and the line representing the assumed substrate surface beneath the cladding using some built-in Matlab functions and some basic math. First I'll find the slope of any line perpendicular to the assumed substrate. Then for each of the track maxima I'll use that perpendicular slope and the calculated distance to plot the line representing the track height for each track.

```
    DistanceSlope1 = Slope2Sub(substate_equation,x);
    for i = 1:10
        Distance(i) =
PointLineDistance(substate_equation,xp(i),yp(i),x(2),x(numel(x)));
        [posx,posy] = POS(xp(i),yp(i),DistanceSlope1,Distance(i));
        plot([xp(i) posx],[yp(i) posy],'r');
    end
    TrackHeightData(:,k) = Distance(:);
    legend('Data','Track Peaks','Substrate','Track Heights')
    hold off
end
```

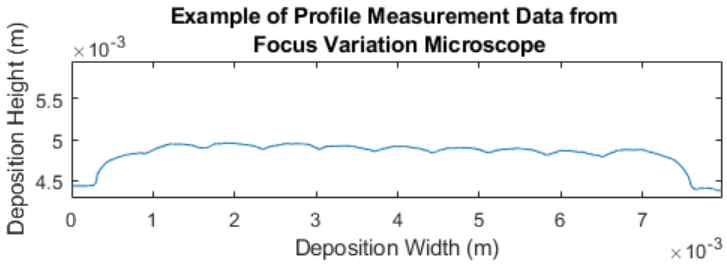

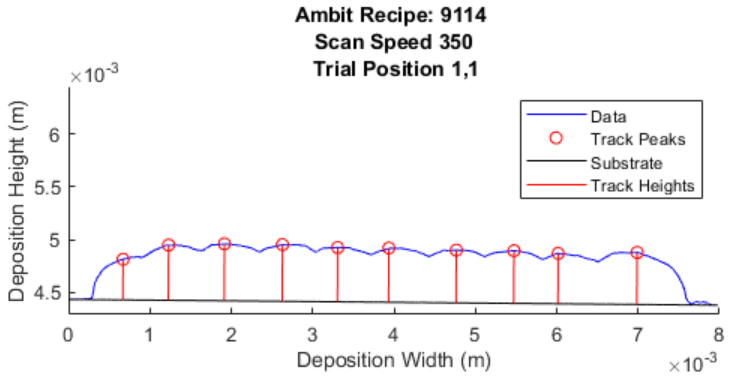

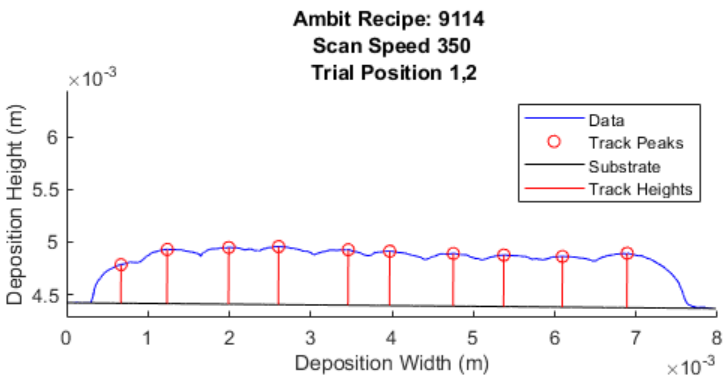
Ambit Recipe: 9114
Scan Speed 350
Trial Position 1,2
Deposition Height (m)
Deposition Width (m)
Data
Track Peaks
Substrate
Track Heights

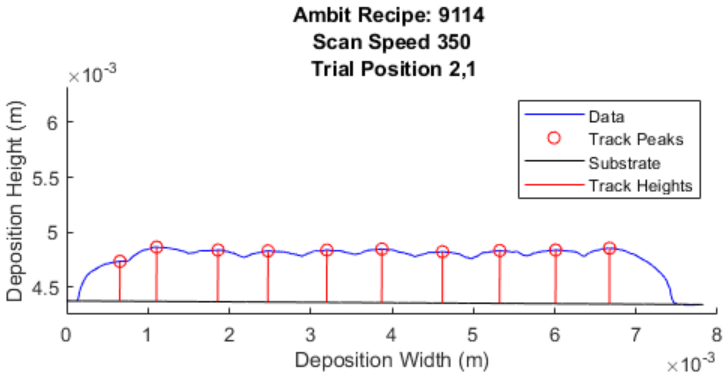
Ambit Recipe: 9114
Scan Speed 350
Trial Position 2,1
Deposition Height (m)
Deposition Width (m)
Data
Track Peaks
Substrate
Track Heights

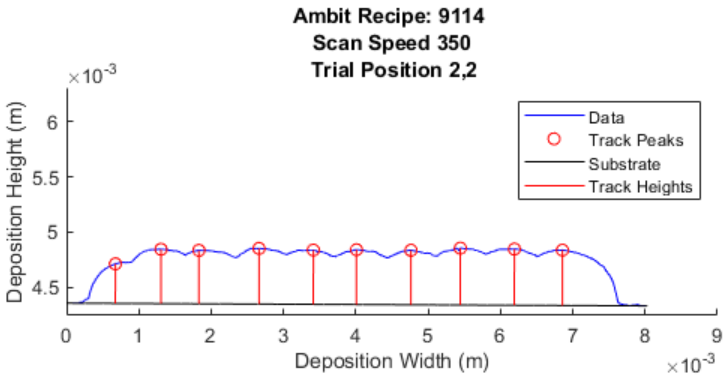
Ambit Recipe: 9114
Scan Speed 350
Trial Position 2,2
Deposition Height (m)
Deposition Width (m)
Data
Track Peaks
Substrate
Track Heights

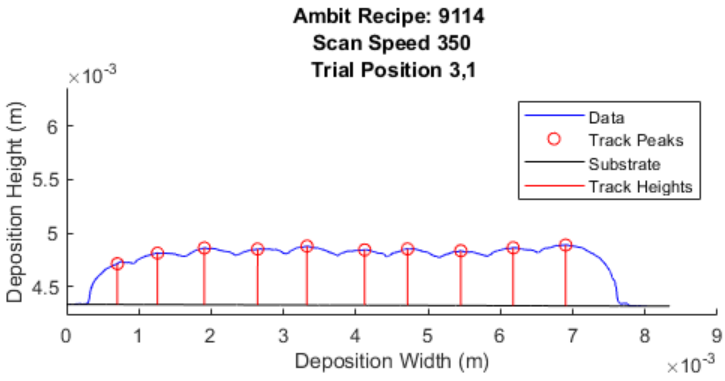
Ambit Recipe: 9114
Scan Speed 350
Trial Position 3,1
Deposition Height (m)
Deposition Width (m)
Data
Track Peaks
Substrate
Track Heights

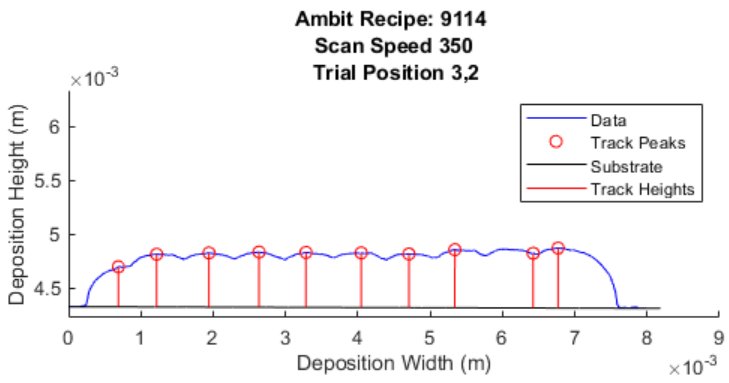

With the data sets visualized I can separate any sets that don't behave well and use the rest to create a model for the track height as a function of track number for this recipe set. To do this I will first collect the track height data, average them respective of track number, then create a polyfit that works well with the data.

```
 TrackHeightData(:,2) = [];
 TrackHeightData(:,3) = [];
 TrackHeightAverages = mean(TrackHeightData,2);
 TrackNumbers = [1:10];
 TrackHeightModel = polyfit(TrackNumbers,TrackHeightAverages,6);
 T = TrackHeightModel; %for sprintf ease later
 TH = polyval(T,TrackNumbers);
```

This section handles plotting the track height averages.

```
 THM = figure();
 plot(TrackNumbers,TrackHeightAverages);axis padded,hold on
 plot(TrackNumbers,TH,'ro')
 THAvg = mean(TrackHeightAverages([2:10]));
 yline(THAvg,'g-.')
 ylim([min(TrackHeightAverages)*.95 max(TrackHeightAverages)*1.1]);THM.Position
= [681 559 560 310];
 xlabel('Track Number');ylabel('Clad Height (m)');
 legend('TrackHeightAverage','TrackHeightModel','Avg Stable Track
Height',"Location","best")
 title(sprintf('Track Height Average & Model\nTrack Height =
%1.3dt^5+%1.3dt^4+%1.3dt^3+\n%1.3dt^2+%1.3dt+%1.3d\nwhere t is track
number\nAverage Stable Track Height =
%2.4d',T(1),T(2),T(3),T(4),T(5),T(6),THAvg));
```

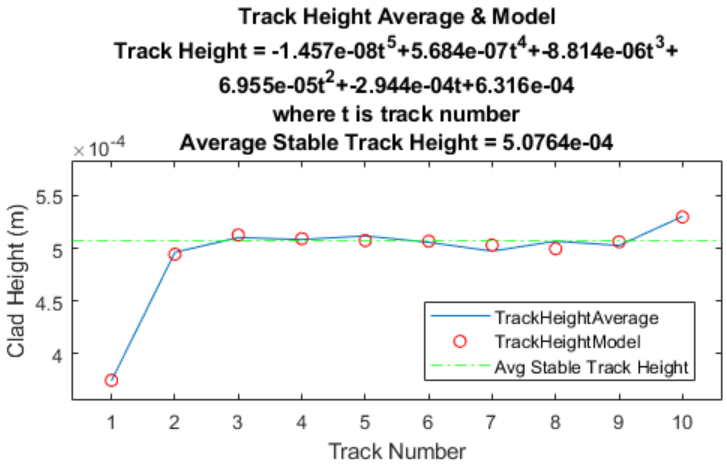


```
function Distance = PointLineDistance(LineEq,x0,y0,x1,x2)
y1 = polyval(LineEq,x1);
y2 = polyval(LineEq,x2);
numerator = abs(((x2-x1)*(y1-y0)) - ((x1 - x0)*(y2-y1)));
denominator = sqrt((x2-x1)^2 + (y2-y1)^2);
Distance = numerator/denominator;
end

function SlopeToSubstrate = Slope2Sub(LineEq,x)
x1 = x(2); %first x is usually 0, so use x(2)
y1 = polyval(LineEq,x(2));
x2 = x(numel(x));
y2 = polyval(LineEq,x(numel(x)));
SlopeLineEq = (y2 - y1)/(x2 - x1);
SlopeToSubstrate = -(1/SlopeLineEq);
end

function [psx psy] = POS(x1,y1,Slope,Distance)
psx = x1 - (Distance/sqrt(1+Slope^2));
psy = y1 - (Distance*Slope)/sqrt(1+Slope^2);
end
```

A.6 Matlab multi-layer analysis example

General Housekeeping

```
clear,clc
format long
```

Reading the data into a table from the csv and preparing the characters for good plot titles.

```
RSS = ['9114_350'];
TrialNum = ['\11';'\12';'\21';'\22';'\31';'\32'];
for i = 1:6
    fnames(i,:) = append(RSS,TrialNum(i,:));
end
titles = char(fnames);
AmbitRecipe = titles(:,1:4);
ScanSpeed = titles(:,6:8);
TrialPos = string(insertAfter(cellstr(titles(:,10:11)),1,","));
for k = 1:size(fnames,1);
    p = readtable(fnames(k,:),"ReadVariableNames",false);
```

Separate and rename the table variables for ease of use.

```
    x = p{:,"Var1"}; y = p{:,"Var2"};
    if k == 1
        ExampleData = figure();
        plot(x,y); axis image; ylim([min(y)*.98 max(y)*1.2]);
        title(sprintf('Example of Profile Measurement Data from \n Focus
Variation Microscope'))
        xlabel('Deposition Width (m)');ylabel('Deposition Height (m)');
    end
```

Create the graphics figure for plotting and turn "hold" on so subsequent plots are in the same figure. Also, add some padding to the plot with limits.

```
    DetailedPlots = figure();
    hold on;
    plot(x,y,'b');DetailedPlots.Position = [681 559 560 250];
    xlabel('Deposition Width (m)');ylabel('Deposition Height (m)');
    title(sprintf('Ambit Recipe: %s \n Scan Speed %s \n Trial Position
%s',AmbitRecipe(k,:),ScanSpeed(k,:),TrialPos(k,:)));
    yHigh = max(y)*1.3; yLow = min(y)*0.98; ylim([yLow,yHigh]);
```

Using the built-in Matlab function "islocalmax" to find the local extremes, which should represent the clad heights of the individual tracks. Then plotting those maxima. To fine tune this process I will first create some variables to control the inputs for the "islocalmax" function, then I can adjust these inputs for each data set respectively using a conditional statement for each iteration of the loop. If the data set does not behave well I can further fine tune the process by creating smaller section in the data to use in the function.

```
    CP = round(linspace(1,numel(y),12));
    offsets = [10 -20 20 0 0 0 0 0 0 0 0 0];
    CheckPoints = CP + offsets;
%     plot(x(CheckPoints),y(CheckPoints),'g*')
    for i = 1:10
        xCladSection = x([CheckPoints(i):CheckPoints(i+1)]);
        yCladSection = y([CheckPoints(i):CheckPoints(i+1)]);
        TrackHeight = islocalmax(yCladSection,'MaxNumExtrema',1);
        if i == 1
            TrackHeight = numel(yCladSection);
        end
        xp(i) = xCladSection(TrackHeight);
        yp(i) = yCladSection(TrackHeight);

    end
    plot(xp,yp,'ro')
```

Section below will sort some of the data points into sections that represent the substrate surface so that it can be plotted for visualization and track height calculation.

```
    g = 10;
    xstart = x([2:2+g]);xend = x([end-g:end]);
    ystart = y([2:2+g]);yend = y([end-g:end]);
    w(:,1,k) = vertcat(xstart,xend);
    w(:,2,k) = vertcat(ystart,yend);
```

Now I will create a function from the data points that represent the substrate surface, using "polyfit", so that I can plot the assumed surface below the depositions.

```
    substate_equation = polyfit(w(:,1,k),w(:,2,k),1);
    substrate_surface = polyval(substate_equation,x);
    plot(x,substrate_surface,'k');
```

Now I can find the distance between each of the track maxima and the line representing the assumed substrate surface beneath the cladding using some built-in Matlab functions and some basic math. First I'll find the slope of any line perpendicular to the assumed substrate. Then for each of the track maxima I'll use that perpendicular slope and the calculated distance to plot the line representing the track height for each track.

```
    DistanceSlope1 = Slope2Sub(substate_equation,x);
    for i = 1:10
        Distance(i) =
PointLineDistance(substate_equation,xp(i),yp(i),x(2),x(numel(x)));
        [posx,posy] = POS(xp(i),yp(i),DistanceSlope1,Distance(i));
        plot([xp(i) posx],[yp(i) posy],'r');
    end
```

```
    TrackHeightData(:,k) = Distance(:);
    legend('Data','Track Peaks','Substrate','Track Heights')
    hold off
end
```

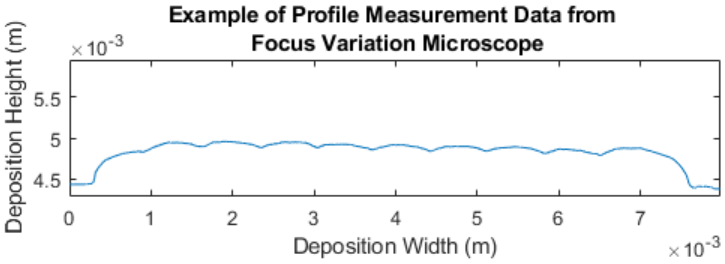

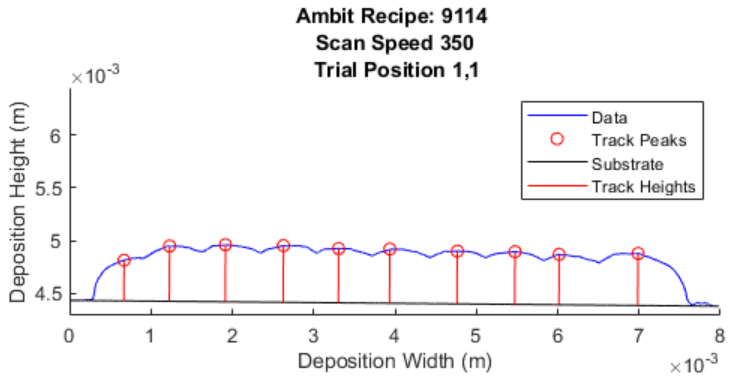

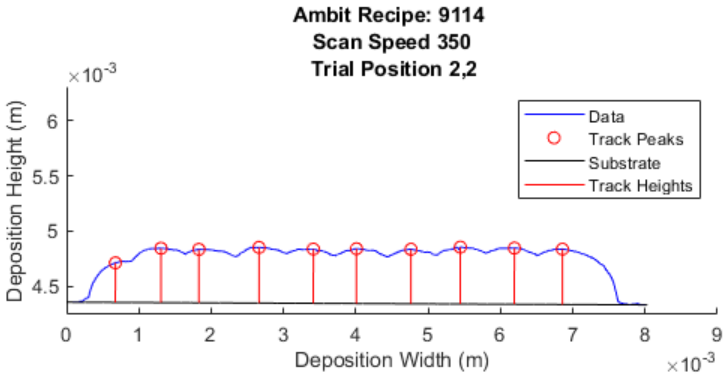

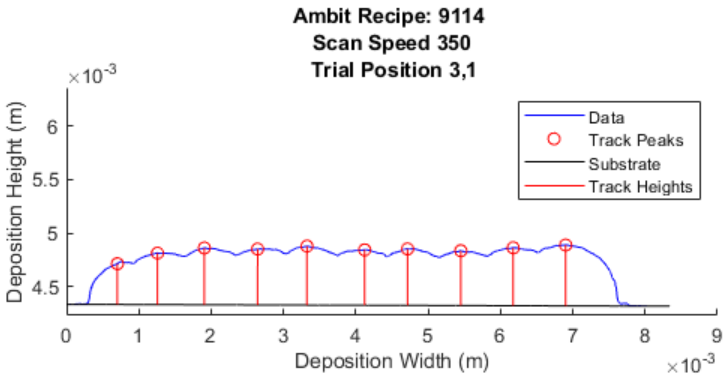

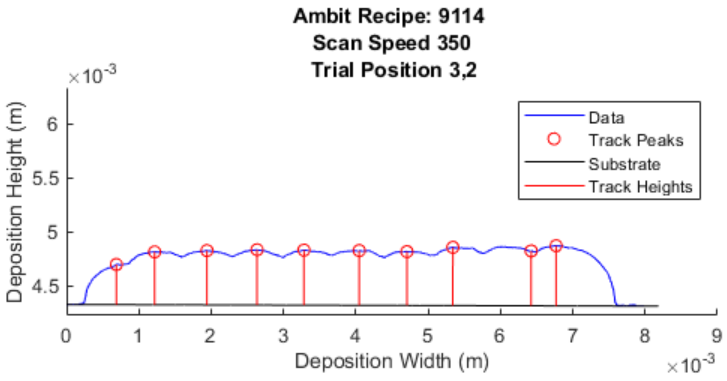

With the data sets visualized I can separate any sets that don't behave well and use the rest to create a model for the track height as a function of track number for this recipe set. To do this I will

first collect the track height data, average them respective of track number, then create a polyfit that works well with the data.

```
 TrackHeightData(:,2) = [];
 TrackHeightData(:,3) = [];
 TrackHeightAverages = mean(TrackHeightData,2);
 TrackNumbers = [1:10];
 TrackHeightModel = polyfit(TrackNumbers,TrackHeightAverages,6);
 T = TrackHeightModel; %for sprintf ease later
 TH = polyval(T,TrackNumbers);
```

This section handles plotting the track height averages.

```
 THM = figure();
 plot(TrackNumbers,TrackHeightAverages);axis padded,hold on
 plot(TrackNumbers,TH,'ro')
 THAvg = mean(TrackHeightAverages([2:10]));
 yline(THAvg,'g-.')
 ylim([min(TrackHeightAverages)*.95 max(TrackHeightAverages)*1.1]);THM.Position
= [681 559 560 310];
 xlabel('Track Number');ylabel('Clad Height (m)');
 legend('TrackHeightAverage','TrackHeightModel','Avg Stable Track
Height',"Location","best")
 title(sprintf('Track Height Average & Model\nTrack Height =
%1.3dt^5+%1.3dt^4+%1.3dt^3+\n%1.3dt^2+%1.3dt+%1.3d\nwhere t is track
number\nAverage Stable Track Height =
%2.4d',T(1),T(2),T(3),T(4),T(5),T(6),THAvg));
```

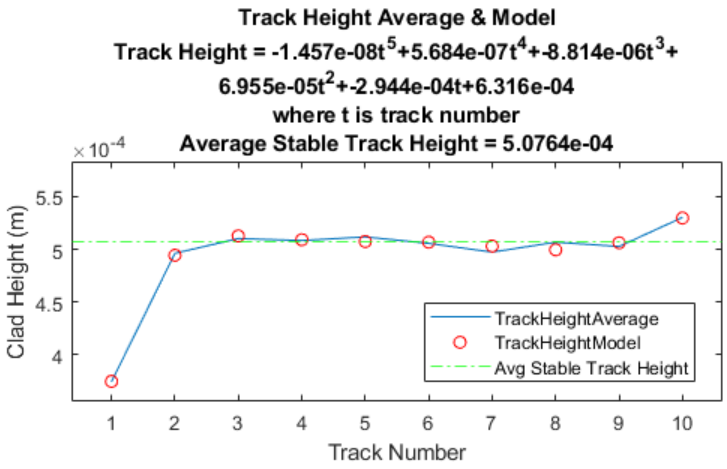

```
function Distance = PointLineDistance(LineEq,x0,y0,x1,x2)
y1 = polyval(LineEq,x1);
y2 = polyval(LineEq,x2);
numerator = abs(((x2-x1)*(y1-y0)) - ((x1 - x0)*(y2-y1)));
denominator = sqrt((x2-x1)^2 + (y2-y1)^2);
Distance = numerator/denominator;
end

function SlopeToSubstrate = Slope2Sub(LineEq,x)
x1 = x(2); %first x is usually 0, so use x(2)
y1 = polyval(LineEq,x(2));
x2 = x(numel(x));
y2 = polyval(LineEq,x(numel(x)));
SlopeLineEq = (y2 - y1)/(x2 - x1);
SlopeToSubstrate = -(1/SlopeLineEq);
end

function [psx psy] = POS(x1,y1,Slope,Distance)
psx = x1 - (Distance/sqrt(1+Slope^2));
psy = y1 - (Distance*Slope)/sqrt(1+Slope^2);
end
```

A.7 Matlab ANOVA and main effect example

```
clear,clc
load('MultiLayerHeightAnovaN.mat')
```

Arrange the data into one matrix

```
[p,tbl,stats,terms] =
anovan(MLHeightMeasured,inputs,'Model','linear','Varnames',{'Powder Flow';'Laser Power';'Scan Speed'});

headingObj = findall(0,'Type','uicontrol','Tag','Heading');
headingObj(1).String = 'ANOVA table : Multi-Layer Average Measured Height';
```

ANOVA table : Multi-Layer Average Measured Height

Source	Sum Sq.	d.f.	Mean Sq.	F	Prob>F
Powder Flow	0.08327	1	0.08327	54.18	0.0018
Laser Power	0.00368	1	0.00368	2.39	0.1967
Scan Speed	0.01345	1	0.01345	8.75	0.0416
Error	0.00615	4	0.00154		
Total	0.10655	7			

Constrained (Type III) sums of squares.

```
 Model1 = stats.coeffs(1:6);
 ModelEquation1 = sprintf('Height = %2.3f*g/min + %2.3f*watts + %2.3f*mm/min
',Model1(1),Model1(2),Model1(3));
 sprintf(ModelEquation1)
```

```
ans = 'Height = 0.375*g/min + -0.102*watts + 0.102*mm/min '
```

```
 rSquared =1 -
(sscanf(sprintf('%s*',tbl{5,2}),'%f*')/sscanf(sprintf('%s*',tbl{6,2}),'%f*'))
```

```
rSquared = 0.9423
```

```
 [p2,tbl2,stats2,terms2] =
anovan(MLHeightMeasured,inputNoLaser,'Model','linear','Varnames',{'Powder
Flow';'Scan Speed'});

 headingObj = findall(0,'Type','uicontrol','Tag','Heading');
 headingObj(1).String = 'ANOVA table : Multi-Layer Average Measured Height';
```

ANOVA table : Multi-Layer Average Measured Height

Source	Sum Sq.	d.f.	Mean Sq.	F	Prob>F
Powder Flow	0.08327	1	0.08327	42.36	0.0013
Scan Speed	0.01345	1	0.01345	6.84	0.0474
Error	0.00983	5	0.00197		
Total	0.10655	7			

Constrained (Type III) sums of squares.

```
 Model2 = stats2.coeffs(1:5);
 ModelEquation2 = sprintf('Height = %2.3f*g/min + %2.3f*mm/min
',Model2(1),Model2(3));
 sprintf(ModelEquation2);

 rSquared =1 -
(sscanf(sprintf('%s*',tbl2{4,2}),'%f*')/sscanf(sprintf('%s*',tbl2{5,2}),'%f*'))
```

```
rSquared = 0.9078
```

```
 slope1 = (sOne(1)-sOne(3))/(sOne(2)-sOne(4));
 slope2 = (stwo(1)-stwo(3))/(stwo(2)-stwo(4));
 slope3 = (sthree(1)-sthree(3))/(sthree(2)-sthree(4));
 mlhplot = figure();
 m = maineffectsplot(MLHeightMeasured,inputs,'varnames',{sprintf('F
g/min\nSlope=%2.2f',slope1),sprintf('P watts\nSlope=%2.2f',slope2),sprintf('S
mm/min\nSlope=%2.2f',slope3)});
 y = ylabel('Multi-layer clad height (mm)');
```

```
 t = title(sprintf('Main Effect Plots : Multi-layer height vs\nPowder Flow Rate,
Laser Power, Scanning Speed'));
 set(t,'Position',get(t,'Position')+[-2.6 0 0])
 set(y,'Position',get(t,'Position')+[-4.5 -0.12 0])
```

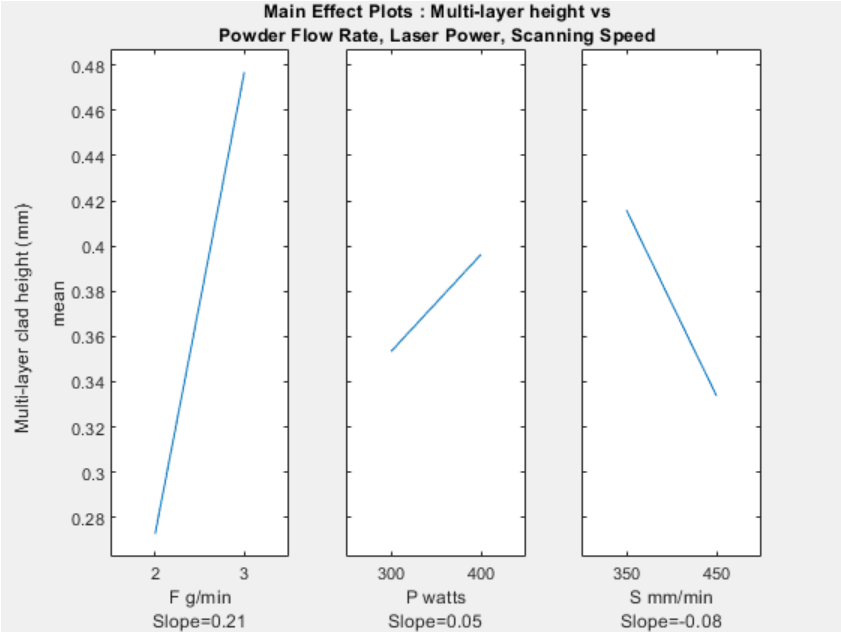


```
 set(0,'DefaultFigureColor',[1 1 1])
```

REFERENCES

1. ISO/ASTM International. ISO/ASTM 52900: Additive manufacturing - General principles and Terminology. Int Stand. 2015;5(978-84-9042-335–6):1–26.

2. Qi H, Azer M, Singh P. Adaptive toolpath deposition method for laser net shape manufacturing and repair of turbine compressor airfoils. Int J Adv Manuf Technol. 2010;48(1–4):121–31.

3. Amine T, Newkirk JW, Liou F. An investigation of the effect of direct metal deposition parameters on the characteristics of the deposited layers. Case Stud Therm Eng [Internet]. 2014 Jul 1 [cited 2020 Apr 25];3:21–34. Available from: https://www.sciencedirect.com/science/article/pii/S2214157X14000070

4. Camarena OKG. Hybrid additive manufacturing for tooling applications. Instituto Tecnológico y de Estudios Superiores de Monterrey School of Engineering and Sciences; 2020.

5. Cheng B, Chou K. Melt pool geometry simulations for powder-based electron beam additive manufacturing. 24th Int SFF Symp - An Addit Manuf Conf SFF 2013. 2013;644–54.

6. Yu J, Lin X, Wang J, Chen J, Huang W. Mechanics and energy analysis on molten pool spreading during laser solid forming. Appl Surf Sci [Internet]. 2010;256(14):4612–20. Available from: http://dx.doi.org/10.1016/j.apsusc.2010.02.060

7. Walker TR, Bennett CJ, Lee TL, Clare AT. A novel numerical method to predict the transient track geometry and thermomechanical effects through in-situ modification of the process parameters in Direct Energy Deposition. Finite Elem Anal Des [Internet]. 2020;169(October 2019):103347. Available from: https://doi.org/10.1016/j.finel.2019.103347

8. Picasso M, Marsden CF, Wagniere JD, Frenk A, Rappaz M. A simple but realistic model for laser cladding. Metall Mater Trans B. 1994;25(2):281–91.

9. Huang Y, Khamesee MB, Toyserkani E. A new physics-based model for laser directed energy deposition (powder-fed additive manufacturing): From single-track to multi-track and multi-layer. Opt Laser Technol [Internet]. 2019 Jan 1 [cited 2020 Apr 23];109:584–99. Available from: https://www.sciencedirect.com/science/article/pii/S0030399218309058

10. Bhardwaj T, Shukla M, Paul CP, Bindra KS. Direct Energy Deposition - Laser Additive Manufacturing of Titanium-Molybdenum alloy: Parametric studies, microstructure and mechanical properties. J Alloys Compd [Internet]. 2019;787:1238–48. Available from: https://doi.org/10.1016/j.jallcom.2019.02.121

11. Shim DS, Baek GY, Seo JS, Shin GY, Kim KP, Lee KY. Effect of layer thickness setting on deposition characteristics in direct energy deposition (DED) process. Opt Laser Technol

[Internet]. 2016;86:69–78. Available from: http://dx.doi.org/10.1016/j.optlastec.2016.07.001

12. Wang S, Zhu L, Fuh JYH, Zhang H, Yan W. Multi-physics modeling and Gaussian process regression analysis of cladding track geometry for direct energy deposition. Opt Lasers Eng [Internet]. 2020;127(November 2019):105950. Available from: https://doi.org/10.1016/j.optlaseng.2019.105950

13. Bax B, Rajput R, Kellet R, Reisacher M. Systematic evaluation of process parameter maps for laser cladding and directed energy deposition. Addit Manuf [Internet]. 2018;21(January):487–94. Available from: https://doi.org/10.1016/j.addma.2018.04.002

14. Wolff SJ, Webster S, Parab ND, Aronson B, Gould B, Greco A, et al. In-situ Observations of Directed Energy Deposition Additive Manufacturing Using High-Speed X-ray Imaging. Jom. 2021;73(1):189–200.

15. Kim DK, Woo W, Kim EY, Choi SH. Microstructure and mechanical characteristics of multi-layered materials composed of 316L stainless steel and ferritic steel produced by direct energy deposition. J Alloys Compd [Internet]. 2019;774:896–907. Available from: https://doi.org/10.1016/j.jallcom.2018.09.390

16. Vakondios D, Kyratsis P, Yaldiz S, Antoniadis A. Influence of milling strategy on the surface roughness in ball end milling of the aluminum alloy Al7075-T6. Meas J Int Meas Confed [Internet]. 2012;45(6):1480–8. Available from: http://dx.doi.org/10.1016/j.measurement.2012.03.001

17. Grzeski W. A revised model for predicting surface roughness in turning. Wear. 1996;194:143–8.

18. ISCAR. ISCAR ’s Quick Reference Guide for Die and Mold Making. 2017;1–160. Available from: https://www.google.com/url?sa=t&rct=j&q=&esrc=s&source=web&cd=&cad=rja&uact=8&ved=2ahUKEwjew9fAk6L5AhVXFrkGHVL_Av8QFnoECAIQAQ&url=https%3A%2F%2Fwww.iscar.com%2FCatalogs%2Fpublication-2017%2FDie_and_Molds_User_Guide_7861458_2017.pdf&usg=AOvVaw1GTFkNdJ62CkJ

19. Kaynak Y, Kitay O. Porosity, surface quality, microhardness and microstructure of selective laser melted 316l stainless steel resulting from finish machining. J Manuf Mater Process. 2018;2(2).

20. ISO/ASTM International. Tool life testing in milling - Part 2: End milling - ISO 8688-2. Geneve, Switzerland: ISO; 1989.

21. Cassier Z, Prato Y, Muñoz-Escalona P. Built-up edge effect on tool wear when turning steels at low cutting speed. J Mater Eng Perform. 2004;13(5):542–7.

22. Grzesik W. Hybrid additive and subtractive manufacturing processes and systems: A review. J Mach Eng. 2018;18(4):5–24.

23. Ituarte IF, Coatanea E, Salmi M, Tuomi J, Partanen J. Additive Manufacturing in Production: A Study Case Applying Technical Requirements. Phys Procedia [Internet]. 2015;78:357–66. Available from: http://dx.doi.org/10.1016/j.phpro.2015.11.050

24. Alvarez P, Montealegre MÁ, Pulido-Jiménez JF, Arrizubieta JI. Analysis of the process parameter influence in laser cladding of 316l stainless steel. J Manuf Mater Process. 2018;2(3).

25. Ramirez-cedillo E, Uddin MJ, Sandoval-robles JA, Mirshams RA. Process planning of L-PBF of AISI 316L for improving surface quality and relating part integrity with microstructural characteristics. 2019;

26. Carmignato S, De Chiffre L, Bosse H, Leach RK, Balsamo A, Estler WT. Dimensional artefacts to achieve metrological traceability in advanced manufacturing. CIRP Ann. 2020;69(2):693–716.

27. Wang H, Liu W, Tang Z, Wang Y, Mei X, Saleheen KM, et al. Review on adaptive control of laser-directed energy deposition. Opt Eng. 2020;59(07):1.

28. Denlinger ER, Heigel JC, Michaleris P, Palmer TA. Effect of inter-layer dwell time on distortion and residual stress in additive manufacturing of titanium and nickel alloys. J Mater Process Technol [Internet]. 2015;215:123–31. Available from: http://dx.doi.org/10.1016/j.jmatprotec.2014.07.030

29. Cabanettes F, Joubert A, Chardon G, Dumas V, Rech J, Grosjean C, et al. Topography of as built surfaces generated in metal additive manufacturing: A multi scale analysis from form to roughness. Precis Eng [Internet]. 2018;52(October 2017):249–65. Available from: https://doi.org/10.1016/j.precisioneng.2018.01.002

30. Sikan F, Wanjara P, Gholipour J, Atabay SE, Brochu M. Effect of substrate condition on wire fed electron beam additive deposition. Mater Sci Eng A [Internet]. 2022;849(June):143448. Available from: https://doi.org/10.1016/j.msea.2022.143448

31. Wang Z, Palmer TA, Beese AM. Effect of processing parameters on microstructure and tensile properties of austenitic stainless steel 304L made by directed energy deposition additive manufacturing. Acta Mater [Internet]. 2016;110:226–35. Available from: http://dx.doi.org/10.1016/j.actamat.2016.03.019

32. Yazar KU, Pawar S, Park K, Choi S. Jo ur. Mater Charact [Internet]. 2022;112148. Available from: https://doi.org/10.1016/j.matchar.2022.112148

33. Jones DJ. Hybrid DED Training AMBIT ™ In a nutshell CNC Machine. 2019.

34. Carpenter-Additive. PowderRange 316L - Datasheet [Internet]. 2020. p. 1–2. Available from: https://www.google.com/url?sa=t&rct=j&q=&esrc=s&source=web&cd=&ved=2ahUKEwij6buXhbr5AhUVBLkGHWR3AAQQFnoECAQQAw&url=https%3A%2F%2Fwww.carpenteradditive.com%2Fhubfs%2FResources%2FData%2520Sheets%2FPowderRange_316L_Datasheet.pdf&usg=AOvVaw31gDVHw29QfbIBoiZkN

35. Zhu Z, Dhokia V, Nassehi A, Newman ST. Investigation of part distortions as a result of hybrid manufacturing. Robot Comput Integr Manuf [Internet]. 2016;37:23–32. Available from: http://dx.doi.org/10.1016/j.rcim.2015.06.001